

AD-A094 511

BATTELLE COLUMBUS LABS OH

F/S 7/4

COMPUTATIONAL STUDY OF NONADIABATIC EFFECTS IN ATOM-MOLECULE RE--ETC(U)

DEC 80 M J REDMON

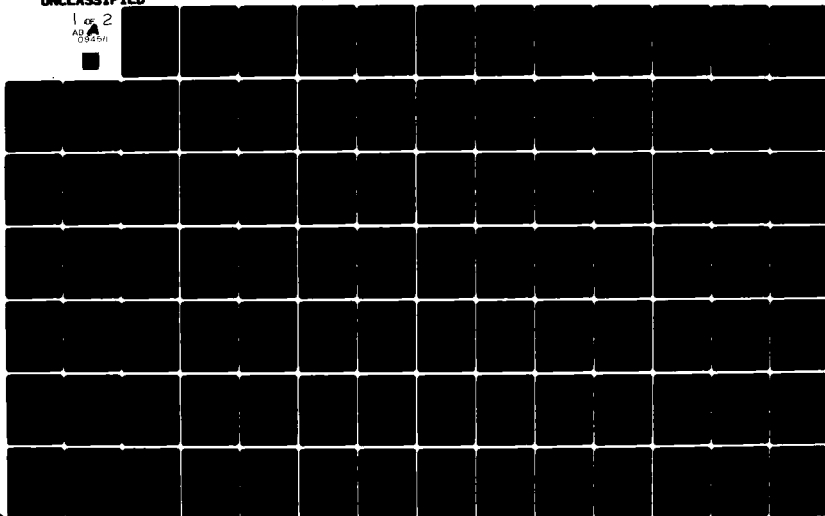
F49620-79-C-0050

NL

UNCLASSIFIED

AFOSR-TR-81-0007

1 of 2
AD
0945/11



AD A094511

DBJ FILE COPY


Battelle
Columbus Laboratories
LEVEL
Report

12

SPIC

Approved for public release;
distribution unlimited.

12

Final Technical Report

on

COMPUTATIONAL STUDY OF NONADIABATIC EFFECTS
IN ATOM-MOLECULE REACTIVE SCATTERING

to

AIR FORCE OFFICE OF SCIENTIFIC RESEARCH

December 10, 1980

Prepared by

Michael J. Redmon

BATTELLE
Columbus Laboratories
505 King Avenue
Columbus, Ohio 43201

AIR FORCE OFFICE OF SCIENTIFIC RESEARCH (AFSC)
NOTICE OF TRANSMITTAL TO DDC
This technical report has been reviewed and is
approved for public release IAW AFR 190-12 (7b).
Distribution is unlimited.
A. D. BLOSE
Technical Information Officer

DECLASSIFIED
E

TABLE OF CONTENTS

	<u>Page</u>
I. STATEMENT OF WORK	1
II. DESCRIPTION OF PROBLEM	1
III. RESEARCH OBJECTIVES	5
IV. RESEARCH ACCOMPLISHMENTS	5
V. RECOMMENDATIONS FOR FURTHER WORK	9
VI. SCIENTIFIC PERSONNEL SUPPORTED DURING THIS PROJECT	10
VII. PUBLICATIONS AND PRESENTATIONS RESULTING FROM THIS REPORT	11
REFERENCES	13

APPENDIX A

RECENT RESULTS FROM THREE DIMENSIONAL QUANTUM REACTIVE SCATTERING THEORY

APPENDIX B

AN ANALYTICAL FIT TO AN ACCURATE AB INITIO (1A_1) POTENTIAL SURFACE OF H_2O .

APPENDIX C

AB INITIO TREATMENT OF ELECTRONICALLY INELASTIC $K + H$ COLLISIONS USING
A DIRECT INTEGRATION METHOD FOR THE SOLUTION OF THE COUPLED-CHANNEL
SCATTERING EQUATIONS IN ELECTRONICALLY ADIABATIC REPRESENTATIONS

Accession For	
NTIS GRA&I	<input checked="" type="checkbox"/>
DTIC TAB	<input type="checkbox"/>
Unannounced	<input type="checkbox"/>
Justification	
By	
Distribution/	
Availability Codes	
Dist and/or	
Dist	Special
A	

FINAL TECHNICAL REPORT
on
Contract # F49620-79-C-0050
COMPUTATIONAL STUDY OF NONADIABATIC EFFECTS
IN ATOM-MOLECULE REACTIVE SCATTERING
to
Air Force Office of Scientific Research
December 10, 1980

I. STATEMENT OF WORK

Conduct a theoretical research program to develop quantum mechanical methods of studying nonadiabatic effects in three-dimensional atom-diatom collisions.

II. DESCRIPTION OF PROBLEM

Chemical dynamics has reached the stage of development that allows the first-principles determination of detailed state-to-state information for many kinetic processes.⁽¹⁾ These new experimental and theoretical methods are beginning to provide information of significant importance to military technology in such areas as chemical and excimer laser development, studies of the interaction of modern weapons systems with the atmosphere, the characterization of the radiation from rocket plumes, and combustion and propellant research.^(2,3) All of these areas require rate data for specific quantum transitions as input to sophisticated kinetic codes.

In many instances, the transitions of interest are difficult to investigate experimentally due to short lifetimes, low intensities, competing processes, or simply economic factors. Theoretical approaches can not only provide information of extreme utility to the experimentalist as support for the interpretation of data, but in their own right can be the most cost-effective means of obtaining such information.⁽⁴⁾

The goal of this research program is to develop new and more efficient quantum scattering methods that will be useful in applications to state-to-state collision processes involving two- and three-atom systems. The emphasis is on nonadiabatic processes, particularly those that involve the transfer of electronic energy. This approach is based on the coupled-channel method, and stresses reliable approximations that allow the study of light, first-row molecular systems involving up to three atoms. An important constituent of the present approach is the incorporation of potential energy surfaces and couplings obtained from ab-initio quantum chemistry. The suitable analytical representation of such surfaces is an important component of this research.

The Born-Oppenheimer (BO) separation of electronic and nuclear motion is a valuable tool in molecular theory since many low-energy collision processes are often adequately described by considering motion on a single potential energy surface. For inelastic collisions where avoided crossings or small separations between electronic states occur, and for reactions which involve the breaking of chemical bonds and reorganization of spin couplings, the BO approximation can be a poor one. In such cases it is necessary to consider the mixing of two or more adiabatic electronic states that arise due to nuclear motion.

Quantum chemistry is concerned with solution of the Schrödinger equation for electronic motion that results from application of the Born-Oppenheimer approximation. The set of solutions (adiabatic) to the electronic problem can be used as a basis for expanding the total wavefunctions for nuclear motion. When the BO approximation is valid, the wavefunctions for nuclear motion adequately describe molecular collisions on the appropriate potential surface (neglecting spin effects).

These adiabatic electronic functions can often be strongly coupled by operators neglected in the BO separation.⁽⁵⁾ For body-fixed coordinates (BF), in which the electronic problem is conveniently solved, these operators take the form of BO couplings for internal motion and coriolis couplings resulting from tumbling of the BF axis. Spin-orbit interaction is normally neglected in solving for the electronic eigenfunctions, but it must be included with the nonadiabatic couplings for a proper treatment of the collision problem. Other terms in the Breit-Pauli hamiltonian resulting from removing the center-of-mass motion may be neglected in problems of chemical interest.

Since most quantum coupled-channel methods make use of partial-wave expansions, studies of interacting open-shell species must explicitly consider the various angular momentum couplings that occur. Several quantum treatments of multiple-surface effects in $F + H_2$ have done so. Miller and Wyatt⁽⁶⁾ and DeVries and George⁽⁷⁾ utilize the valence bond character of DIM theory in their formulations, while Rebentrost and Lester⁽⁸⁾ employ SCF wavefunctions. Depending on the spin and angular momentum of the collision partners, different coupling schemes are required. These studies are the only ones reported for the interaction of a structured atom with a molecule in a $^1\Sigma$ state. Extensions to open-shell molecules are necessary to reach the ultimate goal of this project.

All three studies mentioned above employ diabatic representations for solving the coupled equations.⁽⁵⁾ These are usually obtained by various prescriptions from the adiabatic representation, and are not unique. They can be obtained by a unitary transformation that globally eliminates certain couplings. The advantage of diabatic representations is that one can minimize or eliminate the large couplings due to nuclear motion and instead employ a nondiagonal representation of the electronic hamiltonian. By eliminating the first derivative term, the coupled equations can be integrated using very efficient algorithms. Similar couplings appear for vibrational and rotational motions in reaction coordinate formulations of reactive scattering. Although the equations can be integrated with such terms included, better stability is obtained if they are eliminated.⁽⁹⁾ Since ab initio adiabatic potential surfaces and their couplings are employed in this approach, it is important that adequate methods be developed for integrating the appropriate coupled equations.

In summary, this research program attempts to bring together the computational tools necessary to determine from first-principles, state-to-state probabilities for quantum transitions involving rotational, vibrational, and electronic degrees of freedom for atom-diatomic molecule collisions. In Part III we highlight the principal objectives of this program, and in Part IV we examine the goals achieved during the past 18 months. Part V provides recommendations for further work.

III. RESEARCH OBJECTIVES

The overall objectives of this research program are as follows:

- Extend the 3-D reaction coordinate theory of chemical reactions to include nonadiabatic electronic transitions.
- Investigate various decoupling approximations for reducing the complexity of the coupled equations.
- Develop systematic approaches for the analytical representation of ab initio potential-energy surfaces and couplings.
- Develop efficient algorithms for the integration of coupled equations involving nonadiabatic couplings between rotational, vibrational, and electronic states.
- Implement these methods into efficient scattering codes.
- Apply these codes to a variety of problems of current interest.

IV. RESEARCH ACCOMPLISHMENTS

This research contract was originally funded as a 36-month effort, but this was reduced to 18 months because the principal investigator left Battelle. In spite of the short duration of this project, there have been a number of accomplishments that will form the basis of a practical method for studying electronic excitation in molecular collisions.

As a result of early work on this project, rate constants from 3-D reactive scattering calculations for $F + H_2$ and $H + H_2(V=1)$ are shown to be in general agreement with experiment (see Appendix A). Recent experiments on $F + H_2$ suggest the existence of a resonance⁽¹⁰⁾ predicted earlier by our theoretical approach.⁽¹¹⁾ Surface fitting procedures have been developed for fitting ab initio potential energy surfaces (see

Appendix B). A variety of techniques for integrating coupled equations were investigated, in part in collaboration with the NRCC workshop on computational algorithms in scattering theory. These methods were applied to a variety of vibrationally and rotationally nonadiabatic processes (Appendix A) and to electronically nonadiabatic processes in $K + H$ collisions (Appendix C).

Specific accomplishments are as follows:

- Previously computed reaction probabilities for $F + H_2$ were used to determine cross sections and rate constants for this reaction. This is the first 3-D quantum mechanical calculation of the rate of a chemical reaction other than $H + H_2$. Arrhenius parameters from the theoretical calculations are in reasonable agreement with experiment. Perhaps the most important result is that it is possible to compute probabilities at enough values of energy and total angular momentum to obtain total state-to-state cross sections over the range of energies required to compute a thermal rate. This is further discussed in Appendix A.
- Quantal rate constants calculated at 300 K for $H + H_2(V=1)$ agree with some experimental results and are in apparent disagreement with classical mechanics. The potential surface used in this study is not very reliable, but gives rates for $V=0$ in good agreement with experiment and other theoretical values (see Appendix A). This work is discussed

in some detail in a recent review by Schatz.⁽¹²⁾ Again, it is significant that these calculations are possible with modest computing resources. The $H + H_2(V=1)$ calculations were done on a VAX minicomputer!

- Methods have been developed, based on the many-body approach of Murrell, to obtain analytical representations of three- and four-atom potential energy surfaces. To date applications have been made to $O(^1D) + H_2(^1\Sigma_g^+)$, $C(^3P) + O_2(^3\Sigma_g^-)$, $O(^3P) + H_2O$ and $O(^3P) + CO_2$. Quartic force fields for H_2O and CO_2 are accurately reproduced with this technique (see Appendix B).
- Codes for generating 3-D electronic correlation diagrams in reaction coordinates, including rotational-vibrational degrees of freedom, have now been developed. These are general codes capable of treating one potential surface at a time and are not restricted to linear reaction intermediates. An analytical representation of the potential surfaces for each electronic state is required input. Systems studied so far are $F + H_2$, $H^+ + H_2$, $O(^3P) + H_2$, and $O(^1D) + H_2$.
- 3-D translational wavefunctions have been obtained for $F + H_2$, along with density and flux maps. The 3-D flux maps show whirlpool structure similar to the $F + H_2$ collinear reaction previously studied. This will be

presented in a forthcoming paper.⁽¹³⁾ This is an unusual method of interpreting scattering calculations and should lead to an increased understanding of molecular reaction mechanisms.

- An integral equation method developed previously⁽¹⁴⁾ has been tested against some of the more modern algorithms^(15,16), and in many instances is seen to be competitive. This algorithm is expected to be particularly useful in applications to energy-dependent potentials such as occur in reactive scattering problems.
- Several scattering codes incorporating electronic coupling, using different integrators, have been written and tested. Two of the integrators use accurate and reliable finite-difference methods. The others use more efficient potential-following techniques. The finite difference codes can be used to test the accuracy of the potential-following codes during preliminary studies on new systems.
- Adiabatic potential energy curves and nonadiabatic first-derivative couplings for the X, A, and $C^1\Sigma^+$ states of KH have been obtained by an ab initio pseudopotential method.⁽¹⁷⁾ The important splitting between the X and A curves is in good agreement with experiment. These curves and couplings are useful for dynamical studies on this system (see Appendix C).

- The ab initio potentials were used to calculate electronically inelastic transition probabilities and cross sections for low-energy K + H collisions. The $4^2P \rightarrow 4^2S$ quenching cross section varies between $2 \times 10^{-4} a_0^2$ and $10 \times 10^{-4} a_0^2$ between .022 eV and 1.10 eV relative translational energy. This study is a prelude to the study of K + H₂.

The ultimate goal of this program, namely, the treatment of electronic transitions in a 3-D atom-diatomic molecule reaction, was not realized due to time constraints. The manner in which the present study can be extended to this process is discussed in the next section.

V. RECOMMENDATIONS FOR FURTHER WORK

Progress to date has been made in (1) developing efficient computational tools for integrating coupled equations, (2) studying 3-D chemical reactions on single, adiabatic potential energy surfaces, and (3) developing a formalism for including electronic transitions in atomic collisions. The following recommendations should receive serious consideration to fully utilize the effort expended on this project.

- Perform reactive scattering calculations for O(³P) + H₂. Ab initio potential surfaces exist for this system, as do classical trajectory results and experimental results. This will provide yet another reaction for which 3-D quantum results are available. This was scheduled for the current project, and all necessary codes are in hand.

- Incorporate electronic degrees of freedom into existing scattering codes. This was started during this project, and the 3-D reactive code has been partly generalized. This is a straightforward extension of methods currently in hand, at least for singlet diatomic fragments.
- Develop strategies for treating arbitrary electronic angular momentum in a total angular momentum representation.
- Investigate necessary decoupling approximations suitable for studying vibronic transitions.
- Perform electronically nonadiabatic nonreactive calculations on $\text{Na} + \text{H}_2$ or $\text{K} + \text{H}_2$. This will test the machinery necessary for the reactive problem.
- Perform electronically nonadiabatic reactive calculations on $\text{Na} + \text{H}_2$ or $\text{K} + \text{H}_2$. These reactions are endothermic by about 2.3 eV and 2.7 eV, respectively, and will require a large number of channels. Reliable approximations make these problems tractable on existing machines.

VI. SCIENTIFIC PERSONNEL SUPPORTED DURING THIS PROJECT

Dr. Bruce C. Garrett

Dr. Michael J. Redmon

Dr. Isaiah Shavitt

VII. PUBLICATIONS AND PRESENTATIONS RESULTING FROM THIS PROJECT

A. Publications

1. "Recent Results from Three-Dimensional Quantum Reactive Scattering Theory," Int. J. Quantum Chem. Symp. 13, 559 (1979).
2. "Integral Equations with Reference Potentials," in Proceedings of the Workshop on Algorithms and Computer Codes for Atomic and Molecular Quantum Scattering Theory, Vol. I, L. Thomas, Ed., NRCC Proceedings No. 5, LBL 9501, Lawrence Berkeley Laboratory, Berkeley, CA 94720 (June, 1979).
3. "Applications of Integral Equations with Reference Potentials to the NRCC Close-Coupling Test Problems (INSCAT)," in Proceedings of the Workshop on Algorithms and Computer Codes for Atomic and Molecular Quantum Scattering Theory, Vol II, L. Thomas, Ed., NRCC Proceedings No. 5, LBL-9501, Lawrence Berkeley Laboratory, Berkeley, CA 94720 (July 1, 1980).
4. "An Analytical Fit to an Accurate ab initio (1A_1) Potential Surface of H_2O ," with G. C. Schatz, Chem. Phys. (in press).
5. "Ab initio Treatment of Electronically Inelastic $K + H$ Collisions Using a Direct Integration Method for the Solution of the Coupled-Channel Scattering Equations in Electronically Adiabatic Representations," with B. C. Garrett, D. G. Truhlar, and C. F. Melius, J. Chem. Phys. (in press).

6. "An Analytical Fit to the Ground State Potential Surface of CO_2 ," with G. C. Schatz, in preparation.

B. Presentations, Meetings

1. 34th Annual Molecular Spectroscopy Symposium, Columbus, OH, June 1979.
2. NRCC Close-Coupling Workshop, Part I, Argonne National Laboratory, June 1979.
3. Gordon Research Conference on Few-Body Problems, Wolfsboro, NH, August 1979.
4. AFOSR Molecular Dynamics Contractor's Meeting, Seiler Labs., Colorado Springs, October 1979.
5. NRCC Close-Coupling Workshop, Lawrence Berkeley Laboratory, October 1979.
6. Workshop on Excitation Cross Sections, in conjunction with AFOSR/AFRPL Aerospace Sciences Contractors meeting, AFRPL, Lancaster, CA, March 1980.
7. Visit to AFWL for meeting on possible technology transfer, Chemical Laser Branch, March 1980.
8. Midwest Theoretical Chemistry Conference, Minneapolis, MN, May 1980 (by B. C. Garrett).
9. Canadian Theoretical Chemistry Conference, Banff, Alberta, June 1980.
10. Second Chemical Congress of the North American Continent, Las Vegas, August 1980.
11. AFOSR Molecular Dynamics Contractor's Meeting, AFGL, Cambridge, MA, October 1980.

REFERENCES

1. State-to-State Chemistry, P. R. Brooks and E. F. Hayes, eds., ACS Symposium Series 56 (American Chemical Society, Washington, DC, 1977).
2. L. Wilson, "Report of Workshop on State-to-State Molecular Dynamics," AFOSR Physics 77-111, June 1976.
3. T. C. Collins and D. Stewart, "Report on Conference on Chemistry and Physics of Plumes," AFOSR Physics 77-062, July 1976.
4. M. J. Redmon, R. J. Bartlett, B. C. Garrett, G. D. Purvis, III, P. M. Saatzer, G. C. Schatz, and I. Shavitt, "Collisional Excitation of H₂O by O-Atom Impact: Classical Dynamics on an Accurate ab initio Potential Energy Surface," in Potential Energy Surfaces and Dynamics Calculations, D. G. Truhlar, ed. (Plenum 1981).
5. B. C. Garrett and D. G. Truhlar, "The Coupling of Electronically Adiabatic States in Molecular Collisions," in Theoretical Chemistry: Advances and Perspectives, Vol. 8, edited by D. Henderson (Academic Press, New York, 1980).
6. D. L. Miller and R. E. Wyatt, "Electronuclear Basis for Three-Dimensional Electronic Nonadiabatic Chemical Reactions," J. Chem. Phys. 67, 1302 (1977).
7. P. DeVries and T. F. George, "Quantum Mechanical Theory of a Structured Atom-Diatom Collision System: A + BC('Σ)," J. Chem. Phys. 67, 1293 (1977).
8. F. Rebertus and W. A. Lester, Jr., "Nonadiabatic Effects in the Collision of F(2P) with H₂ ('Σ_g⁺). II. Born-Oppenheimer and Angular Momentum Coupling in Adiabatic and Diabatic Representations," J. Chem. Phys. 64, 3879 (1976).
9. M. J. Redmon and R. E. Wyatt, "Computational Methods for Reactive Scattering," Int. J. Quantum Chem. Symp. 11, 343 (1977).
10. R. K. Sparks, C. C. Hayden, K. Shobatake, D. M. Neumark, and Y. T. Lee, "Molecular Beam Studies of Reaction Dynamics of F + H₂, D₂," Proc. 3rd Conf. Quantum Chem., Kyoto, Japan (in press).
11. M. J. Redmon and R. E. Wyatt, "Quantum Resonance Structure in the Three-Dimensional F + H₂ Reaction," Chem. Phys. Lett. 63, 209 (1979).
12. G. C. Schatz, "Overview of Reactive Scattering," in Potential Energy Surfaces and Dynamics Calculations, D. G. Truhlar, ed. (Plenum, 1981).

13. J. McNutt, R. E. Wyatt, and M. J. Redmon, "Wavefunction and Flux Analysis for the Three-Dimensional $F + H_2$ Reaction," in preparation.
14. M. J. Redmon and D. A. Micha, "A Computational Method for Multi-channel Scattering Calculations. Applications to Rotational Excitation and Long-Lived States in $He-N_2$," *Chem. Phys. Lett.* **28**, 341 (1974).
15. M. J. Redmon, "Reference Potentials with Integral Equations," in Algorithms and Computer Codes for Atomic and Molecular Quantum Scattering Theory, Vol. I, L. Thomas, ed., NRCC Proceedings No. 5, LBL-9501, Lawrence Berkeley Laboratory, Berkeley, CA 94720 (June 1979).
16. M. J. Redmon, "Applications of Integral Equations with Reference Potentials to the NRCC Close-Coupling Test Problems (INSCAT)," in Algorithms and Computer Codes for Atomic and Molecular Quantum Scattering Theory, Vol II, L. Thomas, ed., NRCC Proceedings No. 5, LBL-9501, Lawrence Berkeley Laboratory, Berkeley, CA 94720 (July 1980).
17. B. C. Garrett, M. J. Redmon, D. G. Truhlar, and C. F. Melius, "Ab initio Treatment of Electronically Inelastic $K + H$ Collisions Using a Direct Integration Method for the Solution of the Coupled-Channel Scattering Equations in Electronically Adiabatic Representations," *J. Chem. Phys.* (in press). See Appendix C.

APPENDIX A

Recent Results from Three-Dimensional Quantum Reactive Scattering Theory

MICHAEL J. REDMON

Chemical Physics Group, Battelle-Columbus Laboratories, Columbus, Ohio 43201,
U.S.A.

Abstract

Results from recent three-dimensional natural coordinate reactive scattering calculations are presented. Extensions of the scattering method of Wyatt to systems with nonlinear intermediates are discussed. Rate constants for the reaction $\text{H} + \text{H}_2$ ($v = 1$) at 300 K are presented and compared with classical trajectory calculations and with experiment. The quantum results are in reasonable agreement with experiment, but the classical results greatly underestimate the reaction rate. Total cross sections and relative rate constants are presented for the $\text{F} + \text{H}_2$ ($v = 0$) reaction and compared with classical results and experiment. Total cross sections for the $\text{H} + \text{O}_2$ reaction are presented that demonstrate the enhancement of reaction caused by reagent vibrational energy.

1. Introduction

There has been considerable progress in the development of quantum mechanical methods for obtaining state-to-state cross sections and rate constants for simple chemical reactions. Beginning with the early work on the $\text{H} + \text{H}_2$ reaction [1-4], the computational technology has continuously developed so that converged close-coupled results now exist for this system [5-7]. Recently, a calculation has been reported [7] on an accurate fit [8] to the definitive Liu-Siegbahn surface [9]. It should now be possible to obtain accurate *ab initio* dynamical information for $\text{H} + \text{H}_2$ and its isotopes for comparison with experiment.

Progress has also been made in developing methods based on close-coupling techniques for treating 3-D (three-dimensional) systems other than $\text{H} + \text{H}_2$ [10-12]. Extensions to reactions involving heavier atoms are difficult due to asymmetries in the reaction coordinates and to the enormous increase in the number of coupled channels necessary for convergence of the computed probabilities. The large number of channels accessible at thermal collision energies requires the use of centrifugal decoupling approximations for total angular momentum $J > 0$. These can be so-called J_z -conserving approximations [13], in which the number of channels used in expanding the wavefunction is approximately the same as for $J = 0$, or centrifugal sudden approximations [14], in which the orientation of the system is frozen during a collision, resulting in an enormous reduction in the number of coupled equations. Both of these approximations are adequate for total reaction cross sections for $\text{H} + \text{H}_2$, and the J_z -conserving approximation reproduces accurate close-coupling results for

individual rotational transitions to 7% [10]. It has so far not been possible to test these approximations for heavier systems by comparison with close-coupling calculations. It is felt that the J_z -conserving approximation should be reliable for other reactions with linear intermediates.

In this article we present a review of some recent results of 3-D reactive scattering calculations for $F + H_2$, $H + H_2$, and $H + O_2$. These calculations used Wyatt's formulation of the 3-D quantum scattering problem [15] with the natural collision coordinates (NCC) of Marcus [16]. The calculations employed the code REACTOR, written by the author while at the University of Texas at Austin, and which was used in the previous calculations reported for $F + H_2$ [10-12]. The latest version incorporates modifications necessary for treating reactions with a nonlinear intermediate, such as $H + O_2$, and also uses the R -matrix propagation method [17]. These extensions are examined, although computational details are not presented here. The approximations employed are discussed insofar as they might be expected to affect the reported results. A recent review has been given by Wyatt [18].

In Sec. 2 we discuss some improvements in the NCC approach. In Sec. 3 we present results for several systems, including rate constants for the $F + H_2$ reaction, and make comparisons with experiment and classical trajectory calculations. We also compare our calculations of reaction rates for vibrationally hot $H + H_2$ with some new experiments and with classical mechanics. Finally, we discuss new applications of the method to the $H + O_2$ reaction.

2. Recent Developments in NCC Reactive Scattering Methodology

A. More Schizophrenia in Reaction Coordinates

The unique feature of Marcus' natural collision coordinates [16] is that the translation, vibration, and rotation coordinates (s, ρ, γ) all vary smoothly from a set appropriate for describing the relative motion of an atom C colliding with a diatomic molecule AB to a set appropriate for describing the relative motion of atoms A or B with the molecules BC or AC . This is accomplished in the following way. The body-fixed (x, X) = (0, 0) plane is chosen as the instantaneous plane of the three atoms, with collinear motion defined in the (z, Z) plane. Deviations from collinear motion require excursions of the system into the (y, Y) plane, and are defined by the quantity $m \geq 0$ with magnitude $(y^2 + Y^2)^{1/2}$. As discussed by Marcus [16], keeping m positive avoids one source of double counting of configurations. The smooth transformation between reactant and product coordinates is obtained by requiring a local Cartesian constraint

$$y \sin \alpha(s) + Y \cos \alpha(s) = 0 \quad (1)$$

at each point along the reference curve defined by the translational coordinate s . $\alpha(s)$ is an arbitrary switching angle [16] that varies smoothly between zero for reactant configurations and ξ_∞ (skew angle of the mass-weighted coordinates) for product configurations. The z axis points initially to the reagent atom, and switches smoothly so that it points to the product atom after the collision.

Rather than use the coordinate m , it is more convenient to discuss the motion by using the local radial and bending coordinates (r, γ) , to which m is related by the expression

$$m = r \sin \gamma; \quad (2)$$

where r is measured (in a constant s plane) from the z axis and γ is referenced to the collinear plane. This is useful in writing the Hamiltonian for the system since γ becomes a convenient coordinate for representing internal rotational motion. A problem that arises, which was not discussed by Marcus, is that there are values of γ (near $\pi/2$) for which the coordinates become multiply valued whenever the switching angle $\alpha(s)$ is not exactly equal to one of its asymptotic values. This is a direct consequence of the constraint expressed by Eq. (1). This situation is illustrated in Figure 1, where the hatched area for $\gamma > \gamma_m$ represents the region in which configurations are identical to some for $\gamma < \gamma_m$. Configurations for $\gamma = \gamma_m$ correspond to isosceles triangle geometries, and when $s = 0$ and $\alpha = 1/2 \xi_\infty$, $\gamma_m = 45^\circ$, which corresponds to equilateral triangle configurations for H_3 and H_3^+ .

This characteristic of NCC was not noted in early applications [6, 10, 11] because the bending potential was parametrized and fit to small deviations from linearity (small γ). It was observed by this author during attempts to accurately represent the $F + H_2$ surface in NCC. It becomes particularly important for systems with stable nonlinear intermediates such as H_3^+ and HO_2 . In fact, for $H^+ + H_2$, the most stable configuration follows the curve $\gamma = \gamma_m$ in Figure 2, corresponding to C_{2v} configurations. It seems necessary to replace Eq. (2) with

$$m = r \sin \delta \gamma, \quad (3)$$

with the scale factor $\delta(s)$ defined so that $\delta \gamma = \gamma_m$ for $\gamma = \pi/2$. This introduces

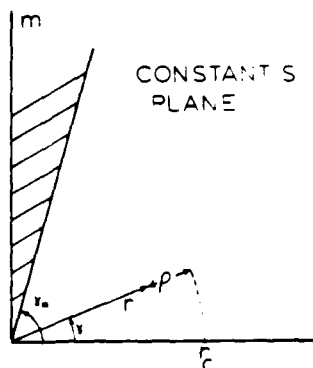


Figure 1. A constant s plane showing the multivalued region for $\gamma > \gamma_m$ that must be avoided in doing scattering calculations. When the switching angle equals an asymptotic value, $\gamma_m = 1/2 \pi$.

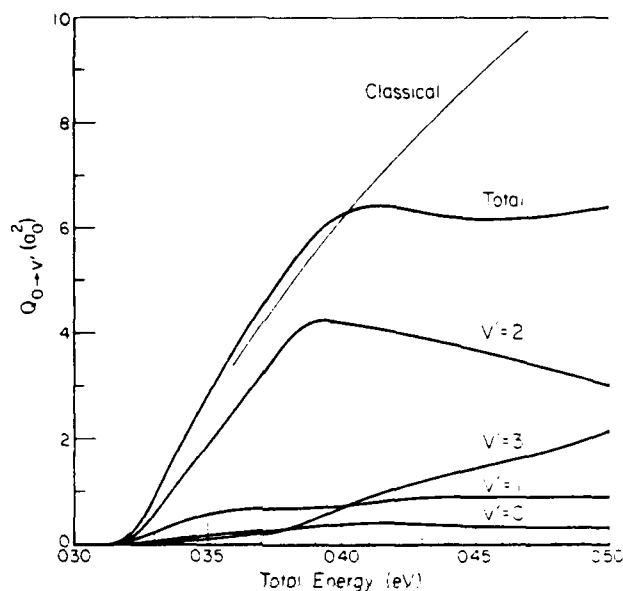


Figure 2. A comparison of the variation of the switching angle $\alpha(s)$ with reaction coordinate, and the corresponding value of γ_m which defines isosceles triangle geometries for the three-atom system

additional complications into an already formidable kinetic energy operator [15], but some procedure for maintaining $\gamma < \gamma_m$ is necessary for accurate computations in NCC. It should be pointed out that this schizoid region is different from the one associated with three-atom dissociation regions of NCC [19], which are effectively handled for low-energy collisions by using a circular arc to define the reference curve, and choosing an appropriate turning center.

B. Extensions to Systems with Noncollinear Reaction Paths

NCC theory was originally formulated with applications to $\text{H} + \text{H}_2$ in mind. Since for this reaction the minimum energy path is collinear, terms in the kinetic energy that are small except for large deviations from collinearity were dropped, and others were approximated by evaluating them on the reaction path [6, 15]. This near-linear intermediate approximation has been used in all NCC calculations reported so far. We have recently added the additional terms that contribute for $J = 0$ and now neglect only those that are zero within the J_z -conserving approximation. Elkowitz has suggested that the inertia coefficients can be evaluated on the noncollinear reaction path, in the spirit of the linear intermediate approximation [20]. He has shown that the Hamiltonian then reduces exactly to the one used previously [15] when the reaction path is collinear. We

have chosen instead to accurately compute the matrix elements over the vibrational motion, which can be large, but to set γ equal to γ_0 , its local value on the reaction path, to approximate some of the integrals over the bending coordinate. This leads to a considerable simplification in matrix element computation, and seems reasonable since we are looking toward developing useful decoupling procedures, and not exact close coupling. The new methods of evaluating matrix elements were used for the $H + O_2$ calculations discussed in this article.

3. Selected Results for Three Representative Reactions

In this section we present some recent results for the $H + H_2$, $F + H_2$, and $H + O_2$ reactions. These systems are useful for demonstrating the range of applicability of the method, as $F + H_2$ is highly exoergic, while $H + O_2$ is endoergic and has a stable nonlinear intermediate with a 2-eV well. The goal of our current effort is to develop techniques for determining total state-to-state cross sections and rate constants for atom-diatomic molecule reactions involving relatively light atoms.

A. Rate Constants for the $H + H_2$ Reaction

In their work on this reaction, Schatz and Kupperman [5] computed rate constants for the Porter-Karplus surface and found good agreement with classical mechanics at 600 K. However, at 300 K there were significant differences between the quantum and classical results. It is of interest to compare quantum and classical calculations on a surface with the correct barrier height, and for vibrationally excited reagents, since reactions of vibrationally hot hydrogen are of current astrophysical interest. We have chosen the Yates-Lester surface [21], and computed distinguishable atom rate constants for the processes $H + H_2(v = 0, j = 0) \rightarrow H + H_2(v = 0, \Sigma j')$, and $H + H_2(v = 1, j = 0) \rightarrow H + H_2(v = 0, \Sigma j')$. The results are summarized in Table I. We find, as did Schatz, that the classical rates at 300 K are significantly lower than the quantum results. For the ground-state reaction, this is presumably due to tunneling. For vibrationally excited hydrogen, tunneling is probably less important, and the enhanced rate is the result of interference effects among the various reactive and non-reactive pathways that suddenly become assessable near a threshold.

We find that the cooling rate for $H_2(v = 1)$ is slightly larger for the non-reactive pathway than for the reactive pathway, as predicted from $J = 0$ probabilities [18]. This is in contradiction to the assumptions made by Heidner and Kasper in analyzing their experiments [22], where the nonreactive contribution to the cooling was assumed negligible.

In comparison with recent hydrogen maser experiments [23], we find that our overall rates are generally in much better agreement with experiment than classical results on the Yates-Lester surface (at 300 K), although we are perhaps underestimating the contribution due to the resonant exchange process $H + H_2(v = 1) \rightarrow H + H_2(v = 1)$. We are currently examining the possibility that the

TABLE I Rate constants^a for the H + H₂ reaction at 300 K

	classical ^a	quantum ^b	experiment
$k_0^{R \rightarrow +}$	--	1.3×10^8	$c_{1.2 \times 10^8}$ $d_{3.3 \times 10^8}$
k_1^R	5.1×10^{10}	(3×10^{12})	$d_{3.1 \times 10^{12}}$
k_1^N	(2.4×10^{10})	8.2×10^{12}	--
k_{10}	--	(1×10^{13})	$e_{1.8 \times 10^{11}}$
k_{10}^R	3.6×10^{10}	2.6×10^{12}	--

^a Units are cm³ sec⁻¹ mole⁻¹. Values in parenthesis are estimates.

^b k_1 refers to reaction from H₂ ($v = 0, j = 0$) to all final states. k_{10} refers to reaction from H₂ ($v, j = 0$) to H₂ ($v' = 0, \Sigma j'$).

^c Classical results on the Yates-Lester surface from I. W. M. Smith, Chem. Phys. Lett. **47**, 219 (1977).

^d 3-D quantum results for the Yates-Lester surface, this work.

^e W. Schultz and D. J. LeRoy, J. Chem. Phys. **42**, 3869 (1965).

^f Reference 23.

^g Reference 22.

linear intermediate approximation might lead to underestimation of the probabilities for this process.* It should be noted that these rates are computed from distinguishable atom cross sections for comparison with classical mechanics, and are for reagent H₂ in its lowest rotational state. Our conclusion is that the use of classical mechanics for this system is justified only for translational temperatures well above 300 K.

B. Quantum Effects in the Three-Dimensional F + H₂ Reaction

This reaction was the first one studied beyond H + H₂ by a full 3-D quantum mechanical method [10, 11]. One of the important reasons for studying this system was to see to what extent the very significant differences between quantum and classical collinear calculations [24] might be modified in three dimensions. The original 3-D quantum calculation was restricted to total angular momentum $J = 0$, but it showed that the Feshbach resonance mechanism that dominates the low-energy collinear reaction probability [25] for the process F + H₂ ($v = 0$) \rightarrow H + HF ($v' = 2$) persists in three dimensions. It was later demonstrated by summing over J to obtain a total cross section for this process that the quantum cross section had a distinct maximum just above threshold, while the classical result continued to grow [12].

Our current quantum scattering codes are efficient enough to allow computations in which the potential parameters of the surface are varied. This allows us to examine the sensitivity of the dynamics to various features of a potential

* The author wishes to thank J. M. Bowman for useful discussions of this point.

surface. This approach can be used to aid those doing *ab initio* calculations of potential energy surfaces in selecting those regions of a surface that require significant effort. This has been done successfully for the collinear $F + H_2$ reaction [25, 26]. We are presently performing 3-D calculations for $F + H_2$ with a variety of bending potentials and present in Figure 3 cross sections for a fit to the famous surface 5 of Muckerman [27]. This differs from the potential used previously [10, 11] in that this fit gives a better description of the local rotor eigenvalue spectrum. The previous potential allowed for less hindered rotational motion near the saddle point than the one used here, and produced reaction cross sections about 30% larger near the threshold. Results for all of the potentials we have used are similar, and all show a maximum in the $v' = 0 \rightarrow 2$ cross section. As Figure 3 shows, this produces a leveling off in the total reaction cross section that is not observed in the classical result [12]. This is direct evidence that a quantum mechanical resonance mechanism results in an energy dependence in the reaction cross section that is not reproduced by classical mechanics, which should be experimentally verifiable.

We have calculated state-to-state rate constants, and present them in Table II, along with classical and experimental results where possible. We find that 67% of the available energy ends up as product vibration, in excellent agreement with experiment and classical mechanics. The ratio of rate constants k_1/k_2 is also in good agreement, but the ratio k_3/k_2 is not. We find a significant amount of flux ends up in $v' = 0$ excitation and is significantly affected by variations in the bending potential, as is to a lesser extent $v' = 3$. Classical mechanics produces no reaction into $v' = 0$, and collinear quantum calculations show less reaction into this state than 3-D calculations. Modifications to the bending potential can introduce wells in the $v' = 0$ and $v' = 1$ correlation diagrams and affect the amount of reaction into those states, just as modifications in the vibrational levels themselves can drastically affect collinear probabilities [25]. This sensitivity to features of the bending potential should ultimately lead to refinements in our knowledge about this system.

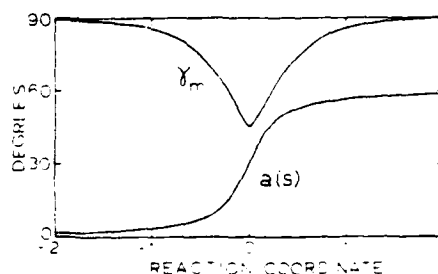


Figure 3. Cross sections for the reaction $F + H_2(v' = 0, j' = 0) \rightarrow H + HF(v', \Sigma')$. The total reaction cross section is shown and compared with the classical result of ref. 28.

TABLE II. Comparison of theoretical and experimental results for the 3-D F + H₂ reaction

	classical	quantum ^b	experiment
$E_a/\text{kcal mol}^{-1}$	1.937 ^d	1.55	1.6 ^c
$\log A/\text{cm}^3 \text{ s}^{-1} \text{ mol}^{-1}$	13.2 ^d	13.65	14.2 ^c
$\sigma_{v'}/\sigma_{v=0}$.665 ^d	.67	.66 ^d
$k_{v'}/k_{\text{max}} (300^\circ\text{K})^{d,e}$			
$v' = 0$	0	.07	--
$v' = 1$.22	.24	.31
$v' = 2$	1.00	1.00	1.00
$v' = 3$.26	.13	.47
$Q_{v'}/Q_{\text{max}} (E_{\text{re}} = 2 \text{ eV})^{d,e,f}$			
$v' = 0$	0	.06	--
$v' = 1$.23	.26	--
$v' = 2$	1.00	1.00	--
$v' = 3$.54	.47	--

^a Classical results of J. C. Polanyi and J. L. Schreiber, Faraday Discuss. Chem. Soc. **62**, 267 (1977); T and f selected from a 300-K Boltzmann distribution

^b This work. Quantum calculations for H₂ ($v = 0, j = 0$), HF (Σ^+, Σ^+); thus $\log A$ should be underestimated.

^c K. H. Homann *et al.* Ber. Bunsenges. Phys. Chem. **74**, 585 (1970).

^d J. C. Polanyi and K. B. Woodall, J. Chem. Phys. **57**, 1574 (1972)

^e Classical cross sections of ref. 28

^f Quantum cross sections, this work and ref. 12.

C. A Quantum Mechanical Study of the H + O₂ Reaction

We have applied the nonlinear intermediate version of REACTOR to the H + O₂ reaction, using a LEPS surface of Gauss with an angle-dependent Sato parameter [29]. This reaction is of practical interest because it is an important chain propagation step in many combustion systems and difficult to study experimentally. Thus, a detailed theoretical investigation of the kinetics of this system is warranted.

From a theoretical viewpoint, this reaction presents many new features. It is endothermic by about $\frac{1}{2}$ eV and has a metastable intermediate with a 2-eV well. The integration of classical trajectories for this system is complicated by the occurrence of many long-lived complexes which often lead to trajectories that cannot be back-integrated [29]. The quantum calculations are made difficult by the existence of so many open channels.

In Table III we present total cross sections for formation of OH ($v = 0$) from various vibrational states of O₂. The calculations are not fully converged due to core limitations on the CDC 7600 (we were limited to about 70 channels). We are presently using a VAX 11/780 where core size is not a limitation and hope to converge the J_z -conserving calculations for this system.

The dependence of reaction cross section on reagent vibrational energy follows the trends expected for an endoergic system from the work of Polanyi and co-workers. This trend was also noted by Gauss for this system. The classical cal-

TABLE III. Cross sections at 1-eV total energy for the process $H + O_2 (v = 0, j = 0) \rightarrow O + OH$ ($v' = 0; \Sigma_j'$).

v	E_{re} (eV)	$\sigma_{v0}^{(0)}$
0	.903	.16
1	.711	.26
2	.522	.30
3	.338	.77
4	.159	3

culations showed no tendency of O_2 ($v = 0$) to react, yet the quantum results indicate that it should. Gauss essentially found no reaction below $v = 4$. We find the cross sections are small for $v < 4$, but are considerably larger than the classical result. Gauss estimates that his $v = 4$ cross section could be low by as much as a factor of 10, due to the inability of his integrator to follow many complex trajectories. We are presently trying to estimate the error in our result due to the limited basis set employed.

We find that nonreactive collisions tend to produce vibrationally excited O_2 , which in turn can react rapidly with hydrogen. A detailed study of this system would probably produce many new results and add considerably to our knowledge of elementary combustion processes.

Acknowledgments

The author wishes to acknowledge his collaborator over the past few years on the $F + H_2$ calculations, Professor Robert Wyatt of the University of Texas at Austin. He also wishes to thank the National Resource for Computation in Chemistry for granting in-house user rates for the $H + O_2$ calculations.

This work was supported in part by Battelle Corporate Technical Development, the U. S. Army Research Office, and by the Air Force Office of Scientific Research, United States Air Force (AFSC), under contract No. F49620-79-C-0050. The United States Government is authorized to reproduce and distribute reprints for governmental purposes notwithstanding any copyright notation hereon.

Bibliography

- [1] D. A. Micha, *Ark. Fys.* **30**, 411 (1965).
- [2] K. T. Tang and M. Karplus, *Phys. Rev. A* **4**, 1844 (1971).
- [3] P. McGuire and D. A. Micha, *Mol. Phys.* **25**, 1335 (1973).
- [4] G. Wolken, Jr. and M. Karplus, *J. Chem. Phys.* **60**, 351 (1974).
- [5] G. C. Schatz and A. Kupperman, *J. Chem. Phys.* **62**, 2502 (1975); **65**, 4642 (1976); **65**, 4665 (1976).
- [6] A. B. Elkowitz and R. E. Wyatt, *J. Chem. Phys.* **62**, 2504 (1975); **63**, 702 (1975).
- [7] R. B. Walker, E. B. Stechel, and J. C. Light, *J. Chem. Phys.* **69**, 2922 (1978).
- [8] D. G. Truhlar and C. G. Horowitz, *J. Chem. Phys.* **68**, 2466 (1978).
- [9] P. Siegbahn and B. Liu, *J. Chem. Phys.* **68**, 2457 (1978).
- [10] M. J. Redmon and R. E. Wyatt, *Int. J. Quantum Chem. Symp.* **9**, 403 (1975).

- [11] M. J. Redmon and R. E. Wyatt, *Int. J. Quantum Chem. Symp.* **11**, 343 (1977).
- [12] M. J. Redmon and R. E. Wyatt, *Chem. Phys. Lett.* **63**, 209 (1979).
- [13] A. B. Elkowitz and R. E. Wyatt, *Mol. Phys.* **31**, 189 (1976).
- [14] J. M. Bowman and Ki Tung Lee, *J. Chem. Phys.* **68**, 3940 (1978).
- [15] R. E. Wyatt, *J. Chem. Phys.* **56**, 390 (1972).
- [16] R. A. Marcus, *J. Chem. Phys.* **49**, 2610 (1968).
- [17] J. C. Light and R. B. Walker, *J. Chem. Phys.* **65**, 4272 (1976).
- [18] R. E. Wyatt, in *State-to-State Chemistry*, P. R. Brooks and E. F. Hayes, Eds., *ACS Symp. Ser. No. 56* (ACS, Washington, DC, 1977).
- [19] J. C. Light, in *Methods in Computational Physics*, B. Alder, S. Fernbach, and M. Rotenberg, Eds. (Academic, New York, 1971), Vol. 10.
- [20] A. B. Elkowitz, *Mol. Phys.* (to be published).
- [21] A. C. Yates and W. A. Lester, *Chem. Phys. Lett.* **24**, 305 (1972).
- [22] R. F. Heidner III and J. V. V. Kasper, *Chem. Phys. Lett.* **15**, 179 (1972).
- [23] E. B. Gordon, B. I. Ivanov, A. P. Perminov, V. E. Balalaev, A. N. Ponomarev, and V. V. Filatov, *Chem. Phys. Lett.* **58**, 425 (1978).
- [24] G. C. Schatz, J. M. Bowman, and A. Kupperman, *J. Chem. Phys.* **58**, 4023 (1973).
- [25] S. L. Latham, J. F. McNutt, R. E. Wyatt, and M. J. Redmon, *J. Chem. Phys.* **69**, 3746 (1978).
- [26] J. N. L. Conner, W. Jakubetz, and J. Manz, *Mol. Phys.* **35**, 1301 (1978).
- [27] See ref. 4.
- [28] A. Komornicki, S. Morokuma, and T. F. George, *J. Chem. Phys.* **67**, 5012 (1977).
- [29] A. Gauss, Jr., *J. Chem. Phys.* **68**, 1689 (1978).

Received March 30, 1979

QUANTUM RESONANCE STRUCTURE IN THE THREE-DIMENSIONAL F + H₂ REACTION *

Michael J. REDMON

*Chemical Physics Group, Battelle, Columbus Laboratories,
Columbus, Ohio 43201, USA*

and

Robert E. WYATT

*Department of Chemistry, University of Texas,
Austin, Texas 78712, USA*

Received 22 March 1979

Evidence for a quantum resonance in the three-dimensional F + H₂ ($v = 0, j = 0$) → FH($v' = 2$, all j') + H reaction is presented. Relative to the collinear reaction, this resonance is much broader and is shifted by about 0.1 eV to higher energies. This resonance has not been predicted in previous quasiclassical trajectory computations, or in approximate quantum calculations.

1. Introduction

The F + H₂ chemical reaction has been the subject of extensive experimental [1] and theoretical study [2], at least in part because of its dominant role in powerful F₂/H₂ chemical lasers. On the theoretical side, the reaction has been attacked from the viewpoints of classical, semiclassical, and quantum dynamics. Prior quantum studies consist of exact collinear computations on several different potential surfaces [2] and approximate (Born [3] and distorted-wave [4]) three-dimensional treatments. In addition, we have reported preliminary quantum results on the 3D reaction which are based upon numerical integration of large systems of quantum close-coupled equations [5].

In this study, the energy dependence of reaction probabilities and cross sections for the reactions F + H₂ ($v = 0, j = 0$) → FH(v' , all j') + H are reported over the total energy range $0.32 \leq E_{\text{tot}} \leq 0.50$ eV ($E_{\text{trans}} = E_{\text{tot}} - 0.27$ eV). Evidence is presented for a broad

resonance in the $v = 0 \rightarrow v' = 2$ cross section, with a peak in the cross section just below 0.4 eV. Resonance structure of this type has not been predicted in either quasiclassical trajectory calculations or in approximate quantal calculations [3,4]. However, the magnitude of the cross section and the energy region where the resonance occurs suggest that further crossed molecular beam experiments would be extremely interesting in testing these predictions. A brief survey of the scattering methodology is presented in section 2. New results on reaction probability surfaces and cross sections are then presented in sections 3 and 4, respectively.

2. Scattering theory

The scattering wavefunction at total angular momentum J is expanded in products of adiabatic hindered asymmetric top wavefunctions [2,6], $\Omega_{jl}^{JM}(\theta\phi\chi\gamma; s)$, times local Morse oscillator functions, $H_v(\rho; s)$

$$\Psi_{v_0 j_0 l_0}(\theta\phi\chi s \rho \gamma) = \mathcal{G}^{-1/2} \sum_{v' j' l'} T_{v_0 j_0 l_0 v' j' l'}^J(s)$$

$$\times \Omega_{j' l'}^{J M}(\theta\phi\chi\gamma; s) H_{v'}(\rho; s), \quad (1)$$

* This research was supported in part by the National Science Foundation, the Robert A. Welch Foundation, and Battelle Memorial Institute.

where $\{\theta, \phi, \chi\}$ are Euler angles used to orient the top, and $\{s, \rho, \gamma\}$ are natural translation-vibration-bending coordinates [2,6]. Also \mathcal{G} is a metric coefficient which is used to scale the wavefunction in order to simplify the structure of the close-coupling equations for the translational wavefunctions, $T_{v_0 j_0 l_0 v j l}^J(s)$. In the computational results reported here, 60 rovibrational channels were employed, with the distribution 12/12/12/8/6/2/2/2/2/2, where the total number of even j plus odd j rotational functions in each of the ten lowest vibrational levels is indicated. At the highest energy studied here, six of these vibrational levels are asymptotically closed in products.

For all computations with $J > 0$, the J_z conserving approximation [7] was employed to restrict the number of orbital angular momentum (l) values in eq. (1) to a single "dominant" term for each value of j and J . The same algorithm for selecting $l(j, J)$ was successfully employed in earlier $H + H_2$ reactive scattering calculations [7]. In that case, cross sections within about 7% of the accurate values were generated with the J_z conserving approximation.

The close-coupled equations for the translational wavefunctions were numerically integrated with the boundary value R -matrix propagation method [8]. Elements of the S -matrix were then directly generated from the arrangement channel R -matrices. Reaction probabilities for $F + H_2(v=0, j=0) \rightarrow FH(v', \text{all } j')$ + H reactive collisions are defined by

$$P_{0v'}^J(E) = \sum_{j'=0}^{(\text{open})} \sum_{l'=l(j-j')}^{J+j'} |S_{00j \rightarrow v'j'l'}^J(E)|^2 \quad (2)$$

and were computed for total energies in the range 0.32 eV $\leq E \leq$ 0.50 eV, and for $0 \leq J \leq 26$ (in ranges of J for which $P_{0v'}^J$ was slowly varying, computations were performed at every other J value).

In these scattering calculations, we have used a variety of potential surfaces, all based in part on surface 5 (M5) of Muckerman [9]*. The different surfaces share the collinear surface of M5, but they differ in the range and degree of angular anisotropy of the bending potentials. The bending potentials all have the same functional form, $V_{\text{bend}}(\gamma, s) = \frac{1}{2} V_0(s) (1 - \cos 2\gamma)$, but differ in the position along the reaction coordinate

(determined by s) of maximum hindrance to rotation. The surface used for the results reported here is similar to the M5 surface for small deviations from collinearity in the transition state region. On the approach or departure from the transition state, the bending potential is similar to the one employed in recent trajectory studies [12].

3. Reaction probability surfaces

In fig. 1a we present sections through the reaction probability surface for producing $FH(v'=2)$. For each value of the total angular momentum J , the variation of probability with energy is qualitatively similar to that obtained from a collinear calculation on the M5 surface [10,13]**. As E increases, there is a rapid increase and then decrease in the probability, followed by a fairly constant value at higher energies. One striking effect in fig. 1a is the J -dependence of the curves at different constant energy sections. At the position of the $J=0$ resonance maximum and below, the curves decrease monotonically with J , whereas at higher energies the curves are initially fairly constant with J , but re-tune onto higher resonance values at a value of J that increases with energy. The locus of these maxima in the $E-J$ plane follows the "resonance ridge" that begins for $J=0$ at the maximum in the probability curve, and progressively moves to higher J with increasing energy. The maximum probability on the ridge gradually decreases as E and J increase. The P_{02}^J curves for the 3D reaction are broader than the collinear result [10,13,14] due to the participation of many (twelve in these calculations) rotor states in the resonance mechanism, and to changes in the shape of the vibrational-rotation adiabatic energy correlation curves with increasing values of J .

In our earlier collinear calculations on this reaction [13], we have identified the resonance mechanism in the $0 \rightarrow 2$ process. It arises from internal excitation and then de-excitation of the FHH intermediate in the beginning of the $FH + H$ exit valley into primarily the $v=3$ and 4 states (which may be approximately identified as asymmetric stretch states) of the vibrational energy correlation curves. Qualitative similarity between the collinear and 3D results (at each J) suggests

* See ref. [10] for M5 parameters. For early classical results on predecessors of the M5 surface see ref. [11].

** For extensive bibliographies see refs. [13,14].

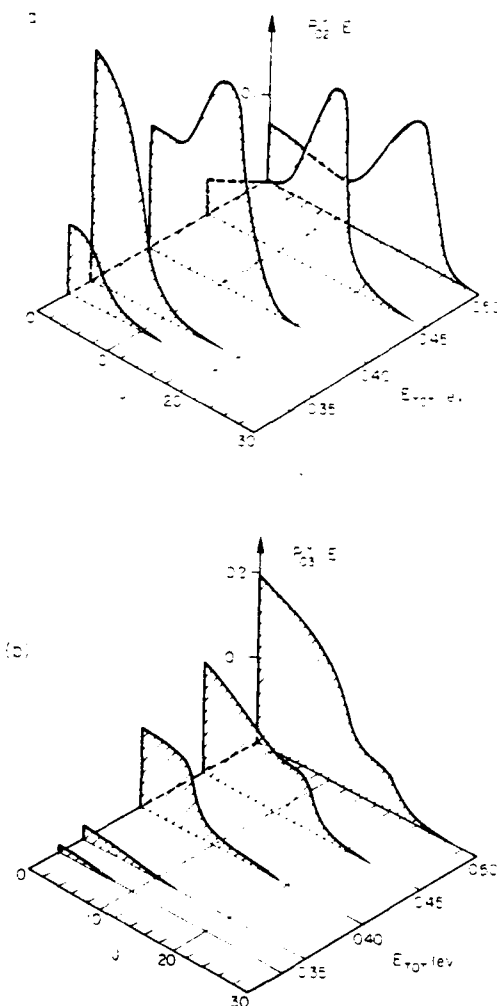


Fig. 1. Reaction probability surface for $F + H_2(v=0, j=0) \rightarrow H + HF(v'=2, j'=all)$. (b) Reaction probability surface for $F + H_2(v=0, j=0) \rightarrow H + HF(v'=3, j'=all)$. Translational energy = total energy - 0.27 eV.

that the same mechanism is operating in the 3D collisions.

It is known from other work that variations in the collinear surface in the saddle-point and downhill regions [13] and variations of the overall exothermicity and product vibrational spacing [14] drastically affect computed reaction probabilities, by shifting or elimi-

nating resonances or by creating new ones. The effects we observe by varying the bending potential are not nearly as severe as those resulting from changes in the collinear surface, and mainly serve to alter the magnitudes of the resonance probabilities and the values of J that contribute most to the integral cross sections.

4. Reaction cross sections

In fig. 2 we present the energy dependence of cross sections for reaction of ground state H_2 to form HF. Also shown is a classical total cross section on a slightly different potential surface [12]. There is good agreement below the resonance maximum, but above that energy the quantal and classical results differ substantially. The classical result continues to rise, while the quantum total cross section levels off, due to the resonance in the $0 \rightarrow 2$ cross section. In earlier collinear studies [10], the classical total reaction probability was also found to exceed (by about a factor of two) the quantum result, between the classical threshold at 0.29 eV and the energy region where the $0 \rightarrow 3$ reaction probability begins to grow (0.4 eV). However, the $0 \rightarrow 2$ resonance width in fig. 2 is much broader than in the collinear calculations (where the width is about

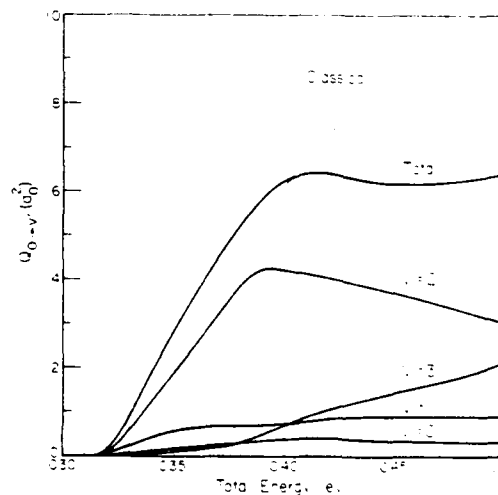


Fig. 2. Cross sections for forming vibrationally excited HF, for all open HF vibrational manifolds. The classical result is from ref. [12].

0.01 eV). The broadening mechanism in the 3D case arises both from the participation of many rotor states, and the detailed angular momentum dependence of the "resonance ridge" in fig. 1a. In our studies on other potential surfaces with different bonding potentials, the $0 \rightarrow 2$ cross section above 0.40 eV never showed smooth growth that could be extrapolated from the lower energy region, as in the classical 3D calculations [9-12]. The quantum $0 \rightarrow 2$ cross sections for different bending potentials ranged from about 3.0 to 5.5 a_0^2 at 0.50 eV and thus showed either a definite leveling-off or a slight decline, relative to the values near 0.40 eV. The peak $0 \rightarrow 2$ cross section near 0.40 eV ranged from 4 to 6 a_0^2 , except for one model bending potential which maximized the angular anisotropy near the beginning of the exit valley, where the peak cross section was 11 a_0^2 .

Further analysis of these cross sections indicates that 67% of the available energy appears as product vibration at the $0 \rightarrow 2$ resonance maximum (0.4 eV), in agreement with both experiment [1,15] and trajectory calculations [9-11] in the low energy region.

5. Conclusions

These quantum scattering calculations of reaction probabilities and cross sections for the three-dimensional low energy electronically adiabatic $F + H_2$ reaction have demonstrated resonance structure for the $v = 0 \rightarrow v' = 2$ process which is much broader and at 0.1 eV higher energy than the collinear resonance, and which is not predicted by quasiclassical trajectory calculations. Contribution of this resonance to the shape of the total cross section has not been shown experimentally. The extension of previous crossed molecular

beam studies (on the $F + D_2$ reaction [16]) in the resonance energy region between $E_{\text{trans}} = 0.05$ eV to $E = 0.23$ eV could test these predictions. Resonance structure in this reaction should be more amenable to experimental study than the vibrational resonance predicted for the $H + H_2$ reaction [17].

References

- [1] J.C. Polanyi and J.L. Schreiber, *Faraday Discussions Chem. Soc.* 62 (1977) 267.
- [2] R.E. Wyatt, in: *State-to-state chemistry*, eds. P.R. Brooks and E.F. Hayes, ACS Symposium Series No. 56, p. 185.
- [3] A. Kafri, Y. Shimoni, R.D. Levine and S. Alexander, *Chem. Phys.* 13 (1976) 323.
- [4] Y. Shan, B.H. Choi, R.T. Poe and K.T. Tang, *Chem. Phys. Letters* 57 (1978) 379.
- [5] M.J. Redmon and R.E. Wyatt, *Intern. J. Quantum Chem.* 11S (1977) 343; 9S (1975) 403.
- [6] A.B. Elkowitz and R.E. Wyatt, *J. Chem. Phys.* 63 (1975) 702.
- [7] A.B. Elkowitz and R.E. Wyatt, *Mol. Phys.* 31 (1976) 189.
- [8] J.C. Light and R.B. Walker, *J. Chem. Phys.* 65 (1976) 4272.
- [9] J.T. Muckerman, private communication.
- [10] G.C. Schatz, J.M. Bowman and A. Kuppermann, *J. Chem. Phys.* 63 (1975) 674.
- [11] J.T. Muckerman, *J. Chem. Phys.* 56 (1972) 2997.
- [12] A. Komornicki, K. Morokuma and T.F. George, *J. Chem. Phys.* 67 (1977) 5012.
- [13] S.L. Latham, J.F. McNutt, R.E. Wyatt and M.J. Redmon, *J. Chem. Phys.* 69 (1978) 3746.
- [14] J.N.L. Connor, W. Jakubetz and J. Manz, *Mol. Phys.* 35 (1978) 1301.
- [15] M.J. Berry, *J. Chem. Phys.* 59 (1973) 6229.
- [16] T.P. Schafer, P.E. Siska, J.M. Parson, F.P. Tully, Y.C. Wong and Y.T. Lee, *J. Chem. Phys.* 53 (1970) 3385.
- [17] G.C. Schatz and A. Kuppermann, *Phys. Rev. Letters* 35 (1975) 1267.

APPENDIX B

An Analytical Fit to an Accurate ab initio (1A_1)
Potential Surface of H_2O

Michael J. Redmon⁺ and George C. Schatz^{*}

Chemical Physics Group
Battelle's Columbus Laboratories, Columbus, Ohio 43201

(Received 7/18/80)

⁺ Present address: Chemical Dynamics Corporation,
1550 W. Henderson Road, Columbus, Ohio 43220

^{*} Alfred P. Sloan Research Fellow. Permanent address: Department of
Chemistry, Northwestern University, Evanston, IL 60201

ABSTRACT

The accurate ab initio MBPT quartic force field of Bartlett, Shavitt and Purvis has been fit to an analytical function using a method developed by Sorbie and Murrell (SM). An analysis of this surface indicates that it describes most properties of the H_2O molecule very accurately, including an exact fit to the MBPT force field, and very close to the correct energy difference between linear and equilibrium H_2O . The surface also reproduces the correct diatomic potentials in all dissociative regions, but some aspects of it in the "near asymptotic" $\text{O}(^1\text{D}) + \text{H}_2$ region are not quantitatively described. For example, the potential seems to be too attractive at long range for $\text{O} + \text{H}_2$ encounters, although it does have the correct minimum energy path geometry and correctly exhibits no barrier to O atom insertion. Comparisons of this surface with one previously developed by SM indicates generally good agreement between the two, especially after some of the SM parameters were corrected, using a numerical differentiation algorithm to evaluate them. A surface developed by Schinke and Lester (SL) is more realistic than ours in the $\text{O}(^1\text{D}) + \text{H}_2$ regions, but less quantitative in its description of the H_2O molecule. Overall, the present fit appears to be both realistic and quantitative for energy displacements up to 3-4 eV from H_2O equilibrium, and should therefore be useful for spectroscopic and collision dynamics studies involving H_2O .

I. INTRODUCTION

In a recent paper, Bartlett, Shavitt and Purvis¹ presented the results of an accurate ab initio calculation of the ground state quartic force field of H_2O . This calculation used a many body perturbation theory (MBPT) method including up to quadruple excitations and a large basis set (39-STO) wave function to evaluate all of the 31 quadratic, cubic and quartic force constants in the generalized valence force field. Not all of these force constants have been determined experimentally, but where accurate values are known, the MBPT values are in good agreement with them. Indeed the MBPT force field may be better than experiment, but in order to use this force field for spectroscopic or scattering calculations, it must be extended to map out regions of nuclear configuration space away from the H_2O equilibrium geometry.

In this paper, we use the method of Sorbie and Murrell² to fit the MBPT surface to an analytical function. This function identically reproduces the MBPT H_2O quartic force field, and correctly describes the $O(^1D) + H_2$ and $OH(^2\Pi) + H$ dissociative channels at infinite separation. In between these limits, a smooth interpolation is provided. We also describe a simple numerical algorithm for generating the parameters used in the Sorbie-Murrell (SM) fitting method, and we correct their fit to the spectroscopically derived force field of Hoy, Mills and Strey (HMS).³

Besides the SM surface, other complete surfaces for $H_2O(^1A_1)$ have been generated by Tully^{4a}, by Whitlock, Muckerman and Fischer^{4b} (WMF) and by Schinke and Lester⁵ (SL). Tully and WMF used the valence bond diatomics in molecules (DIM) method to construct their potential surfaces. The two

surfaces are not identical because of differences in integral evaluation, but neither surface describes the H_2O molecule with anything close to spectroscopic accuracy. SL used a Sorbie-Murrell-like function to fit the ab initio surface of Howard, McLean and Lester⁶ (HML), but unlike SM (see Section II), they obtained the coefficients in their fit by a least squares analysis. A fairly widely scattered set of ab initio points was used for the fit, with the result that their surface describes the $\text{O} + \text{H}_2$ and $\text{OH} + \text{H}$ regions more accurately than SM, but their H_2O force field is much less accurate (though still better than the DIM ones).

Because calculated rather than experimental dissociation energies were used for all or parts of the potential surfaces of Tully, WMF and SL, certain energetic aspects of these surfaces are in error. For example, the energy associated with dissociation of H_2O to $\text{O}(^3\text{P}) + 2\text{H}(^2\text{S})$ is 10.08 eV experimentally, but only 9.37 eV on Tully's surface, 9.16 eV on WMF's and 8.95 eV on SL. Likewise, the $\text{OH}(^2\Pi)$ dissociation energy is 4.63 eV experimentally, but 4.54 eV on Tully, 4.58 eV on WMF and 4.04 eV on SL. Both Tully and WMF do correctly describe the energy associated with $\text{O}(^1\text{D}) + \text{H}_2 \rightarrow \text{O}(^3\text{P}) + 2\text{H}(^2\text{S})$ (2.79 eV) but SL's value is 1.87 eV. In this paper, we use the experimental dissociation energies so as to insure the proper energetics in all arrangement channels.

Because the ab initio MBPT points are clustered close to the H_2O equilibrium, the present fit describes the H_2O molecule properties much more accurately than the $\text{O} + \text{H}_2$ and $\text{OH} + \text{H}$ regions. This is like the SM surface, but in the present case, certain MBPT derived quartic force constants not available to SM have been included in the fitting process. We will examine here the influence of these additional constants on the long range nature of

the surface. In addition, a general comparison of the H_2O molecule properties of the SM, MBPT and SL surfaces will be made.

II. EVALUATION OF FITTED SURFACE

The functional form of the fitting surface for H_2O is²

$$V_{H_2O}(R_1, R_2, R_3) = V_{OH}(R_1) + V_{OH}(R_2) + V_{HH}(R_3) + V_3(R_1, R_2, R_3) \quad (1)$$

where R_1 is one of the OH distances, R_2 the other and R_3 the HH distance.

V_{OH} and V_{HH} are the OH and HH ground state potential curves, and are taken from Ref. 7, while V_3 accounts for all 3-body terms in V_{H_2O} . Note that for $R_3 < 1.6707\text{\AA}$, H_2O dissociates into $O(^1D) + H_2(^1\Sigma_g^+)$ but for $R_3 > 1.6707\text{\AA}$, the ground state dissociation channel is $O(^3P) + H_2(^3\Sigma_u^+)$. V_{HH} incorporates this behavior by switching from the $^1\Sigma_g^+$ to the $^3\Sigma_u^+$ potential curves at that R_3 value. This leads to a cusp in both V_3 and V_{H_2O} asymptotically and necessitates the use of a discontinuous form for V_3 in order to make V_{H_2O} continuous near the H_2O equilibrium geometry.

The functional form of V_3 is given by²:

$$V_3 = A(1 - \tanh \gamma_1 S_1 / 2)(1 - \tanh \gamma_2 S_2 / 2)(1 - \tanh \gamma_3 S_3 / 2)P(S_1, S_2, S_3) \quad (2)$$

where $S_i = R_i - R_i^0$ ($i = 1, 2, 3$) and R_i^0 is the i th H_2O equilibrium internuclear distance. A , γ_1 , γ_2 and γ_3 are parameters and P is a polynomial in S_1 , S_2 and S_3 . This polynomial will have a different representation inside the above mentioned cusp than outside, and we denote these two polynomials as P^{in} and P^{out} , respectively.

As discussed in Ref. 2, the coefficients in P^{in} are conveniently evaluated when an analytical representation of the H_2O force field is known

(near equilibrium) by relating the derivatives of this force field (evaluated at equilibrium) to those of P^{in} . Although explicit analytical expressions for these polynomial coefficients were given in Ref. 2, their evaluation is tedious for all but the simplest types of force fields. A much easier evaluation of these coefficients can be accomplished by numerical differentiation of

$$P = \frac{V_{H_2O} - V_{OH}(R_1) - V_{OH}(R_2) - V_{HH}(R_3)}{(1 - \tanh \gamma_1 S_1/2)(1 - \tanh \gamma_2 S_2/2)(1 - \tanh \gamma_3 S_3/2)} \quad (3)$$

When derivatives of (3) are evaluated at the equilibrium position, the resulting values are simply proportional to the polynomial coefficients in P^{in} . P^{out} can be similarly evaluated by requiring that the derivatives of the potential at $S_3 = S_3$ (cusp) (with $S_1 = S_2 = 0$) be continuous. By using the previously obtained P^{in} to evaluate V_3 for S_3 slightly inside the cusp in Eq. (3) and V_{HH} for S_3 slightly outside, numerical differentiation of Eq. (3) directly yields the coefficients of the polynomial outside, as expanded about the cusp position. P^{out} can then be reexpanded about the equilibrium position, if desired, by evaluating its numerical derivatives at that position. Note that the same numerical differentiation program is used three times in this evaluation, once in determining P^{in} and twice for P^{out} . By programming this algorithm in double precision (64 bit words) and using a judicious choice of finite difference increment (1×10^{-5} bohr for the first and second derivatives, 5×10^{-4} for 3rd and 4th), even the simplest differentiation formulas⁸ enable the determination of 4th derivatives to 3-4 significant figures (with much higher significance for the lower order derivatives). Moreover, this algorithm is independent of the functional form used to represent the ab initio potential near the equilibrium position.

The matching procedure at $S_3 = S_3$ (cusp) does not guarantee continuity of the potential across the cusp for $S_1 \neq S_2$. This deficiency was corrected by switching between polynomials at the cusp using the expression

$$P = A^{\text{in}} p^{\text{in}} \sin^2 \omega + A^{\text{out}} p^{\text{out}} \cos^2 \omega \quad (4)$$

where

$$\omega = \frac{\pi}{4} [1 - \tanh \gamma_s [S_2 - S_2(\text{cusp})]] \quad (5)$$

The value of parameter γ_s determines the range of mixing of the two polynomials on either side of the cusp.

The resulting polynomial coefficients using the SDQ-MBPT(4) potential force field of Ref. 1 are listed in Table I (labelled MBPT). Also given are the other parameters in V_3 mentioned previously (γ_1 , γ_2 and γ_3 are taken from Ref. 2), and the analogous coefficients and parameters in a fit (using our method) to the spectroscopically derived force field of Hoy, Mills and Strey³ (labelled HMS). This latter force field was also fit by Sorbie and Murrell, and in Table I, we list their parameters (labelled SM). Since the same method of fitting was used in each application, the SM and HMS parameters should be identical. Table I indicates that most of the parameters agree to 3-4 significant figures. Two sets of coefficients are very different however. The SM coefficient multiplying S_1 is of similar magnitude but opposite in sign to ours for both p^{in} and p^{out} , while the coefficient multiplying $S_1^3 S_2$ differs by a factor of about 3. The origin of these differences is not known, but in the next section, we shall see that they cause SM's potential to have slightly different quartic force field parameters than HMS, even though SM is supposed to be a fit to HMS.

Comparison of the HMS and MBPT parameters in Table I indicates good agreement for the lower order coefficients, but only qualitative agreement

for the higher order ones. The influence of these higher order coefficients on features of the potential surface will be considered in the next two sections.

III. PROPERTIES OF FITTED SURFACES

A. H_2O Force Field Parameters

The first requirement of the MBPT fitted surface is that it should be able to reproduce the MBPT quartic force field exactly. A convenient representation of this surface involves an expansion in scaled normal mode coordinates.⁹ If Q_s is the normal coordinate for mode s , then the dimensionless coordinate q_s is defined by

$$q_s = 2\pi \left(\frac{c\omega_s}{h} \right)^{1/2} Q_s \quad (6)$$

and the potential V_{H_2O} is expanded as

$$\begin{aligned} V_{H_2O}/hc = & \frac{1}{2}(\omega_1 q_1^2 + \omega_2 q_2^2 + \omega_3 q_3^2) \\ & + k_{111} q_1^3 + k_{122} q_1 q_2^2 + k_{133} q_1 q_3^2 + k_{211} q_2 q_1^2 \\ & + k_{222} q_2^3 + k_{233} q_2 q_3^2 + k_{1111} q_1^4 + k_{1122} q_1^2 q_2^2 \\ & + k_{1133} q_1^2 q_3^2 + k_{2222} q_2^4 + k_{2233} q_2^2 q_3^2 + k_{3333} q_3^4 \end{aligned} \quad (7)$$

Values of the coefficients in this expansion for the fitted MBPT surface are given in Table II. The MBPT fitted surface is labelled MBPT-F, while the quartic representation used to generate the fit is labelled MBPT-Q. Likewise, our fit to the HMS-Q surface is labelled HMS-F, while Sorbie and Murrell's fit is labelled SM-F. Also included in this Table are the analogous coefficients obtained from SL's surface.⁵

We note first in Table II that all the quartic parameters obtained from our fits to HMS-Q and MBPT-Q agree with those of the surface being fit to within 0.3 cm^{-1} or better. The agreement should, of course, be exact, and for most parameters, it is. A few parameters are slightly different, probably because of round-off errors in the 4th derivative evaluation used to generate the fitted surfaces.

SM-F's parameters differ from HMS-Q by as much as 7.7 cm^{-1} , probably because of the differences in coefficients noted in Table I. SL's parameters in Table II are very different from either MBPT-Q or HMS-Q (over 330 cm^{-1} for ω_1) although most of the parameters have at least qualitatively reasonable values. The large differences between the SL results and those of the other surfaces are at least partially due to the lower accuracy of the ab initio results being fit,⁶ and partially to the least squares procedure used by SL to fit HML's points (SL's fitting method places less emphasis on the H_2O equilibrium geometry). It should be noted that the equilibrium H_2O geometry of these surfaces shows variations similar to those between the force constants. This is indicated in Table III, where the OH equilibrium distances and H_2O angle are listed. Also included in the table are the values of $V_{\text{H}_2\text{O}}$ at equilibrium for a number of H_2O potential surfaces. As noted in the introduction, the values for the SL, WMF and Tully surfaces differ by roughly 1 eV from the experimental value.

B. Other Properties of MBPT-F and Other Surfaces

In Fig. 1 is plotted $V_{\text{H}_2\text{O}}$ as a function of the H_2O bending angle θ (with $S_1 = S_2 = 0$) for the MBPT-Q, MBPT-F and SL surfaces. The corresponding curves for HMS-Q and HMS-F are quite similar to MBPT-Q and MBPT-F,

respectively, in the figure. Notice how the MBPT-F curve is considerably more repulsive than MBPT-Q for small ϕ and less for large ϕ . The SL curve is qualitatively similar to MBPT-F for large ϕ but not for small.

Of particular interest in the analysis of the bending potential is the characterization of linear H_2O . None of the quartic force fields are even qualitatively correct for that geometry since the correct potential has a saddle point there while the quartic representations have a nonzero value of $\partial V_{\text{H}_2\text{O}}/\partial \phi$ at $\phi = \pi$. All of the fitted surfaces do have saddle points, and the properties of those are summarized in Table IV. Of particular importance in this table is the energy difference ΔV between the saddle point energy and the water equilibrium energy. Experimental estimates of this barrier¹⁰ indicate a value 1.37 eV, which is in best agreement with the MBPT-F value of 1.296 eV. The HMS-F value (1.168 eV), which is very close to SM-F (1.175 eV), is too low while SL's value (1.708 eV) is much too high. It is also interesting to note that although the HMS-F and MBPT-F R_1 values in Table IV are only slightly smaller ($<0.01\text{\AA}$) than at equilibrium, SL's value is 0.04\AA smaller. SL's saddle point frequencies are also appreciably different ($300\text{--}300\text{ cm}^{-1}$) from MBPT-F or HMS-F.

In Figs. 2 and 3 are plotted contour diagrams of the MBPT-F surface as a function of the two OH distances R_1 and R_2 for the equilibrium and linear H_2O configurations. A cut through Fig. 2 corresponding to symmetric bond stretching displacements is given in Fig. 4. Included in this figure is a comparison of the MBPT-Q, MBPT-F and SL surfaces. There is good agreement between HMS-F and MBPT-F for symmetric bond stretch displacements except at very large and small values of R_1 , so we have not plotted the former curve in the figure. Fig. 4 does indicate that the MBPT-Q potential is more repulsive

than MBPT-F at both large and small R_1 . The difference between MBPT-Q and MBPT-F remains smaller than 0.1 eV for displacements over 2 eV away from equilibrium. This contrasts with the behavior in Fig. 1, which indicates 0.1 eV differences only 0.7 eV above equilibrium. Since the analogous comparison for the asymmetric bond stretching potential indicates excellent agreement between MBPT-Q and MBPT-F for several eV displacements, we conclude that the most serious errors in the quartic representation of the H_2O potential arise for bending displacements. These errors can be important even for the low lying vibrational states of H_2O since the vibrational zero point energy (0.59 eV) is comparable to the energy displacement needed to make the differences between MBPT-F and MBPT-Q large.

Comparison of the SL and MBPT-F curves in Fig. 4 indicates reasonable correspondence for large R_1 corresponding to 3-body dissociation. This indicates that at least for coordinate displacements of the type indicated, the fitted MBPT surface agrees with one known to be more accurate asymptotically.

C. Surface Properties in the $O(^1D) + H_2$ Region

In Fig. 5 are plotted contours of the MBPT-F surface corresponding to C_{2v} symmetry collisions of $O(^1D)$ with H_2 . The distance X in the figure is the oxygen atom to center of mass of H_2 distance. Previous ab initio studies have indicated^{6,11} that the minimum energy path for $O(^1D) + H_2 \rightarrow OH + H$ follows this and similar geometries, and the present MBPT-F surface concurs with this. Two cuts through the contours in Fig. 5 are plotted in Figs. 6 and 7. Fig. 6 plots the MBPT-F, HMS-F and SL values of V_{H_2O} versus X for the equilibrium H_2 value of R_3 , while Fig. 7 presents the analogous plot for the equilibrium H_2O value of R_3 . No barriers are evident in the potential curves

for any of the three surfaces. This agrees with the results of Ref. 5, but disagrees with the barrier found by Gangi and Bader¹¹. Since the experimental activation energy for $O(^1D) + H_2$ is apparently zero¹², we presume that the zero barrier result is correct.

Fig. 6 indicates that for R_3 equal to the H_2 equilibrium value, the MBPT-F and HMS-F potentials exhibit strong attractive behavior at much larger X values than SL. Since the minimum energy paths for large X follow the curves in this figure, we conclude that the HMS-F and MBPT-F minimum energy paths have much more attractive profiles for large X than SL. Close to H_2O equilibrium, the minimum energy paths switch to the curves depicted in Fig. 7, where the MBPT-F, HMS-F and SL curves are quite similar. Thus it is only at larger distances where there is much discrepancy between the surfaces, and we find that even in this limit, the MBPT-F and HMS-F are still very close. This suggests that the quartic terms in the force fields (which differ substantially between MBPT-F and HMS-F) do not play an important role at the larger distances considered. In Ref. 5, the differences between SM-F (which is close to HMS-F) and SL were traced to the switching function parameters γ_1 , γ_2 and γ_3 in V_3 . The values used by SM (and by us) are a factor of two larger than those used by SL. This causes V_3 to be cut-off more rapidly in displacements from equilibrium for the MBPT-F and HMS-F potentials than SL. This explains why the different quartic potentials used by MBPT-F and HMS-F have so little influence on the shapes of the curves in Fig. 6. Since SL's curves agreed well with HML's ab initio results in this region, it seems likely that the SL curve is more accurate than MBPT-F and HMS-F in this region. This difference does not have a strong effect on the thermal rate constants, however. At 300 K, SL found that thermal rate constants for their surface were about a factor of 2 lower than SM-F. Since both results were within experimental

uncertainties, no definitive statement concerning the relative accuracies of the two surfaces can be made based on this comparison. The larger value of the SM-F rate constant is consistent with the longer range of the attractive part of that potential surface. This is very likely to be true with the MBPT-F surface as well.

It is also of interest to examine the behavior of the potentials for linear OHH configurations. Here, in agreement with Ref. 5, we find that the SM-F, HMS-F and MBPT-F surfaces exhibit wells while the SL surface has a small barrier followed by a monotonic decrease in energy along the reaction path going to OH + H. The MBPT-F well occurs at $R_1 = 1.054\text{\AA}$, $R_3 = 1.005\text{\AA}$, and has an energy of -5.961 eV relative to $O(^3P) + 2H(^2S)$ (1.329 eV below the $OH(^2\Sigma^-) + H$ arrangement channel energy). The HMS-F well occurs at $R_1 = 1.029\text{\AA}$, $R_3 = 1.016\text{\AA}$, with an energy of -6.076 eV (1.444 eV below OH + H). The SM-F well occurs at $R_1 = 1.02\text{\AA}$, $R_3 = 1.02\text{\AA}$, and is 1.47 eV below OH + H⁵. The SL barrier is at $R_1 = 1.18\text{\AA}$, $R_3 = 0.76\text{\AA}$, and has an energy 1.3 kcal/mole above $O(^1D) + H_2$ (2.23 eV above OH + H). The wells observed for the MBPT-F, HMS-F and SM-F are all well above H_2O equilibrium, but they are probably artifacts, as no ab initio or semi-empirical evidence supports their existence.⁵ The MBPT-F well is only slightly smaller than HMS-F, which indicates that neither the additional quartic terms present in the MBPT-Q potential nor the more accurate MBPT-Q force constants has much influence on this artifact.

IV. CONCLUSION

In this paper, the accurate MBPT quartic force field of Bartlett, Shavitt and Purvis has been fit to an analytical function using a method developed by Sorbie and Murrell. Properties of this surface have been analyzed and compared with those of previously determined surfaces (including

a reparametrized SM fit to the HMS force field). Our analysis indicates that this fitted MBPT surface describes the properties of the H_2O molecule extremely well. In addition to reproducing the MBPT quartic parameters at the equilibrium geometry, this surface reproduces the known energy associated with straightening the H_2O molecule better than any other global surface. Far away from equilibrium however, this surface is much less accurate. For the $\text{O}(\text{:D}) + \text{H}_2$ arrangement channel, the surface shows a much longer range attractive potential than has been observed in ab initio calculations, although the error in thermal rate constants introduced by this feature is apparently inside experimental uncertainties. In addition, the $\text{O} + \text{H}_2$ linear geometry exhibits a spurious minimum. These errors all arise for geometries where the 3-body part of the potential has largely been damped out, so that the more accurate quartic force field used to represent H_2O in this surface has no corrective influence. Evidently to improve upon the surface in these regions it will be necessary to use higher terms than quartic in the H_2O force field, or an improved choice of the damping coefficients γ_1 , γ_2 and γ_3 , or the explicit incorporation of ab initio points far removed from H_2O equilibrium in the fitting algorithm.

Despite the apparent inadequacies of this surface in the $\text{O}(\text{:D}) + \text{H}_2$ regions, it does provide an excellent representation of the H_2O potential close to equilibrium (probably for energies as high as 3-4 eV above the H_2O minimum). As such, this potential should be useful for spectroscopic studies, and as the intramolecular potential in nonreactive collision problems involving H_2O as one partner. Indeed for both such studies, the MBPT-F surface is much to be preferred over its quartic counterpart, for important deviations between the quartic and full surfaces can occur for bending displacements only 0.7 eV above H_2O equilibrium.

The comparisons of the MBPT-F surface with others indicated that it is very similar both qualitatively and quantitatively to HMS-F (the latter being close to but not quite the same as SM-F). Near H_2O equilibrium, the MBPT-F is qualitatively similar to but quantitatively different from the SL surface, with SL the less accurate, while far from equilibrium (in the $O + H_2$ region), it appears that SL is the more accurate surface. Of course, the exact surface characteristics in the far from equilibrium configurations are still not known very quantitatively.

V. ACKNOWLEDGMENT

G. C. Schatz thanks NSF Grant CHE-7820336 for partial support. He also thanks M. J. Redmon for his generous hospitality during his stay at Battelle Labs.

The authors thank R. J. Bartlett, I. Shavitt and G. D. Purvis, III for useful discussions. They also thank J. N. Murrell for helpful correspondence on the Sorbie-Murrell surface, and R. Schinke and W. A. Lester, Jr. for comments on their surface and for providing a preprint of their work prior to publication. This work was supported in part by the Air Force Office of Scientific Research, United States Air Force (AFSC), under Contract No. F49620-79-C-0050, and by the Air Force Rocket Propulsion Laboratory, United States Air Force (AFSC), under Contract No. F04611-79-0024. The United States Government is authorized to reproduce and distribute reprints for governmental purposes notwithstanding any copyright notation hereon.

REFERENCES

1. R. J. Bartlett, I. Shavitt and G. D. Purvis, III, J. Chem. Phys. 71, 281 (1979).
2. K. S. Sorbie and J. N. Murrell, Mol. Phys. 29, 1387 (1975).
3. A. R. Hoy, I. M. Mills and G. Strey, Mol. Phys. 24, 1265 (1972).
4. (a) J. C. Tully, J. Chem. Phys. 58, 1396 (1973).
(b) P. A. Whitlock, J. T. Muckerman and E. R. Fischer, Report, Research Institute for Engineering Sciences and Department of Engineering, Wayne State University, Detroit, Michigan, 1976.
5. R. Schinke and W. A. Lester, J. Chem. Phys. 72, 3754 (1980).
6. R. E. Howard, A. D. McLean and W. A. Lester, J. Chem. Phys. 70, 4893 (1979).
7. K. S. Sorbie and J. N. Murrell, Mol. Phys. 31, 905 (1976).
8. M. Abramowitz and I. A. Stegun, Handbook of Mathematical Functions, National Bureau of Standards, 1964, pp 883-885.
9. H. H. Nielsen, Rev. Mod. Phys. 23, 90 (1951).
10. P. R. Bunker and J. M. R. Stone, J. Molec. Spect. 41, 310 (1972).
11. R. A. Gangi and R. F. W. Bader, J. Chem. Phys. 55, 5369 (1971).
12. Indirect evidence for this has been discussed by R. F. Heidner and D. Husain, Int. J. Chem. Kin. 5, 819 (1973).

TABLE I. POLYNOMIAL COEFFICIENTS IN 3 BODY FITTING TERM

Term	$p^{in}[S_3 < S_2(\text{cusp})]$			$p^{out}[S_3 > S_2(\text{cusp})]$		
	SM	HMS	MBPT	SM	HMS	MBPT
1	1	1	1	1	1	1
$S_1(S_2)$	1.5421	1.5402	1.5207	1.8750	1.8676	1.8559
S_3	4.6539	4.6551	4.6455	-0.3691	-0.3582	-0.35631
$S_1^2(S_2^2)$	1.5720	1.5748	1.2746	3.1767	3.1773	3.0102
S_3^2	-4.4355	-4.4369	-4.8014	-2.4168	-2.4096	-2.6085
$S_1 S_3(S_2 S_3)$	17.9914	17.995	18.049	3.1803	3.1849	3.2314
$S_1 S_2$	-1.9761	-1.9861	-1.7863	1.2577	1.2402	1.3496
$S_1^3(S_2^3)$	6.5279	6.0132	4.3146	7.1737	6.8763	5.9441
S_3^3	-7.5781	-7.5742	-9.3266	-5.2200	-5.2016	-6.1567
$S_1 S_2^2(S_2 S_1^2)$	4.9240	5.0266	10.088	8.1229	8.1405	10.893
$S_1 S_3^2(S_2 S_3^2)$	11.3559	11.391	14.816	6.2908	6.2925	8.1619
$S_1^2 S_3(S_2^2 S_3)$	22.3568	22.279	21.204	-2.2456	-2.2399	-2.7979
$S_1 S_2 S_3$	23.1978	23.089	12.017	-1.7899	-1.8101	-7.8076
$S_1^4(S_2^4)$	0.6787	-0.5793	-3.6377	0.3677	-0.3056	-1.9708
S_3^4	-11.4851	-11.478	-14.031	-6.7255	-6.7552	-8.1599
$S_1^3 S_2(S_2^3 S_1)$	1.5255	0.5220	-2.5556	0.8266	0.3061	-1.3837
$S_1^2 S_2^2$	-5.7924	-5.9434	4.2511	-3.1387	-3.2029	2.3532
$S_1^3 S_3(S_2^3 S_3)$	59.6057	59.011	63.497	9.1025	8.8604	11.376
$S_1^2 S_3^2(S_2^2 S_3^2)$	-22.2496	-22.368	-21.790	-15.1988	-15.311	-15.008
$S_1 S_3^3(S_2 S_3^3)$	20.8998	20.982	23.152	8.0856	8.1767	9.3882
$S_1 S_2 S_3^2$	-18.3900	-18.712	-20.269	-13.1075	-13.316	-14.186
$S_1^2 S_2 S_3(S_1 S_2^2 S_3)$	93.5650	93.800	86.304	15.9060	16.160	12.198
$A^{in}(\text{eV})$	-0.9418	-0.94159	-0.94354			
$A^{out}(\text{eV})$	-1.7381	-1.7346	-1.7344			
$S_3(\text{cusp})(\text{\AA})$	0.1568	0.15677	0.15638			
$\gamma_1, \gamma_2(\text{\AA}^{-1})$	4.5348	4.5348	4.5348			
$\gamma_3(\text{\AA}^{-1})$	2.0	2.0	2.0			
$R_{OH}^o(\text{\AA})$	0.9572	0.9572	0.95680			
$R_{HH}^o(\text{\AA})$	1.5139	1.5139	1.51429			
γ_s	--	--	25.0			

TABLE II. QUADRATIC, CUBIC AND QUARTIC FORCE FIELD
PARAMETERS FOR H₂O SURFACES

	HMS-Q	HMS-F	SM-F	MBPT-Q	MBPT-F	SL
ω_1	3831.5	3831.4	3832.0	3865.0	3864.9	3530.2
ω_2	1648.8	1648.8	1648.6	1687.4	1687.4	1568.2
ω_3	3942.2	3942.1	3942.6	3975.0	3975.0	4039.2
k_{111}	-302.5	-302.5	-304.9	-304.2	-304.2	-270.7
k_{222}	63.6	63.6	63.6	42.9	42.9	10.1
k_{122}	167.4	167.4	168.2	148.6	148.6	235.7
k_{211}	-53.1	-53.1	-53.7	-61.8	-61.8	-49.0
k_{133}	-927.8	-927.8	-935.5	-914.1	-914.1	-840.9
k_{233}	-138.8	-138.8	-139.2	-111.7	-111.6	-36.9
k_{1111}	31.9	31.8	31.8	31.5	31.5	34.6
k_{2222}	2.1	2.1	2.1	-2.6	-2.6	25.2
k_{3333}	35.4	35.4	35.3	32.0	32.0	12.0
k_{1122}	-85.6	-85.4	-86.2	-75.1	-74.8	-65.3
k_{1133}	201.3	201.4	201.3	190.3	190.4	152.5
k_{2233}	-101.1	-100.9	-101.5	-91.7	-91.4	-98.0

TABLE III. EQUILIBRIUM PROPERTIES OF H₂O MOLECULE

Surface	$V_{\text{H}_2\text{O}}^{\text{a}}$ (eV)	R_1^{b} (Å)	$\theta_{\text{H}}^{\text{c}}$ (°)
SM-F, HMS-F, Experiment	-10.0705	0.9572	104.52
MBPT-F	-10.0705	0.9568	104.62
SL	-8.95	0.9867	103.98
WMF	-9.16	0.9778	92.81
Tully	-9.37	0.979	100.3

- (a) Potential at H₂O equilibrium geometry [relative to O(³P) + H(²S) + H(²S)]
 (b) OH equilibrium position
 (c) H₂O angle

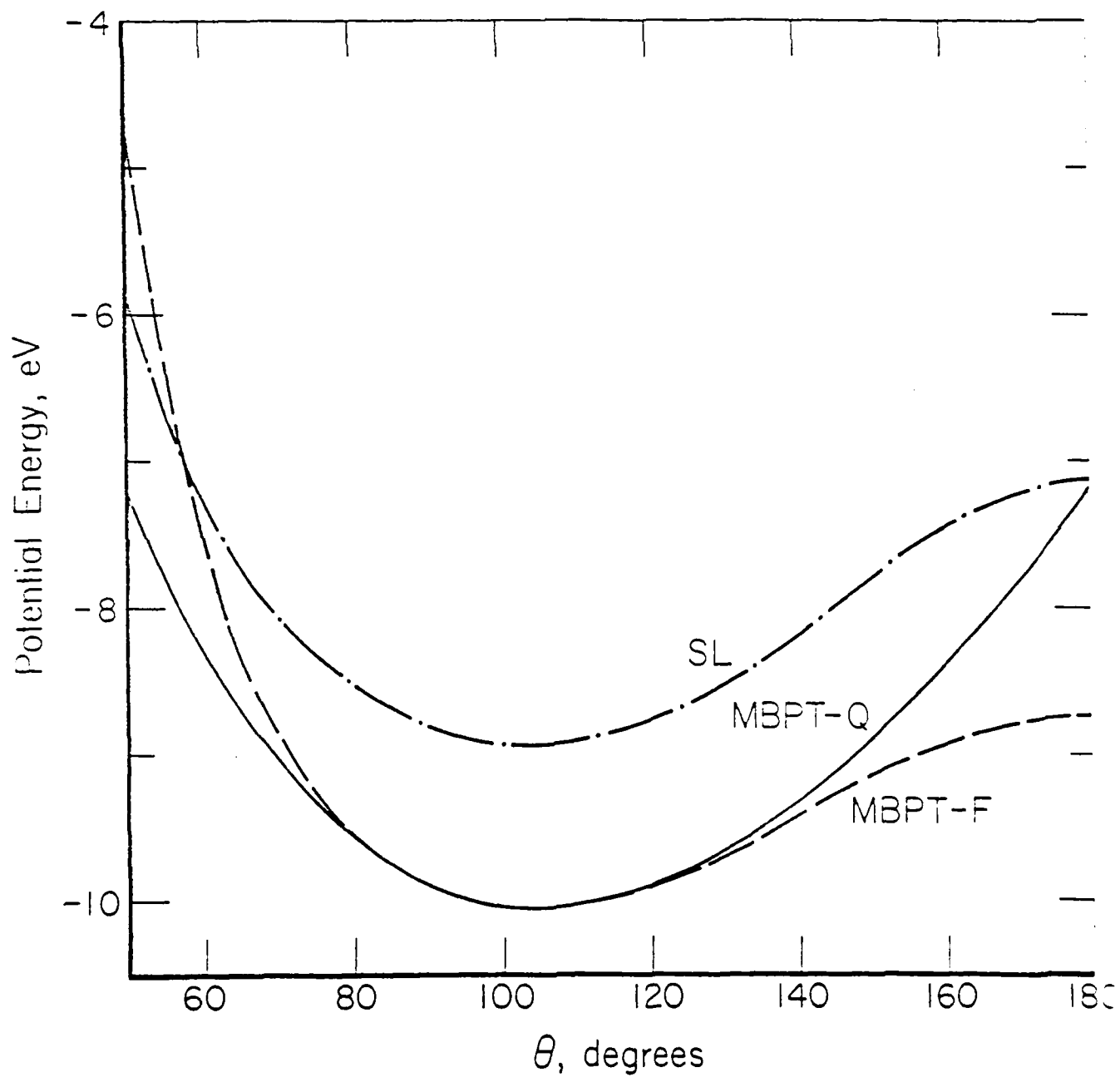
TABLE IV. PROPERTIES OF LINEAR HOH SADDLE POINT

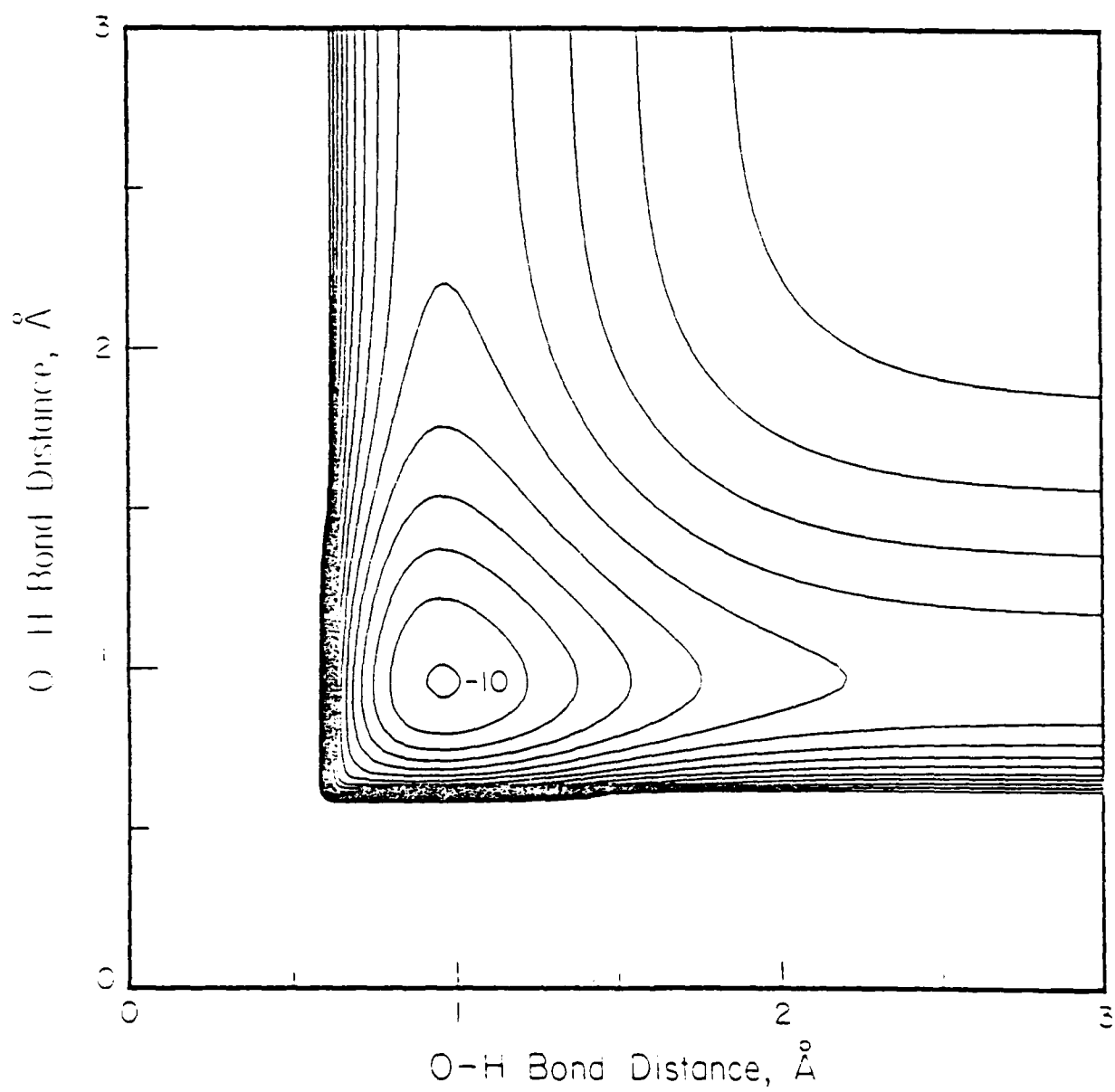
Surface	^a $V_{\text{H}_2\text{O}}$ (eV)	^b ΔV (eV)	^c $R(\text{\AA})$	^d $\omega_1(\text{cm}^{-1})$	^e $\omega_2(\text{cm}^{-1})$	^f $\omega_3(\text{cm}^{-1})$
HMS-F	-8.902	1.168	0.9506	3577	1407i	4064
MBPT-F	-8.774	1.296	0.9480	3595	1502i	4005
SL	-7.083	1.708	0.9469	4399	1867i	4618

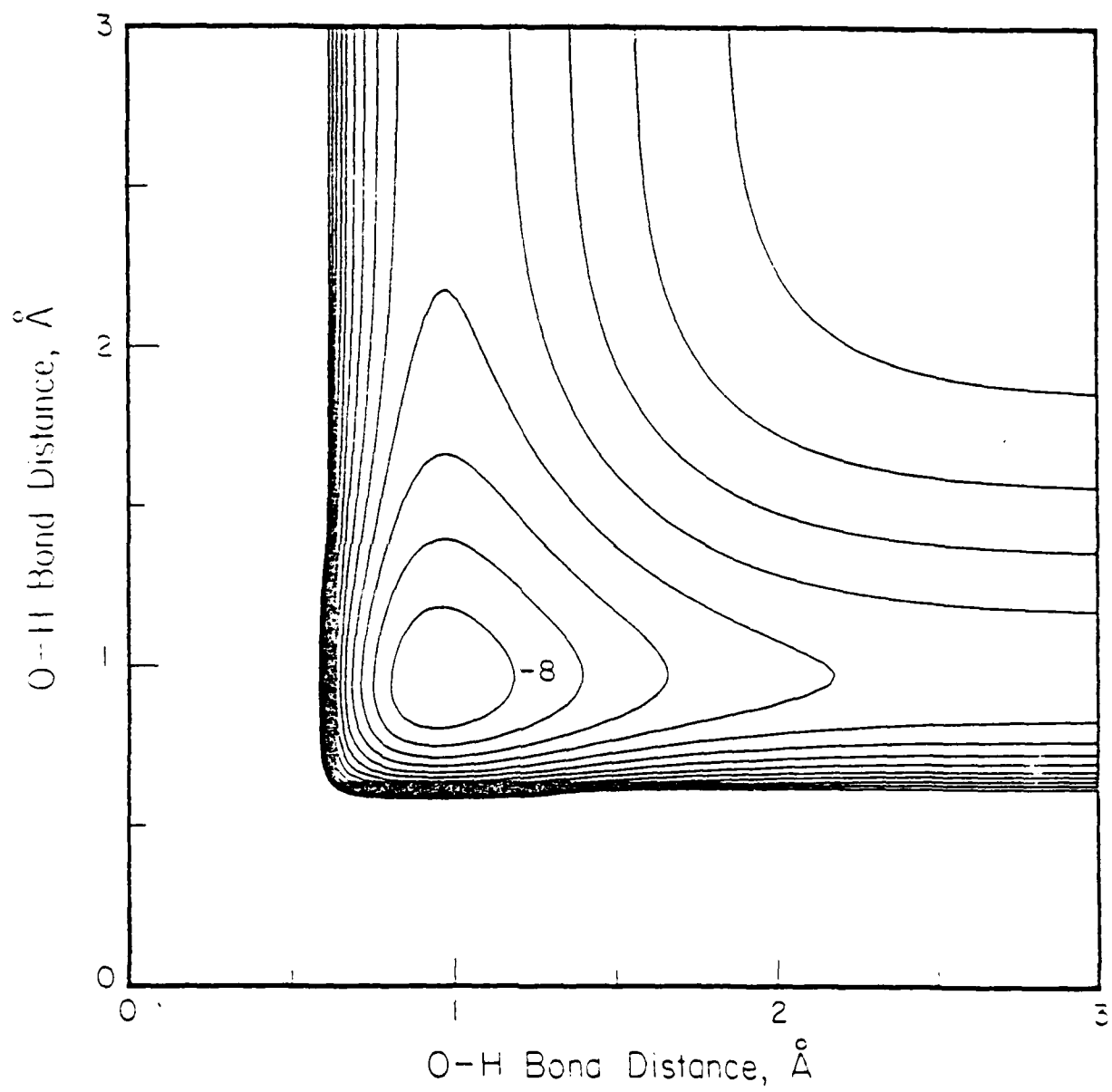
- (a) Potential at saddle point relative to $\text{O}(^3\text{P}) + \text{H}(^1\text{S}) + \text{H}(^1\text{S})$
 (b) Difference between saddle point energy and corresponding H_2O equilibrium energy
 (c) OH distance at saddle point
 (d) Symmetric stretch frequency
 (e) Bend frequency
 (f) Asymmetric stretch frequency

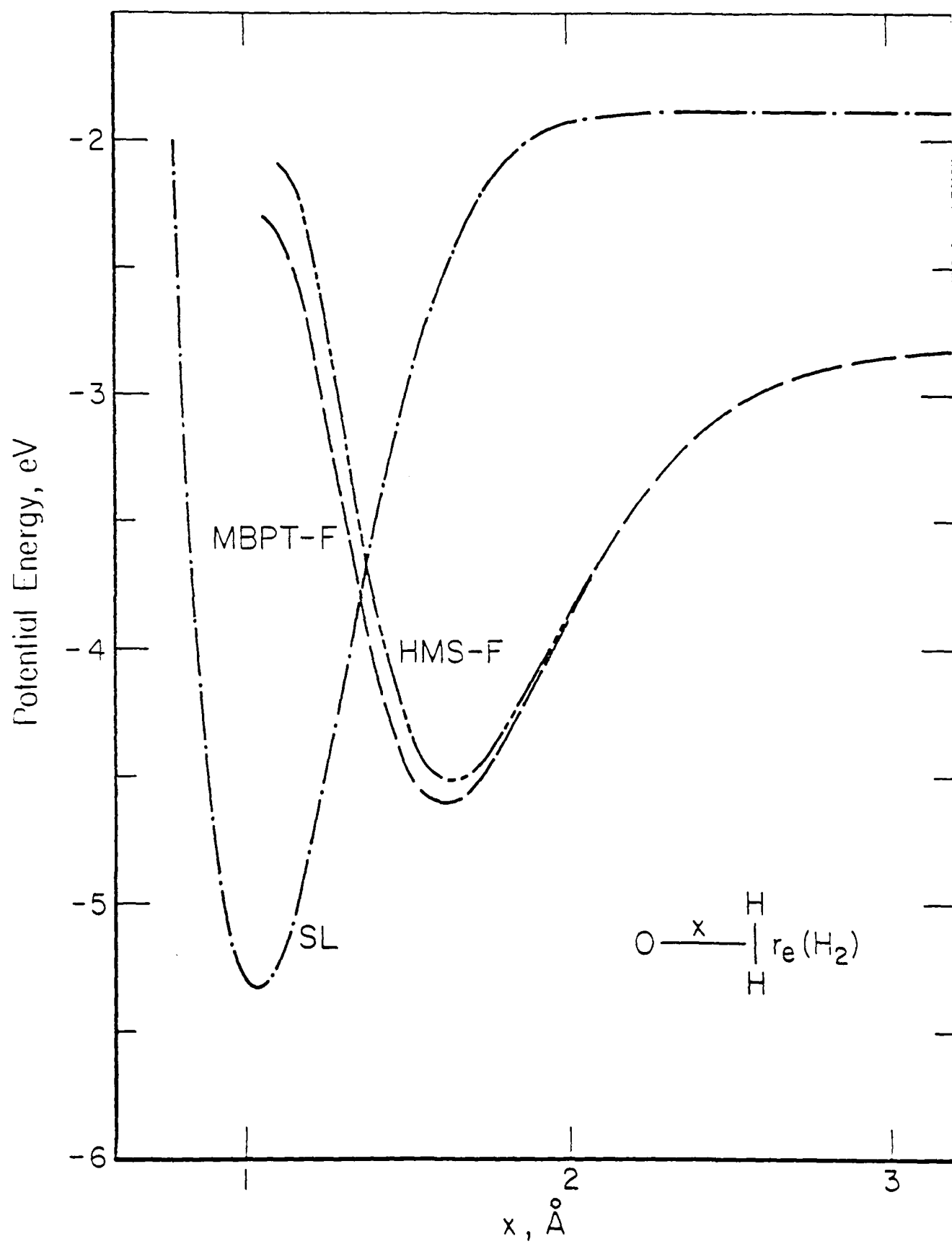
FIGURE CAPTIONS

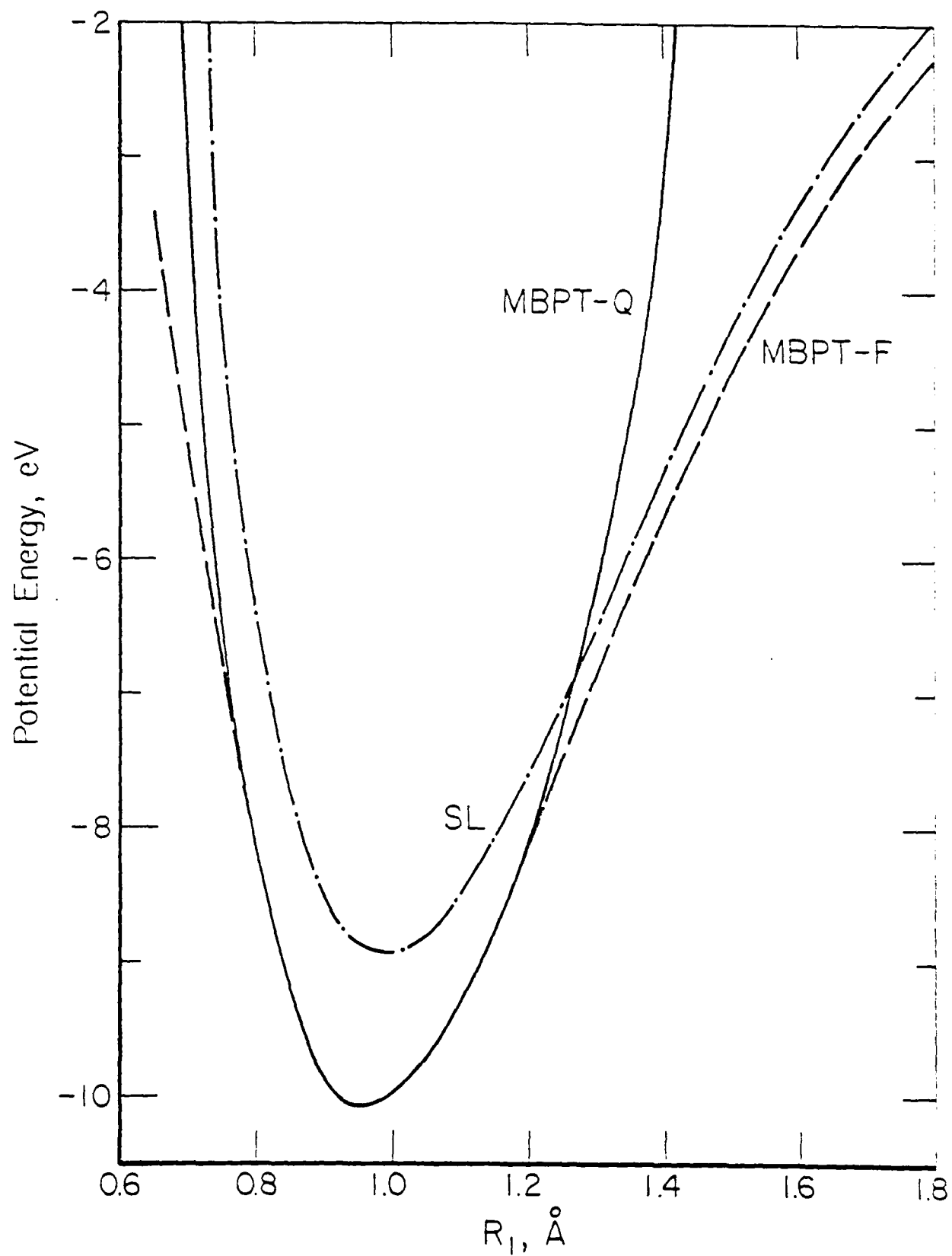
- FIGURE 1. MBPT-Q, MBPT-F and SL potentials (in eV) versus HOH bend angle θ for R_1, R_2 fixed at their equilibrium values.
- FIGURE 2. Equipotential contours of V_{H_2O} (MBPT-F) versus R_1, R_2 for θ fixed at its equilibrium value. Contours are in 1 eV increments starting with the lowest at -10 eV relative to $O(^3P) + 2H(^2S)$.
- FIGURE 3. Contours of V_{H_2O} (MBPT-F) analogous to Fig. 2, but for $\theta = 180^\circ$ (linear HOH).
- FIGURE 4. MBPT-Q, MBPT-F and SL potentials (in eV) versus R_1 for $R_1 = R_2$ and θ at its equilibrium value.
- FIGURE 5. Contours of V_{H_2O} (MBPT-F) versus X and R_3 for perpendicular $O + H_2$ geometries. The distance X is the O to center of mass of H_2 distance. Contours chosen are the same as in Fig. 2.
- FIGURE 6. MBPT-F, HMS-F and SL potentials versus X for perpendicular $O + H_2$ and R_3 equal to the H_2 equilibrium distance.
- FIGURE 7. MBPT-F, HMS-F and SL potentials versus X as in Fig. 6, but for R_3 equal to the H_2O equilibrium H_2 distance.

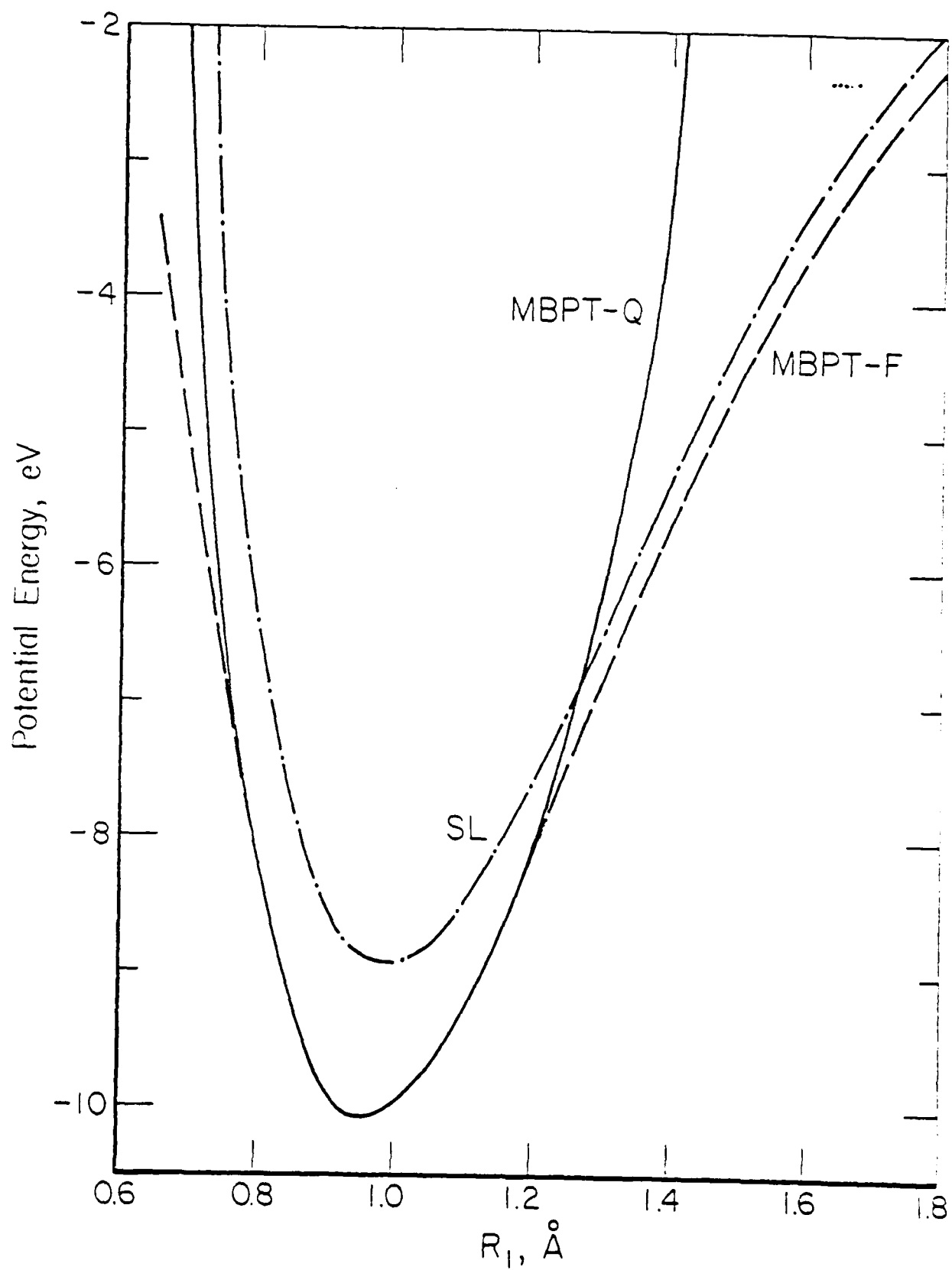


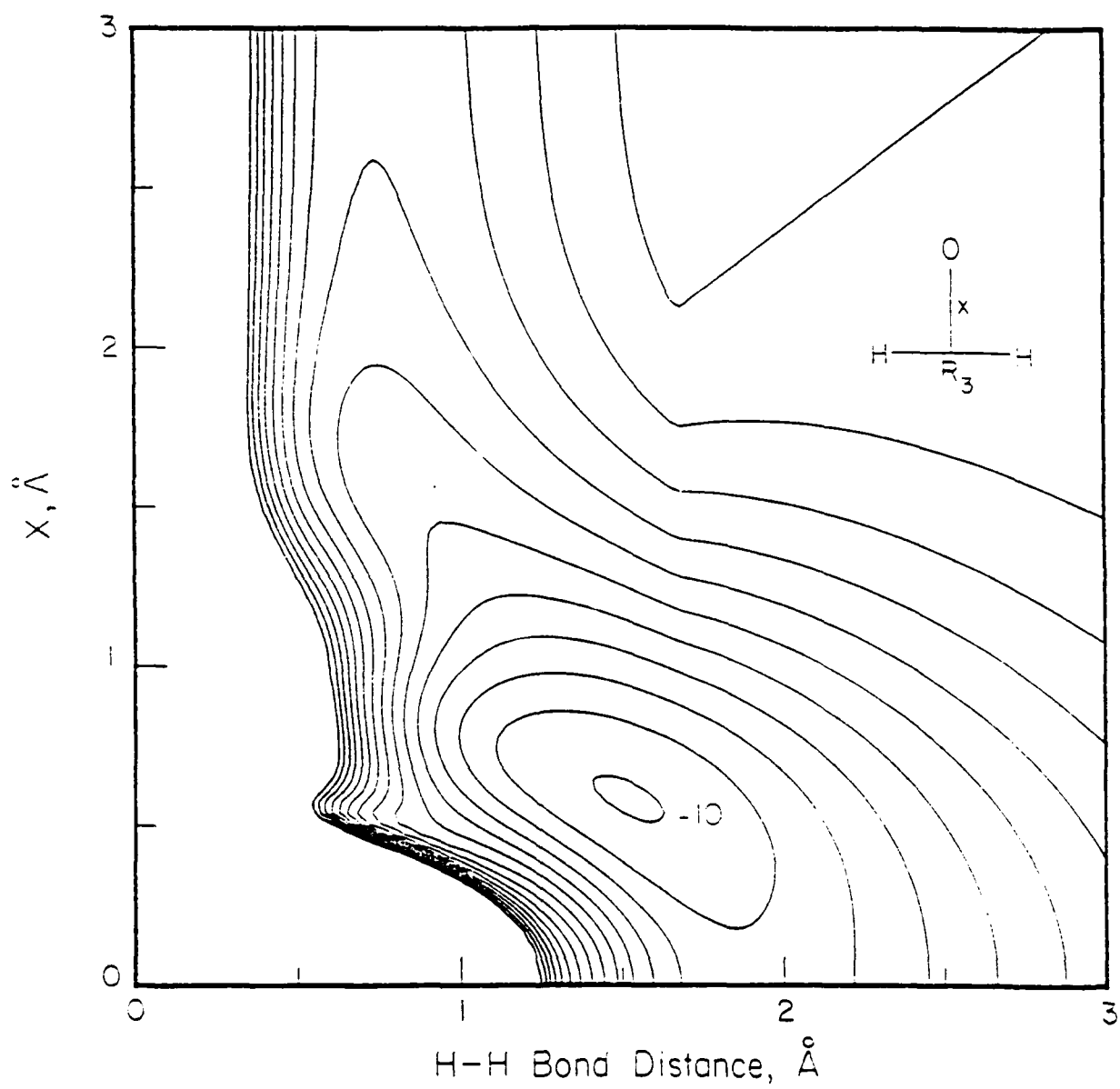


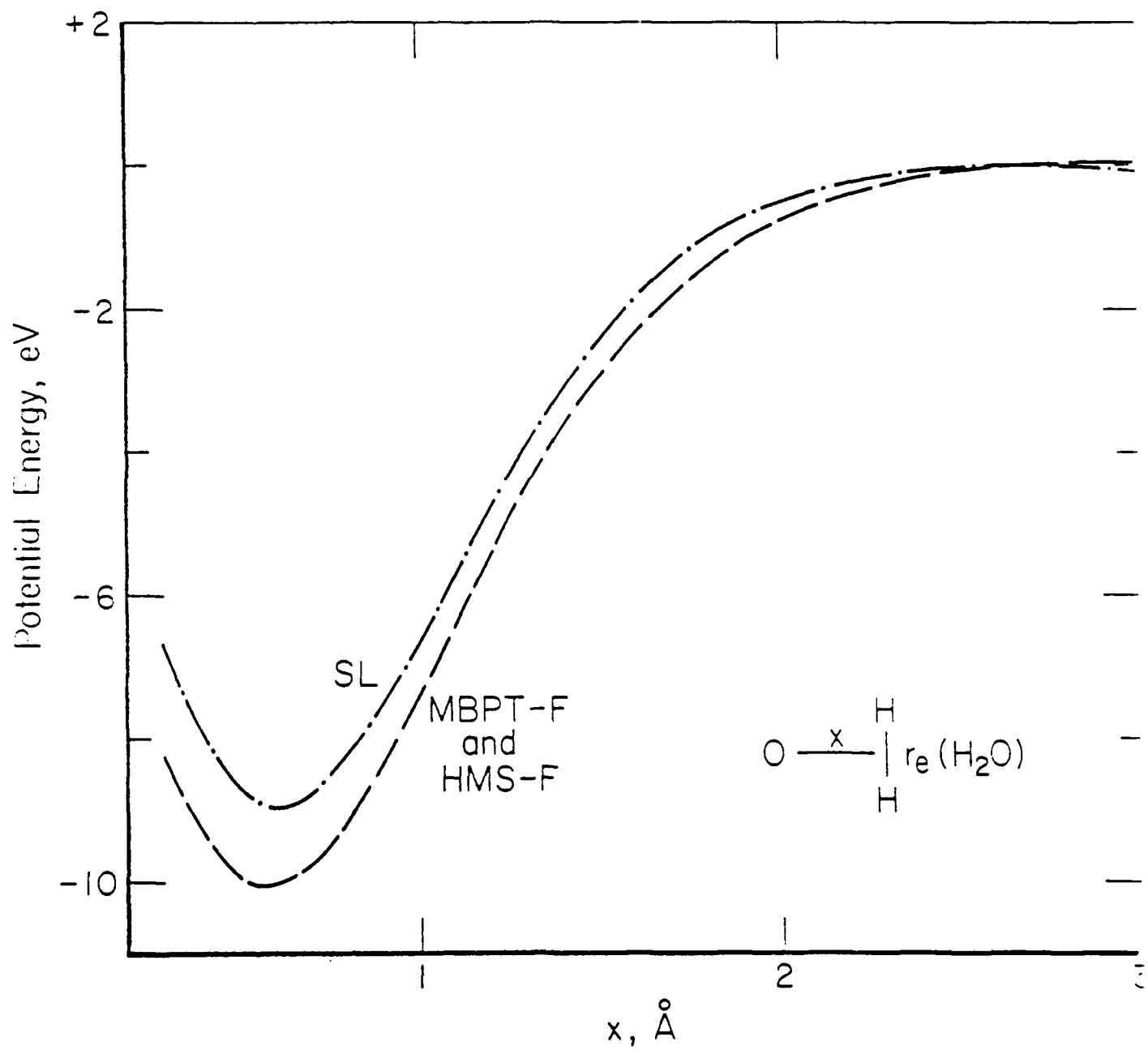












APPENDIX C

Ab Initio Treatment of Electronically Inelastic
K + H Collisions Using a Direct Integration Method
for the Solution of the Coupled-Channel Scattering
Equations in Electronically Adiabatic Representations

Bruce C. Garrett, Michael J. Redmon

Chemical Physics Section, Battelle Columbus Laboratories,
505 King Avenue, Columbus, Ohio 43201

Donald G. Truhlar

Department of Chemistry, University of Minnesota,
Minneapolis, Minnesota 55455

and Carl F. Melius

Sandia Laboratories, Livermore, California 94550

Abstract

We calculate the adiabatic potential energy curves and nonadiabatic first-derivative couplings for the X, A, and C $1\Sigma^+$ states of KH by an ab initio one-electron pseudopotential formalism. The splitting of the X and A curves at the avoided crossing is in good agreement with experiment. The ab initio results are used to calculate the electronically inelastic transition probabilities and cross sections for K + H collisions at low energies by R matrix propagation in the adiabatic representation with exponential sector transformations. Since this method has never been applied before, we made an extensive study of its convergence properties and efficiency. We found it to be a convenient, accurate, and efficient method. The cross sections are changed by about a factor of two when the potential curves are changed by a different treatment of the KH^+ core, but only by about 1% when the assumptions about the nonadiabatic second-derivative coupling terms are altered. Our estimate of the $4^2\text{P} \rightarrow 4^2\text{S}$ quenching cross section at 0.022 eV relative translational energy is $2-4 \times 10^{-4} a_0^2$. This increases to $8-10 \times 10^{-4} a_0^2$ by 1.1 eV. The emphasis in this article is on testing and evaluating the new method for solving the scattering problem rather than on the cross sections themselves.

I. INTRODUCTION

The standard quantum mechanical treatment for low-energy atomic and molecular collisions is the close coupling method.¹ When more than one electronic state must be considered, one can use an adiabatic or a diabatic representation for the electronic wavefunction. The diabatic representation has the mathematical convenience of no derivative coupling operators, but it is not unique.^{2,3} One way to specify it completely is to define it by a transformation from a finite number of adiabatic states, where the transformation is defined by requiring the first-derivative coupling to vanish in the finite manifold. It is also possible to solve the coupling equations directly in the electronically adiabatic representation, including the derivative coupling. A new method for doing this has been proposed by two of the authors,³ and it is applied here for the first time. The method involves R matrix propagation and requires as input only the adiabatic potential curves and first-derivative coupling matrix elements obtainable⁴ from standard electronic structure calculations. For the present application we consider collisions of K with H,⁵⁻¹¹ we consider only radial coupling between $1\Sigma^+$ states, and we obtain the adiabatic potential curves and first-derivative coupling matrices by ab initio methods.

Section II presents the coupled-channels scattering equations and the details of how we solve them. This section also compares the new method to the method Johnson and Levine¹² proposed for this problem and to a method one of us and Wyatt¹³ have applied to solve reactive scattering problems in vibrationally and rotationally adiabatic representations. Section III gives details and results of the electronic structure calculations performed to generate the input to the scattering equations. Section IV presents the

details of the scattering calculations, section V presents results, and section VI is discussion. The emphasis in the present paper is on evaluating the new method for solving the scattering equations rather than on the cross sections themselves.

II. THEORY

A. New method

Consider the coupled Σ states of a diatomic system with nuclear masses m_A and m_B and N_e electrons each of mass m_e . The total Hamiltonian is given by

$$H = \frac{-\hbar^2}{2\mu_{AB}} \frac{1}{R} \frac{\partial^2}{\partial R^2} R + \frac{L^2}{2\mu_{AB} R^2} + H_e(R) - \frac{\hbar^2}{2(m_A + m_B)} \sum_{ij} \nabla_{r_i} \cdot \nabla_{r_j} \quad (1)$$

where R is the internuclear distance, \mathbf{r}_i is the vector from the center of mass of the nuclei to electron i in the body-fixed frame, L is the angular momentum operator of the relative motion of the nuclei, μ_{AB} is the reduced mass for this motion, and H_e is the "electronic Hamiltonian"

$$H_e(R) = - \frac{\hbar^2}{2m_e} \sum_i \nabla_{r_i}^2 + V(\mathbf{x}, R) \quad (2)$$

where we have denoted \mathbf{x} as the collection of electronic coordinates $\{\mathbf{r}_i\}_{i=1}^{N_e}$, and $V(\mathbf{x}, R)$ includes all the pairwise coulomb interactions between nuclei and electrons.

The radial coordinate is subdivided into sectors numbered (i) , and within each sector the total wavefunction $\psi_{q_0}^{(i)}(\mathbf{x}, R)$, where q_0 denotes the initial conditions, is expanded in an orthogonal, approximately adiabatic basis $\psi^a(\mathbf{x}; i)$ which is independent of internuclear coordinate:

$$\psi^{(i)}(\mathbf{x}, R) = [\psi^a(\mathbf{x}; i)]^T \chi^a(R; i) \quad (3)$$

where ψ is a row vector of elements ψ_{q_0} , ψ^a is a column vector, each column of χ^a is a different linearly independent solution, and each row of χ^a corresponds to one of the channels.

The approximately adiabatic basis states in sector (i) are chosen to diagonalize the molecular electronic Hamiltonian in the body-fixed frame at the center R_C^i of the sector, i.e.,

$$\int d\mathbf{x} \phi_q^a(\mathbf{x};i) H_e(R_C^i) \phi_q^a(\mathbf{x};i) = \delta_{q_1 q} \epsilon_q^a(i) \quad (4)$$

Coupled radial equations for each sector (i) are obtained by substituting eqs. (1)-(3) into the time-independent Schrödinger equation for total energy E, and closing on the left with an adiabatic basis function $\phi_{q_1}^a(\mathbf{x},i)$. Neglecting the mass polarization term [last term of eq. (1)] and \hat{L}^2 coupling, the coupled equations in sector (i) are

$$\begin{aligned} \left\{ -\frac{\hbar^2}{2\mu_{AB}} \left[\frac{d^2}{dR^2} - \frac{\ell(\ell+1)}{R^2} \right] + \epsilon_{q_1}^a(i) - E \right\} \chi_{q_1 q_0}^a(R;i) \\ + \sum_q V_{q_1 q}^a(R;i) \chi_{q q_0}^a(R;i) = 0 \end{aligned} \quad (5)$$

where

$$V_{q_1 q}^a(R;i) = \int d\mathbf{x} \phi_{q_1}^{a*}(\mathbf{x};i) H_e(R) \phi_q^a(\mathbf{x};i) - \epsilon_q^a(i) \delta_{q_1 q} \quad (6)$$

The matrix elements $V_{q_1 q}^a(R;i)$ are defined for all values of R in sector (i) using basis functions that would usually be used only for calculations at the center of the sector; these matrix elements are zero at the center R_C^i of each sector. Also, because the basis functions $\phi_q^a(\mathbf{x};i)$ are independent of R within a sector, the coupled radial equations in each sector contain no derivative coupling terms. A more convenient form of eq. (5) is

$$\frac{d^2}{dR^2} \chi_q^a(R;i) = \lambda_q^2(R;i) \chi_q^a(R;i) \quad (7)$$

where

$$\chi^2(R, i) = \frac{2\mu}{\hbar^2} \{ V^a(R; i) + E^a(i) + [\frac{\hbar^2 \lambda(i+1)}{2\mu_{AB} R^2} - E] I_i \} \quad (8)$$

and the diagonal matrix $E^a(i)$ is given by

$$E_{qq_1}^a(i) = \epsilon_q^a(i) \delta_{qq_1} \quad (9)$$

Using standard numerical techniques, the radial wavefunctions $\chi^a(R; i)$ can be propagated from the left side to the right side of sector (i). Continuous solutions with continuous first derivatives are obtained for multi-sector regions by imposing the following matching conditions at each sector boundary

$$\psi_q^{(i-1)}(\chi, R_R^{i-1}) = \psi_q^{(i)}(\chi, R_L^i) \quad (10)$$

$$\frac{d}{dR} \psi_q^{(i-1)}(\chi, R_R^{i-1}) = \frac{d}{dR} \psi_q^{(i)}(\chi, R_L^i) \quad (11)$$

where $R_R^i(R_L^i)$ is the value of R at the right (left) boundary of sector (i).

Substituting eq. (3) into eqs. (10) and (11) and rearranging yields

$$\frac{d}{dR} \chi^a(R_R^{i-1}; i-1) = T(i-1; i) \frac{d}{dR} \chi^a(R_L^i; i) \quad (12)$$

$$\chi^a(R_R^{i-1}; i-1) = T(i-1; i) \chi^a(R_L^i; i) \quad (13)$$

where

$$T_{qq_1}(i-1; i) = \int d\chi \phi_q^{a*}(\chi; i-1) \phi_{q_1}^a(\chi; i) \quad (14)$$

Equations (12) and (13) provide the initial conditions for propagation across sector (i) given the solution in sector (i-1). Thus a continuous solution can be constructed over the entire scattering region. The equations presented so far are essentially the same as those in the method proposed by Johnson and Levine.¹² However, instead of requiring an explicit evaluation

of the inconvenient overlap-type integration in (14), we relate the transformation matrices $T(i-1, i)$ to the standard nonadiabatic derivative coupling matrices.

To accomplish this, we define

$$M_{sq}(R_C^i, y) = \langle \phi_s^a(\chi, R_C^i) | \phi_q^a(\chi, R_C^i + y) \rangle \quad (15)$$

where the matrix element indicates integration over the electronic coordinates. Then

$$T(i, i+1) = M(R_C^i, \frac{h_i + h_{i+1}}{2}) \quad (16)$$

where h_i is the length of sector (i). Differentiating (15), we obtain

$$\frac{\partial}{\partial y} M_{sq}(R_C^i, y) = \langle \phi_s^a(\chi, R_C^i) | \frac{\partial}{\partial y} \phi_q^a(\chi, R_C^i + y) \rangle \quad (17)$$

$$= - \frac{2\mu_{AB}}{\hbar^2} \sum_{s_1} M_{ss_1}(R_C^i, y) F_{s_1 q}^a(R_C^i + y) \quad (18)$$

where $F_{s_1 q}^a(r)$ is the nonadiabatic derivative coupling matrix defined by

$$F_{s_1 q}^a(R) = - \frac{\hbar^2}{2\mu_{AB}} \langle \phi_{s_1}^a(\chi, R) | \frac{\partial}{\partial R} \phi_q^a(\chi, R) \rangle \quad (19)$$

In obtaining eqs. (18) and (17) we assumed that $\phi_{s_1}^a(\chi, i)$ form a complete set of states. When this approximation is used in coupled-channel calculations employing a truncated set of states, its validity can be assured by obtaining converged results with respect to increasing the basis size. The effects of this approximation for finite basis sets are discussed further in the Appendix. Equation (18) can be solved numerically for $M(R_C^i, y)$ using the Magnus method,

$$N(R_C^i, y) = N(R_C^i, 0) \exp [N(R_C^i, y)] \quad (20)$$

where

$$N(R_C^i, y) = -\frac{2u_{AB}}{\hbar^2} \int_0^y dy' F^a(R_C^i + y') \\ + 2\left(\frac{u_{AB}}{\hbar^2}\right)^2 \int_0^y dy' \int_0^{y'} dy'' [F^a(R_C^i + y'), F^a(R_C^i + y'')] + \dots \quad (21)$$

and

$$N(R_C^i, 0) = I \quad (22)$$

Let R_M^i be the midpoint between sector centers

$$R_M^i = \frac{1}{2}(R_C^i + R_C^{i+1}) \quad (23)$$

and expand the coupling matrix in a Taylor series around this point

$$F^a(R_C^i + y) \approx F^a(R_M^i) + (y + R_C^i - R_M^i) \frac{dF^a}{dR}(R_M^i) \quad (24)$$

Substituting (24) into (21) and retaining terms through order $\frac{h_i + h_{i+1}}{2}$ yields

$$N(R_C^i, \frac{h_i + h_{i+1}}{2}) = -\frac{2u_{AB}}{\hbar^2} \left(\frac{h_i + h_{i+1}}{2} \right) F^a(R_M^i) + O\left[\left(\frac{h_i + h_{i+1}}{2}\right)^3\right] \quad (25)$$

and, by (16) and (20),

$$I(i, i+1) = \exp \left[-\frac{2u_{AB}}{\hbar^2} \frac{h_i + h_{i+1}}{2} F^a(R_M^i) \right] + O\left[\left(\frac{h_i + h_{i+1}}{2}\right)^3\right] \quad (26)$$

This completes the derivation of a way to perform the sector-boundary matching of (12) and (13) by using the standard functions $F^a(R)$ rather than the non-standard overlaps of (14).

The essential step in the new method is eq. (26) for the sector transformation matrix. We note that this expression is identical to the sector

transformation matrix given in eq. (12) of reference 13. The derivation and the context are different, however. In reference 13 the problem considered was reactive scattering in a vibrationally-rotationally adiabatic basis, and the propagation of the radial wave functions of (7) from R_L^i to R_R^i was accomplished by the first order Magnus method.^{14,15} In the present case the internal degrees of freedom being considered are the electronic ones, and we will accomplish the propagation across a sector by the R matrix propagation method.^{3,16-18} Comparison of the approaches illustrates that eq. (26) provides a general sector transformation matrix for solving scattering problems in adiabatic bases. For problems involving both electronic and vibrational-rotational degrees of freedom, such as electronically inelastic atom-molecule or molecule-molecule scattering, it is possible either (i) to use (26) or eq. (12) of reference 13 to treat all degrees of freedom in an adiabatic representation or (ii) to treat electronic degrees of freedom in an adiabatic representation and to treat other degrees of freedom by the diabatic representation that is more standard¹⁹ for vibrational-rotational degrees of freedom.

B. Standard methods

To compare with the adiabatic-at-the-center-of-a-sector method given above, we present here the equations for the standard adiabatic and diabatic propagation methods.²⁰

Using a continuous adiabatic basis $\psi^a(x, R)$ the coupled equations analogous to eq. (5) are

$$\left\{ -\frac{\hbar^2}{2\mu_{AB}} \left[\frac{d^2}{dR^2} - \frac{l(l+1)}{R^2} + \frac{2\mu_{AB}E}{\hbar^2} \right] + E^a(R) + 2F^a(R) \frac{d}{dR} + G^a(R) \right\} \psi^a(R) = 0 \quad (27)$$

where

$$E_{qq_1}^a(R) = \epsilon_q^a(R) \delta_{qq_1} \quad (28)$$

$$G_{qq_1}^a(R) = -\frac{\hbar^2}{2\mu_{AB}} \langle \phi_q^a(x, R) | \frac{\partial^2}{\partial R^2} | \phi_{q_1}^a(x, R) \rangle \quad (29)$$

and $F_{\chi}^a(R)$ is defined in (19). Equation (27) contains the radial-derivative couplings $F_{\chi}^a(R)$ and $G_{\chi}^a(R)$, but the angular-derivative couplings do not appear because we restricted ourselves to Σ states at the beginning of section II.A. Note that $\chi_{\chi}^a(R; i)$ and $\chi_{\chi}^a(R)$ become identical in the limit of small sector sizes. The first-derivative coupling term can be eliminated from (27) by transforming to an orthogonal diabatic basis such that the transformation matrix $U(R)$ obeys the following equation

$$\frac{\hbar^2}{2\mu_{AB}} \frac{d}{dR} U^T(R) = F_{\chi}^a(R) U^T(R) \quad (30)$$

The transformed coupled equations are then given by

$$\left\{ -\frac{\hbar^2}{2\mu_{AB}} \left[\frac{d^2}{dR^2} - \frac{l(l+1)}{R^2} + \frac{2\mu_{AB}E}{\hbar^2} \right] + H_{\chi}^d(R) + G_{\chi}^d(R) \right\} \chi_{\chi}^d(R) = 0 \quad (31)$$

where

$$H_{\chi}^d(R) = U(R) E_{\chi}^a(R) U^T(R) \quad (32)$$

$$\chi_{\chi}^d(R) = U(R) \chi_{\chi}^a(R) \quad (33)$$

and the second-derivative coupling in the new basis is

$$G_{\chi}^d(R) = U(R) \left\{ G_{\chi}^a(R) - \frac{dF_{\chi}^a}{dR} + \frac{2\mu_{AB}}{\hbar^2} [F_{\chi}^a(R)]^2 \right\} U^T(R) \quad (34)$$

It can be shown that in the limit of a complete basis

$$G_{\chi}^a(R) = \frac{dF_{\chi}^a}{dR} - \frac{2\mu_{AB}}{\hbar^2} [F_{\chi}^a(R)]^2 \quad (35)$$

and thus $G_{\chi}^d(R)$ vanishes in that limit. The diabatic basis defined by equations (30) and (32) is a P-diabatic basis in the terminology used in references 2 and 3.

III. SYSTEM AND METHODS

The system studied for a test case is $K + H$. The adiabatic potential curves were calculated by a one-electron model^{11,21} for alkali hydrides involving effective core potentials to represent K^+ and H . This method is described in reference 11, and the effective core potentials and orbital basis set used are also given there. The three lowest-energy adiabatic states $\phi_j^a(x;R)$ of $1\sigma^+$ symmetry were calculated by diagonalizing the one-electron Hamiltonian in the orbital basis. The potential curves for these states were calculated by adding the energy of the KH^+ core to the one-electron eigenvalues. The KH^+ core energy is approximated by a full KH^+ calculation or by a calculation on KH^+ employing only a single H $1s$ basis function.¹¹ Following reference 11, we call these two choices methods 2I and 2H, respectively. As discussed there, method 2H is expected to be the more accurate one. The derivative coupling matrix $F_{jk}^a(R)$ was then calculated from the wave functions by using

$$\langle \phi_j^a(x;R) | \frac{\partial}{\partial R} | \phi_k^a(x;R) \rangle = \lim_{\delta \rightarrow 0} \frac{1}{\delta} M_{jk}(R, \delta) \quad (36)$$

since $\langle \phi_j | \phi_k \rangle = 0$. A value of $0.001 a_0$ was used for δ . For calculating the overlap integral $M_{jk}(R, \delta)$, defined by (15), the K nucleus was fixed and the H was moved by the amount δ . This corresponds to placing the origin of the electronic coordinate system at the K nucleus, and it makes the 3×3 submatrix of $F_{jk}^a(R)$ for the states considered here tend to a null matrix at $R = \infty$, which makes it straightforward to impose scattering boundary conditions. Other possible choices of electronic origin are discussed elsewhere.^{3,22}

The calculated adiabatic potential curves $\epsilon_q^a(R)$ are shown in Figure 1, and the calculated first-derivative coupling matrices are shown in Figure 2. In Figure 2 we use the notation

$$\tilde{F}^a(R) = -(\hbar^2/2\mu_{AB}) \tilde{f}^a(R) \quad (37)$$

Transforming away the first-derivative coupling by the 3×3 matrix $\tilde{U}(R)$ yields the diabatic Hamiltonian matrix $\tilde{H}^d(R)$ whose elements are illustrated in Figures 3 and 4.

The results are given in hartree atomic units: 1 a.u. energy = 1 hartree = $1 E_h = 27.212 \text{ eV}$, and 1 a.u. length = 1 bohr = $1 a_0 = 0.52918 \text{ \AA}$.

IV. SCATTERING CALCULATIONS

We will compare several different methods for solving the scattering problem.

A. First order Magnus approximation in the adiabatic representation.

In this method we rewrote (27) as

$$\frac{dY_{\chi}^a}{dR} = A_{\chi}(R) Y_{\chi}^a(R) \quad (38)$$

where

$$Y_{\chi}^a(R) = \begin{pmatrix} \chi^a(R) \\ \frac{d\chi^a}{dR} \end{pmatrix} \quad (39)$$

$$A_{\chi}(R) = \begin{pmatrix} 0 & I_{\chi} \\ D_{\chi}^a(R) & 2F_{\chi}^a(R) \end{pmatrix} \quad (40)$$

and

$$D_{\chi}(R) = \frac{2\mu_{AB}}{\hbar^2} [E_{\chi}^a(R) + G_{\chi}^a(R) + (\frac{\hbar^2 \lambda(\lambda+1)}{2\mu_{AB} R^2} - E) I_{\chi}] \quad (41)$$

Equation (38) was integrated by the first order Magnus approximation

$$Y_{\chi}^a(R+h) = \exp[hA_{\chi}(R+\frac{1}{2}h)] Y_{\chi}^a(R) \quad (42)$$

The exponential was evaluated by a power series, retaining terms through h^7 . Checks showed that the same results were obtained by retaining terms through h^5 .

The scattering matrix was evaluated by applying boundary conditions to $\chi_{\chi}^a(R)$ in the usual way.²³ We employed a fixed stepsize h and decreased it till convergence was obtained for the absolute squares of scattering matrix elements.

B. First order Magnus approximations in the diabatic representation
with power series evaluation of the exponentials. In this method we rewrote
 (31) as

$$\frac{dY^d}{dR} = B(R) Y^d(R) \quad (43)$$

where

$$Y^d(R) = \begin{pmatrix} \chi^d(R) \\ \frac{d\chi^d}{dR} \end{pmatrix} \quad (44)$$

$$B(R) = \begin{pmatrix} 0 & I \\ D^d(R) & 0 \end{pmatrix} \quad (45)$$

and

$$D^d(R) = \frac{2\mu_{AB}}{\hbar^2} [H^d(R) + G^d(R) + (\frac{\hbar^2 \ell(\ell+1)}{2\mu_{AB} R^2} - E) I] \quad (46)$$

Starting with the same input, $E^a(R)$ and $F^a(R)$, as for method A, we integrated
 (30) simultaneously with (43) so that we could calculate $B(R)$ from (32), (45),
 and (46) as we needed it. We assumed $G^d = 0$ as discussed after (34). The
 first order Magnus approximations are

$$U^T(R + \frac{1}{2}h) = \exp[-hF^a(R)] U^T(R - \frac{1}{2}h) \quad (47)$$

and

$$Y^d(R + h) = \exp[hB(R + \frac{1}{2}h)] Y^d(R) \quad (48)$$

In (47) and (48) the exponentials were evaluated by power series through h^7 .
 The boundary conditions and stepsize were handled the same as in method A.

C. First order Magnus approximation in the diabatic representation with analytic evaluation of the exponentials. This method is the same as method B except for the evaluation of the exponentials. The exponential in (48) was evaluated analytically in terms of the eigenvalues and eigenvectors of $\hat{D}^d(R)$ as explained by Light.¹⁵ Since we still assume $\hat{G}^d(R) = 0$, the eigenvalues are the already-available $\epsilon_q^a(i)$ and the eigenvectors are the columns of $U(R_C^i)$. The latter are obtained from (47), but in this method the exponential in (47) was evaluated analytically. Since \hat{F}^a is skew symmetric, the exponential in (47) can be evaluated in terms of f_{12}^a , f_{13}^a , and f_{23}^a . This kind of procedure is very efficient for 2×2 and 3×3 cases, and we used it for the calculations reported here. For matrices of order greater than 3, the exponential of a skew symmetric matrix can be evaluated efficiently by diagonalizing the square of the skew symmetric matrix.^{24,25} The boundary conditions and stepsize were handled the same as in method A.

D. R matrix propagation with adiabatic basis functions at sector centers and with the exponential sector transformation matrix. This is the new method of reference 3 and the present paper. The propagation across a sector was accomplished by the R matrix propagation method,^{3,15-17} using a modified version of an R matrix propagation code that has been discussed elsewhere.^{26,27} Since $\hat{F}^a(R)$ is skew symmetric, the exponential sector transformation matrix (26) was evaluated analytically in terms of F_{12}^a , F_{13}^a , and F_{23}^a as discussed in subsection C above. The method for extracting a scattering matrix from the global R matrix is explained elsewhere.²⁷ We used a variable stepsize algorithm^{26,27} with one stepsize parameter $\epsilon^{(1)}$ for $R < 25 a_0$ and another $\epsilon^{(2)}$ for $R > 25 a_0$. $\epsilon^{(2)}$ was set at a value that yields high accuracy, and $\epsilon^{(1)}$ was decreased till convergence was obtained for absolute squares of scattering matrix elements.

E, F. Numerical integration in the adiabatic representation. For these methods we applied a fixed-stepsize Runge-Kutta-Gill integration²⁸ (method E) or a 5th order variable-stepsize predictor-corrector algorithm²⁹ (method F) to integrate eq. (38). The boundary conditions were handled the same as in method A.

G, H. Numerical integration in the diabatic representation. Finally we applied the Runge-Kutta-Gill (method G) and 5th order variable-stepsize predictor-corrector (method H) methods to simultaneously integrate eqs. (30) and (43). The boundary conditions were handled the same as in method A.

I. Initial values and boundary conditions. For all the methods we started the integration of the radial wavefunctions at small enough R that the results are invariant to further decreasing the starting value. In particular we started the s-wave solutions at $1.1 a_0$ and $2.1 a_0$ for the 2I and 2H potential curves, respectively, for $E = 0.06 E_h$. For higher E we started at smaller R , and for higher ℓ we started at larger R , e.g., $2.2 a_0$ for $\ell = 15$ for the 2H potential curves for $E = 0.06 E_h$. At the starting point the radial wavefunctions were taken as zero and the matrix of radial-wavefunction derivatives was the unit matrix. This generates N linearly independent solutions where N is the number of states retained in the wavefunction expansion. At $R = 70 a_0$, we transformed to the adiabatic representation (only necessary in methods B, C, G, and H) and took linear combinations of the linearly independent solutions to obtain the correct scattering solutions satisfying the Ricatti-Bessel boundary conditions for the radial wavefunctions and their derivatives.

For methods B, C, G, and H we need also specify the initial values for U^T at the center of the first sector. It can be shown that the scattering

matrix obtained by the above procedures is invariant to the starting value of U^T so we started it as the unit matrix. This transformation generates an arbitrary linear combination (with R-independent coefficients) of the physical diabatic states, where the physical ones are the ones that make $H^d(R)$ diagonal at large R. Let $C^T(R)$ denote the transformation matrix for the physical diabatic states. $C^T(R)$ is not needed for scattering calculations but is required to make Figures 3 and 4. It is generated by

$$C^T(R) = U(\text{large } R) U^T(R) \quad (49)$$

where large R = 70 a_0 in practice and both matrices on the right side of (49) are generated by solving (47) with $U^T(R_{\text{start}} + \frac{1}{2}h) = I$.

In all cases we checked that ending the integrations at R = 69 a_0 would have given the same scattering matrices (within 0.1%) as ending at R = 70 a_0 .

J. Stabilizing transformations. For all the methods except R matrix propagation, method D, it is necessary to integrate the radial wavefunction through classically forbidden regions. In such regions one faces the well known problem that components of the solution vectors grow exponentially and can cause the solution vectors to become linearly dependent.³⁰⁻³² This problem is handled by performing a Schmidt orthogonalization of the solution matrix, $X^a(R)$ or $X^d(R)$, after a specified number of integration steps have been taken in regions in which at least one channel is closed. For step-sizes small enough to insure 0.01% accuracy it was found that stabilizing every 20 steps was sufficient so that the transition probabilities were invariant to 6 significant figures to orthogonalizing even more often. Doubling the number of orthogonalizations increased the computer time by only 10%. For the larger stepsizes which give approximately 0.5% accuracy, stabilizations were performed every step in regions in which at least one channel is closed.

V. RESULTS AND DISCUSSION

In all cases we included three states in the coupled-channel calculations.

A. Comparison of methods. We made a detailed study of computational efficiency for the case of the s-wave probabilities at $E = 0.06 E_h$. First we performed some calculations with very small stepsizes (i.e., small sector widths) to get the accurate transition probability P_{12} connecting the first (4^2S) and second (4^2P) atomic states. Then, for the six most efficient methods we performed calculations for a fine grid of fixed stepsizes (methods A, B, C, E, and G) or fixed stepsize parameters $\epsilon^{(1)}$ (method D) to find the minimum computing time required to achieve 0.5% accuracy for this probability. These computing times are given in Table I, where they are expressed as ratios to the computing time required by method D. We see that the new method, i.e., the variable-stepsize R matrix propagation method in the adiabatic representation with the exponential sector transformation matrix, is the most efficient of the seven methods tested in this work. Second most efficient is fixed-stepsize Magnus integration in the diabatic representation with analytic exponentiation. Analytic exponentiation was about twice as fast as using the power series, even though the power series was coded very efficiently to take advantage of the structure of zeroes in the matrices. The Magnus methods could probably be made more efficient by using a suitable variable-stepsize algorithm, but this was not attempted.

It is well known that the most efficient method for one level of accuracy is not necessarily the most efficient method for other levels of accuracy. A more detailed comparison of the two most efficient methods, on the same scale as used for Table I, is given in Table II. Table II shows that the

convergence of both methods is smooth and that method D is also efficient for higher accuracy, e.g., it is 3.7 times more efficient than method C for 0.1% accuracy in P_{12} .

It should be clear that, although eight methods have been compared for the same problem, there has been no attempt to determine the absolutely fastest possible way to solve the coupled-channels problem. The main conclusion of this section is that the R matrix propagation method in the adiabatic representation with the exponential sector transformation matrix, which is a very convenient and stable method, is also very efficient.

B. Probabilities. The s-wave transition probabilities for the two sets of potential curves are shown in Figure 5. These probabilities show regular oscillations as functions of $1/E$, and the envelope of the oscillating probabilities increases with increasing energy above threshold. The small differences between the two sets of potential curves change the phase of the oscillations in the transition probabilities, but they do not make large changes in the magnitudes of the envelopes. For both sets of potential curves P_{12} is in the range $10^{-5} - 10^{-4}$, P_{13} is $10^{-7} - 10^{-6}$, and P_{23} is $10^{-2} - 5 \times 10^{-2}$ for most energies considered.

We performed some extra calculations to check the assumption of a complete set of states for the second-derivative coupling term. In the standard versions of methods A, E, and F, we use equation (35) for G_v^a . This equation is also used to make G_v^d vanish in methods B, C, G, and H, and, as discussed in the appendix, it is required to hold for the equivalence of method D to the other methods. Thus it is interesting to test the sensitivity of the results to the treatment of the second-derivative coupling.

The correct expression for a second-derivative coupling matrix element is

$$G_{ij}^a(R) = \frac{d}{dR} F_{ij}^a(a) + \frac{2\mu_{AB}}{h^2} \sum_k F_{ik}^a(R) F_{kj}^a(R) \quad (50)$$

where the sum over k should include a complete set of states. In (35), however, the sum includes only the N states retained in the expansion (3) of the wavefunction. To test the importance of this truncation in the second term, we repeated the method-A calculations entirely neglecting the second term. The results are given in Tables III and IV. In 27 out of 28 cases, the difference of the results is 1% or less. In the remaining case the difference is 5%. The present test is a very stringent one for eq. (35). First of all, the second derivative coupling is known to be less important in high-energy cases where semiclassical methods are valid,^{22,33,34} but the present tests are low-energy, highly quantal cases. Second, the truncation of the sum in the second term of (50) would be expected to be most valid for large inelastic probabilities dominated by two strongly coupled states. But the present inelastic probabilities are very small and do not correspond quantitatively to a simple two-state avoided crossing.¹⁰ Thus the fact that the second term of equation (35) has only a small effect in the present cases is very encouraging.

It should be noted that approximations to the skew-symmetric first term of equation (35) or (50) are dangerous. If this term is neglected, the calculated probabilities no longer sum to unity or satisfy microscopic reversibility. The second term of (35) is symmetric; thus its neglect does not affect these properties.

C. Cross sections. Cross sections were calculated at two energies, $E = 0.06 E_h$ and $0.10 E_h$. The first of these is only 0.022 eV above the

4^2P threshold at $E = 0.059192 E_h$; thus it is a total energy typical of those contributing to quenching of the 4^2P state under thermal conditions. The second energy is 1.11 eV above the 4^2P threshold. The cross sections are given in Table IV. At $0.06 E_h$, the potential curves obtained by method 2I lead to $4^2P + 4^2S$ quenching cross section 1.9 times smaller than is obtained by method 2H. However at $0.10 E_h$, the method 2I cross sections are 1.3 times larger. Considering the small size of the cross sections and the out-of-phase oscillations in the fixed- ℓ inelastic transition probabilities, the different values obtained for the cross sections are not too surprising. The much larger $4^2P \rightarrow 5^2S$ cross section is less sensitive to the difference in the potential curves.

D. Potential curves and coupling terms. Figure 1 compares the new potential curves to the experimental ones. Method 2I leads to more accurate dissociation energies but method 2H leads to more accurate repulsive walls. The C-state³⁵ curve shows a shoulder at $R = 5-6 a_0$. A similar feature was predicted in reference 7. Reference 7 shows that this shoulder results from an avoided crossing with a state with Rydberg character.

The first-derivative coupling between the X and A states peaks at $8.5 a_0$, and the splitting of the adiabatic energy values is a minimum at $R = 8.9 a_0$. The position and value of the minimum of the adiabatic splitting is compared quantitatively to previous calculations in Table V. The table shows, as is also clear from Figure 1, that the present calculations slightly overestimate the X-A splitting. However the present calculations are more accurate than all previous calculations. There are no experimental results available for the other avoided crossings. There is still quite a bit of uncertainty about the splitting at the A-C avoided crossing, but the two

calculated values for the minimum splitting of the X and C curves are in reasonably good agreement.

The shape of the present diabatic couplings as functions of R are very similar to those calculated previously for KH (see Figure 2 of reference 7). The adiabatic couplings also show a reasonable similarity in shape to those calculated previously (see Figure 17 of reference 7).

E. Semiclassical approximations. Although $F_{12}^a(R)$ and $|\epsilon_1^a(R) - \epsilon_2^a(R)|$ show the behavior associated with an avoided crossing at $R = 8-9 a_0$, Figure 3 shows that the diabatic potential curves do not show such a crossing. Most previous workers have treated the X-A inelastic transition in terms of such a hypothetical diabatic crossing, although there was already some indication in references 3 and 7 that the usual diabatic pictures for the curve crossings in NaH and KH might be inadequate. Nevertheless it is interesting to briefly compare the present inelastic transition probabilities to those obtained by the semiclassical Landau-Zener formula for estimating transition probabilities at adiabatic avoided crossings resulting from diabatic crossings. According to this formula, if the crossing occurs at $R = R_X$, the inelastic s-wave transition probability is^{33,36-38}

$$P_{12}^{LZ} = 2p(1 - p) \quad (51)$$

where

$$p = e^{-w} \quad (52)$$

$$w = \frac{2\pi}{\hbar v} \left| \frac{(H_{12}^d)^2}{d(H_{11}^d - H_{22}^d)/dR} \right|_{R=R_X} \quad (53)$$

and v is the local radial speed at the diabatic crossing, i.e., for an s wave,

$$v = \{2(E - H_{11}^d(R_X))/\mu\}^{1/2} \quad (54)$$

In the two-state approximation, assuming orthogonal diabatic states,

$$H_{12}^d(R_X) = \frac{1}{2}[\epsilon_2^a(R_X) - \epsilon_1^a(R_X)] \quad (55)$$

It is customary,^{5,6,8} for the X-A transition in alkali hydrides, to neglect H_{11}^d and dH_{11}^d/dR at $R = R_X$ and to approximate H_{22}^d by (in atomic units)

$$H_{22}^d(R) \approx IP - EA - \frac{1}{R} - \frac{\alpha}{2R^4} \quad (56)$$

where IP is the ionization potential of M, EA is the electron affinity of H, and α is the sum of the polarizabilities of M^+ and H^- . Putting all these approximations together and noting that $w \gg 1$ yields (in atomic units)

$$P_{12}^{LZ} = 2 \exp \left[- \frac{\pi |\Delta\epsilon(R_X)|^2}{(8E/\mu)^{1/2} (R_X^{-2} + 2\alpha R_X^{-5})} \right] \quad (57)$$

We use $\mu = 1790.83$ a.u. and $\alpha = 218$ a.u., and we take R_X and $\Delta\epsilon(R_X)$ from Table V.

In the more complete Landau-Zener-Stueckelberg theory, the inelastic probability becomes^{36,38-40}

$$P_{12}^S = 2P_{12}^{LZ} \sin^2(\tau + \delta) \quad (58)$$

where τ is the difference in action integrals for the two adiabatic curves and δ is a phase correction:

$$\tau = (2\mu/\hbar^2)^{1/2} \int_{R_{tp1}}^{R_X} [E - \epsilon_1(R)]^{1/2} dr - \int_{R_{tp2}}^{R_X} [E - \epsilon_2(R)]^{1/2} dr \quad (59)$$

where R_{tp1} and R_{tp2} are the classical turning points in adiabatic states 1 and 2 respectively. Equation (58) shows that $2P_{12}^{LZ}$ should be compared to the

upper envelope of the oscillating inelastic transition probability. This comparison is shown in Table VI for those energies at which the close coupling probabilities are maxima (compare Figure 5). The comparison, however, shows that the Landau-Zener formula overestimates the inelastic transition probabilities as compared to the results obtained from the close coupling calculations. The overestimates in Table VI range from a factor of 36 to a factor of 60. Thus this simple high-energy model does not yield accurate transition probabilities at the low collision energies of the present study.

Although the failings of the Landau-Zener theory are well known, even at higher energies,⁴¹ both Faist and Levine⁴² and Andresen *et al.*⁴³ found that it works very well for the ionic-covalent crossing in alkali-halogen collisions, even near threshold. In fact Andresen *et al.*⁴³ concluded that "a similar agreement is expected for all other systems which are dominated by the interaction of a covalent and an ionic channel." By this argument one would expect that it would be accurate for the ionic-covalent interaction leading to P_{12} . In previous work,⁷ however, it has been pointed out that the strong interaction is not well localized in this case and that this would lead to a breakdown of the Landau-Zener method. Furthermore, the fact that the diabatic curves do not cross is an indication that the transition is not an isolated curve crossing. A more quantitative measure of whether this transition should be treated as a curve crossing will be given below.

The other inelastic transitions are more complicated. The second and third diabatic states cross twice, and the first and third diabatic states do not cross. Landau-Zener-type isolated-avoided-crossing treatments are not appropriate for either of these transitions. In the absence of simple

models the full close coupling treatments reported above are the best way to estimate the transition probabilities.

The additional factor in equation (58) results from the interference of the two possible trajectories leading to the same inelastic collision. This effect accounts for the existence of the oscillations in Figure 5. Equation (53) results from a high-energy approximation, retaining only the leading term in $1/v$ in the semiclassical phase integral.⁴⁴ With the same approximation the difference in action integrals becomes

$$\tau = (1/\hbar v) \int_{R_{tp}}^{R_X} \Delta \epsilon(R) dr \quad (60)$$

where the classical turning points are the same to this order. Equation (60) predicts that at high energy the oscillations should be evenly spaced in $1/v$. At the low energies of the present study, the initial and final speeds are appreciably different, and they differ significantly from the local radial speeds at small r . Thus it is not possible to approximate all these speeds by the same v and equation (60) is inapplicable. Nevertheless the regularity in the oscillations is evident in Figure 5.

We have already mentioned that the couplings between the adiabatic curves cannot be treated as simple avoided crossings. To put this on a more quantitative basis we will discuss the classification of the nonadiabatic couplings. One may distinguish two kinds of strong interaction in terms of the following two-state representation

$$\phi_1^a(x, R) = \phi_1^d(x) \cos \theta(R) + \phi_2^d(x) \sin \theta(R) \quad (61)$$

$$\phi_2^a(x, R) = -\phi_1^d(x) \sin \theta(R) + \phi_2^d(x) \cos \theta(R) \quad (62)$$

Using (19), (37), (61), and (62), one finds

$$f_{12}^a(R) = \frac{d\theta}{dR} \quad (63)$$

One can distinguish two prototype cases. In one case, θ changes from 0 at $R = \infty$ to $\pi/4$ (≈ 0.785) at small R . This occurs for a symmetric resonance interaction like $H^+ + H$. In another case θ changes from 0 at $R = \infty$ to $\pi/2$ (≈ 1.57) at small R . This occurs for a diabatic curve crossing. In general one may associate a $\Delta\theta_{ij}$ with each peak in $f_{ij}^a(R)$ by integrating over the range of strong interaction:

$$\Delta\theta_{ij} = \int_{R_1}^{R_2} f_{ij}^a(R) dR \quad (64)$$

For actual cases, $\Delta\theta_{ij}$ may come out somewhere between 0.785 and 1.57 for strong interactions and may be less for weak ones. We applied this model to the present case and the results are given in Table VII. These results show that $\Delta\theta_{12}$ is not close to 1.57. Thus it is an oversimplification to describe the 1-2 ionic-covalent interaction as a simple curve crossing, and this helps to explain the failure of the Landau-Zener method. The adiabats are not merely "switching" from one diabatic to the other; rather there is an appreciable "mixing" contribution. Even the 2-3 interaction, where the diabats cross, is not a pure curve crossing. Table VII shows that the 1-3 interaction is weak.

In order to calculate the $\Delta\theta_{ij}$ values in Table VII, we had to separate the overlapping contributions from two different interaction regions in the vicinity of the sign change in $f_{ij}^a(R)$. We did this by the simplest method, i.e., we integrated from the peak of $f_{ij}^a(R)$ to $R = \infty$ and multiplied by 2. There is an even simpler way to classify the nonadiabatic interactions

that also avoids the question of overlapping wings of the peaks in $f_{ij}^a(R)$. Under simple assumptions in $H_{ij}^d(R)$, one can show on a two-state model that $f_{ij}^a(R)$ for the symmetric resonance has the form $(\beta/4) \text{sech}[\beta(R - R_M)]$ and for the curve cross cases it is a Lorentzian.²² These different shapes may be characterized by defining the unitless interaction parameter:

$$Q_{ij} = [\text{peak value of } f_{ij}^a(R)] \times \text{FWHM}$$

where FWHM is the full width at half maximum of the peak. This leads to $Q_{ij} = 0.66$ for the symmetric resonance case and $Q_{ij} = 1.00$ for the curve crossing cases. We also calculated Q_{ij} for the biggest peak in each $f_{ij}^a(R)$, and the results are in Table VII. This confirms that the 1-2 and 2-3 interactions involve considerable mixing (as in symmetric resonance) as opposed to pure curve crossing. This simple method for characterizing nonadiabatic interactions should be useful for many problems.

VI. CONCLUDING REMARKS

This paper has been concerned with calculational techniques for the calculation of electronically inelastic transition probabilities using ab initio potential energy curves and nonadiabatic radial-first-derivative couplings as input. We have demonstrated that very small transition probabilities can be calculated with high precision using a convenient and accurate method based on R matrix propagation and an exponential sector transformation matrix.

The emphasis in this article is on the techniques for solving the coupled-channel equations to obtain the precise values of the cross sections that correspond to a set of ab initio potential energy curves and nonadiabatic radial-first-derivative couplings. Several other considerations enter when we try to obtain accurate cross sections, i.e., good agreement with experiment or reliable predictions. Only two of these have been considered in this paper, namely, sensitivity to changes in the potential curves and to the treatment of the second-derivative nonadiabatic coupling terms. Some other factors that must be considered in future work to obtain reliable results for the K + H system are sensitivity to change of electronic origin in the radial-first-derivative coupling terms^{3,22,45} and the role of angular-derivative coupling terms.^{22,46} The latter terms couple the Σ states to the Π states, but we have included only Σ - Σ coupling in the present study. Another question, also discussed elsewhere^{2,3,47,48} and also deferred to future work for detailed numerical study, is the question of whether accurate low-energy cross sections can be calculated from ab initio molecular-frame input data without either including plane-wave factors or transforming at large R to a laboratory-frame diagonal representation in which the coupling

vanishes at infinity for any consistent choice of origin for the electronic coordinates. If such a transformation is required, the present method can still be used to integrate out to the large-R transformation distance.

VII. ACKNOWLEDGEMENTS

This work was supported in part by the National Science Foundation under grant no. CHE77-27415 and by the Air Force Office of Scientific Research, United States Air Force (AFSC), under contract no. F40611-79-0024. The United States Government is authorized to reproduce and distribute reprints for governmental purposes notwithstanding any copyright notation thereon.

APPENDIX

In this appendix we discuss the fact that using (18) with an incomplete basis is equivalent to including the full effect of the first derivative coupling matrix $F^a(R)$, but including only part of the second derivative coupling matrix $G^a(R)$.

First note that $U(R)$ defined by (30) and $M(R)$ defined by (18) obey the same differential equation. Note that the sign difference arises in taking the transpose of (30) since $F^a(R)$ is skew symmetric. It has been shown elsewhere³ that the matrices $M(R)$ can be used to construct the transformation $U(R)$ from the adiabatic basis to the diabatic one. Therefore, the two problems are equivalent in the limit of small sector size and since the transformation method, (27)-(34), includes the full effect of the $F^a(R)$ matrix, so will the direct integrationscheme of eqs. (7)-(26).

By using the M matrices to generate the transformation to the diabatic basis $\chi^d(R)$, (7) can be transformed to

$$\frac{d^2}{dR^2} \chi^d(R;i) = D(R;i) \chi^d(R;i) \quad (A-1)$$

where

$$D(R;i) = U(R_C^i) \lambda^2(R;i) U^T(R_C^i) \quad (A-2)$$

and

$$\chi^d(R;i) = U(R_C^i) \chi^a(R;i) \quad (A-3)$$

In enforcing the sector matching conditions (10) and (11), the matrix $T(i-1;i)$ is now replaced by the identity matrix since $F^d(R)$ is identical zero. Therefore, solution of (A-1)-(A-3) is the same as the solution to (31) but neglecting $G^d(R)$. Since $G^d(R)$ vanishes in the limit of a complete set, this neglect is completely justified in the converged limit. Consider, however the case

in which an incomplete basis of the N lowest-energy adiabatic states is included in the coupled-channel equations. Then the terms neglected in assuming $G_{ij}^a(R)$ obey (35) are given by

$$\Delta_{ij}(R) = -\frac{\hbar^2}{2\mu_{AB}} \sum_{k=N+1}^{\infty} \langle \phi_i^a | \frac{\partial}{\partial R} | \phi_k^a \rangle \langle \phi_k^a | \frac{\partial}{\partial R} | \phi_i^a \rangle \quad (A-4)$$

Equation (35) will be a valid approximation for incomplete bases in the case

$$|E_i^a(R) + G_{ii}^a(R)| \gg |\Delta_i(R)| \quad (A-5)$$

Using a Hellman-Feynman type theorem it can be shown that

$$\langle \phi_i^a | \frac{\partial}{\partial R} | \phi_k^a \rangle = \frac{1}{\epsilon_k^a(R) - \epsilon_i^a(R)} \langle \phi_i^a | \frac{\partial H}{\partial R} | \phi_k^a \rangle \quad (A-6)$$

and therefore the conditions for the validity of (35) are

$$|\epsilon_i^a(R) + G_{ii}^a(R)| \gg \frac{\hbar^2}{2\mu_{AB}} \left| \sum_{k=N+1}^{\infty} \frac{\langle \phi_i^a | \frac{\partial H}{\partial R} | \phi_k^a \rangle^2}{[\epsilon_k^a(R) - \epsilon_i^a(R)]^2} \right| \quad (A-7)$$

and

$$|G_{ij}^a(R)| \gg \frac{\hbar^2}{2\mu_{AB}} \left| \sum_{k=N+1}^{\infty} \frac{\langle \phi_i^a | \frac{\partial H}{\partial R} | \phi_k^a \rangle \langle \phi_k^a | \frac{\partial H}{\partial R} | \phi_j^a \rangle}{[\epsilon_k^a(R) - \epsilon_i^a(R)][\epsilon_k^a(R) - \epsilon_j^a(R)]} \right| \quad (A-8)$$

Thus equation (35) is a good approximation if the omitted states lie high enough in energy.

TABLE I. Relative computing times required to obtain 0.5% accuracy

Method	Computing time
D. R matrix propagation	1.0
C. Magnus, diabatic, analytic exponential	2.0
B. Magnus, diabatic, exponential by power series	4
A. Magnus, adiabatic	7
G. Runge-Kutta, diabatic	16
E. Runge-Kutta, adiabatic	16
F. Adams-Moulton, adiabatic	>30 ^a
H. Adams-Moulton, diabatic	>40 ^a

^aIn these two cases the results are still accurate to only 10-50% for the computing times listed. Since these two methods were found to be so inefficient, we did not continue to decrease the stepsize parameter to obtain 0.5% accuracy.

AD-A094 511

BATTELLE COLUMBUS LABS OH
COMPUTATIONAL STUDY OF NONADIABATIC EFFECTS IN ATOM-MOLECULE RE-ETC(U)
DEC 80 M J REDMON F49620-79-C-0050

F/6 7/4

NL

UNCLASSIFIED

AFOSR-TR-81-0007

2 OF 2
AD
D00000

END
DATE
FILMED
2-81
DTIC

TABLE II. Detailed comparison of computational efficiencies of methods
C and D.

Number of sectors or steps	Computing time ^a	P_{12} ^b	% error
Method D			
302	0.85	1.5646(-6) ^c	0.68
358	1.01	1.5617(-6)	0.49
452	1.23	1.5564(-6)	0.37
486	1.33	1.5554(-6)	0.09
520	1.43	1.5550(-6)	0.06
621	1.68	1.5543(-6)	0.02
659	1.73	1.5541(-6)	0.01
926	2.56	1.5539(-6)	-0.01
2344	6.25	1.5539(-6)	-0.01
4671	11.82	1.5540(-6)	0.00
Method C			
453	1.52	1.5741(-6)	1.29
647	2.02	1.5628(-6)	0.57
653	2.03	1.5615(-6)	0.48
680	2.09	1.5612(-6)	0.46
1359	3.55	1.5558(-6)	0.12
1477	4.66	1.5555(-6)	0.10
4527	11.93	1.5541(-6)	0.01
13581	35.76	1.5540(-6)	0.01

^a Same scale as Table I.

^b For 2H potential curves, $\epsilon = 0.06 E_h$, $\lambda = 0$.

^c Numbers in parentheses are powers of ten.

TABLE III. Comparison of s-wave inelastic transition probabilities calculated with two different equations for $G_0^a(R)$.^a

E (eV)	P ₁₂		P ₁₃		P ₂₃	
	$G_0^a = dF_0^a/dR$	Eq. (35)	$G_0^a = dF_0^a/dR$	Eq. (35)	$G_0^a = dF_0^a/dR$	Eq. (35)
1.633	2.03(-7) ^b	2.02(-7)				
1.660	1.38(-7)	1.37(-7)				
1.905	1.60(-5)	1.59(-5)				
1.986	8.41(-6)	8.41(-6)				
2.123	1.11(-5)	1.10(-5)				
2.177	2.62(-5)	2.62(-5)				
2.231	3.30(-5)	3.29(-5)				
2.612	7.09(-6)	7.07(-6)	1.76(-8)	1.75(-8)	8.67(-3)	8.62(-3)
2.645	1.11(-5)	1.11(-5)	3.36(-8)	3.33(-8)	3.51(-3)	3.49(-3)
2.661	1.35(-5)	1.35(-5)	4.40(-8)	4.38(-8)	6.83(-5)	7.17(-5)
2.694	1.95(-5)	1.94(-4)	7.18(-8)	7.16(-8)	1.36(-2)	1.36(-2)
2.721	2.56(-5)	2.56(-5)	1.00(-7)	9.95(-8)	9.06(-3)	9.02(-3)
2.884	7.73(-5)	7.72(-5)	4.58(-7)	4.57(-7)	1.76(-2)	1.76(-2)
2.912	8.39(-5)	8.37(-5)	5.11(-7)	5.10(-7)	2.30(-2)	2.29(-2)

^aMethod 21.

^bNumbers in parentheses are powers of ten.

TABLE IV. Cross sections for excitation and de-excitation processes
in K + H collisions.^a

$E (E_h)$	l_{\max}^b	$\sigma_{12} (a_0^2)$	$\sigma_{21} (a_0^2)^{c,e}$	$\sigma_{13} (a_0^2)$	$\sigma_{23} (a_0^2)^e$
2I potential curves					
0.06	37	$8.40(-6)^d$	$2.08(-4)$		
0.10	165	$1.20(-3)$	$9.80(-4)$	$2.75(-6)$	0.41
2H potential curves					
0.06	36	$1.60(-5)$	$3.96(-4)$		
0.10	>145	$9.24(-4)$	$7.55(-4)$	$1.73(-6)$	0.4

^aCross sections are accurate to about 2% with respect to variations of integration parameters.

^bNumber of partial waves necessary to converge inelastic cross sections to 5 significant figures.

^c $\sigma_{ji} = (k_{i1}^2/k_{j1}^2)\sigma_{ij}$ where $\hbar k_i$ is asymptotic momentum in channel i and d_i is the degeneracy of state i .

^dNumbers in parentheses are powers of ten.

^eIncludes factor of 1/3 for P-state degeneracy.

TABLE V. Predicted positions R_X and values $\Delta\epsilon$ of the large-R minima in the splitting of the adiabatic potential curves for KH.^a

Workers	Ref.	X-A		A-C		X-C	
		R_X (a_0)	$\Delta\epsilon$ (eV)	R_X (a_0)	$\Delta\epsilon$ (eV)	R_X (a_0)	$\Delta\epsilon$ (eV)
Bates-Boyd	4	8.8	0.495	14.3	0.24
Grice-Herschbach	6	8.8	1.06
Numrich-Truhlar	7,10	8.7	0.66	15.2	0.20	12.9	1.74
Janev	8	8.8	0.62
Adelman-Herschbach	9	7.6	1.16	13.75	0.37
Method 2I	present	8.9	0.85	15.1	0.30	13.5	1.81
Method 2H	present	8.9	0.85	15.1	0.30	13.5	1.81
RKR analysis ^b	7,10	9.3	0.78				

^a Calculations listed in chronological order.

^b Experimental.

TABLE VI. Maxima of s-wave inelastic transition probabilities
for $X \rightarrow A$ transition.

E (eV)	P_{12}	
	close coupling	$2P^{LZ}$
Method 2I		
1.91	$1.6(-5)^a$	$8.4(-4)$
2.22	$3.3(-5)$	$1.5(-3)$
2.96	$8.9(-5)$	$4.4(-3)$
Method 2H		
2.00	$2.8(-5)$	$1.0(-3)$
2.34	$3.2(-5)$	$1.9(-3)$
3.11	$1.4(-4)$	$5.2(-3)$

^aNumbers in parentheses are powers of ten.

TABLE VII. Interaction parameters for outermost peaks in $f_{ij}^a(R)$.

i	j	location of max $f_{ij}^a(r)$ (a_0)	$\Delta\theta_{ij}$	Q_{ij}
1	2	8.49	0.840	0.66
2	3	14.82	0.973	0.74
1	3	7.02	0.059	0.03
1	3	11.18	0.071	...

- ¹J. C. Light, in Atom-Molecule Collision Theory, edited by R. B. Bernstein, Plenum, New York, 1979, p. 239; D. J. Kouri, *ibid.*, p. 259.
- ²J. B. Delos and W. R. Thorson, J. Chem. Phys. 70, 1774 (1979).
- ³B. C. Garrett and D. G. Truhlar, in Modern Theoretical Chemistry: Advances and Perspectives, Vol. 6, edited by D. Henderson, Academic, New York, in press.
- ⁴J. C. Browne, Adv. At. Mol. Phys. 7, 47 (1971).
- ⁵D. R. Bates and T. J. M. Boyd, Proc. Phys. Soc. London 69A, 910 (1956).
- ⁶R. Grice and D. R. Herschbach, Mol. Phys. 27, 159 (1974).
- ⁷R. W. Numrich and D. G. Truhlar, J. Phys. Chem. 79, 2745 (1975).
- ⁸R. K. Janev, J. Chem. Phys. 64, 1891 (1976).
- ⁹S. A. Adelman and D. R. Herschbach, Mol. Phys. 33, 793 (1977).
- ¹⁰R. W. Numrich and D. G. Truhlar, J. Phys. Chem. 82, 168 (1978).
- ¹¹C. F. Melius, R. W. Numrich, and D. G. Truhlar, J. Phys. Chem. 83, 1221 (1979).
- ¹²B. R. Johnson and R. D. Levine, Chem. Phys. Lett. 13, 168 (1972).
- ¹³M. J. Redmon and R. E. Wyatt, Int. J. Quantum Chem., Symp. 11, 343 (1977).
- ¹⁴D. Chang and J. C. Light, J. Chem. Phys. 50, 2517 (1969).
- ¹⁵J. C. Light, Methods Comput. Phys. 10, 111 (1971).
- ¹⁶J. C. Light and R. B. Walker, J. Chem. Phys. 65, 4272 (1976).
- ¹⁷E. B. Stechel, R. B. Walker, and J. C. Light, J. Chem. Phys. 69, 3518 (1978).
- ¹⁸J. C. Light, R. B. Walker, E. B. Stechel, and T. G. Schmalz, Computer Phys. Commun. 17, 89 (1979).
- ¹⁹W. A. Lester, in Dynamics of Molecular Collisions, Part A, edited by W. H. Miller, Plenum, New York, 1976, p. 1.
- ²⁰See, e.g., S. A. Evans, J. S. Cohen, and N. F. Lane, Phys. Rev. A 4, 2235 (1971); I. H. Zimmerman and T. F. George, J. Chem. Phys. 63, 2109 (1975).

- ²¹C. F. Melius, Bull. Amer. Phys. Soc. 19, 1199 (1974).
- ²²C. F. Melius and W. A. Goddard III, Phys. Rev. A 10, 1541 (1974).
- ²³See, e.g., L. L. Barnes, N. F. Lane, and C. C. Lin, Phys. Rev. 137, A388 (1965) or W. A. Lester, Jr., Methods Comput. Phys. 10, 211 (1971).
- ²⁴E. Dalgaard and P. Jørgensen, J. Chem. Phys. 69, 3833 (1978).
- ²⁵R. Shepard and J. Simons, J. Chem. Phys., to be published.
- ²⁶D. G. Truhlar and N. A. Mullaney, J. Chem. Phys. 68, 1574 (1978); N. A. Mullaney and D. G. Truhlar, Chem. Phys. Lett. 58, 512 (1978); N. A. Mullaney and D. G. Truhlar, Chem. Phys. 39, 91 (1979).
- ²⁷D. G. Truhlar, N. M. Harvey, K. Onda, and M. A. Brandt, in Algorithms and Computer Codes for Atomic and Molecular Quantum Scattering Theory, Vol. I, edited by L. Thomas, National Resource for Computation in Chemistry, Lawrence Berkeley Laboratory, Berkeley, CA, 1979, p. 220.
- ²⁸M. J. Romanelli, in Mathematical Methods for Digital Computers, Vol. I, edited by A. Ralston and H. S. Wilf, John Wiley and Sons, New York, 1960, p. 110.
- ²⁹W. H. Miller and T. F. George, J. Chem. Phys. 56, 5668 (1972).
- ³⁰M. E. Riley and A. Kuppermann, Chem. Phys. Lett. 1, 537 (1968).
- ³¹W. Eastes and D. Secrest, J. Chem. Phys. 56, 640 (1972).
- ³²R. A. White and E. F. Hayes, J. Chem. Phys. 57, 2985 (1972).
- ³³B. H. Bransden, "Atomic Collision Theory", W. A. Benjamin, New York, 1970, chapters 8 and 9.
- ³⁴M. E. Riley, Phys. Rev. A 7, 626 (1973).
- ³⁵In references 7 and 10 we labelled the $1\Sigma^+$ curves X, A, B,... In the present paper we switch to the convention used in the rest of the literature, i.e., the lowest three $1\Sigma^+$ states are called X, A, and C, and B denotes the lowest 1Π state.
- ³⁶N. F. Mott and H. S. W. Massey, The Theory of Atomic Collisions, 3rd ed., Oxford University Press, London, 1965, pp. 351ff., 804ff.
- ³⁷D. R. Bates, in Quantum Theory I. Elements, edited by D. R. Bates, Academic Press, New York, 1961, p. 293ff.

- ³⁸R. E. Olson, Phys. Rev. A 2, 121 (1970).
- ³⁹M. S. Child, Mol. Phys. 20, 171 (1971), 28, 495 (1974).
- ⁴⁰E. E. Nikitin, Advan. Quantum Chem. 5, 135 (1970).
- ⁴¹See, e.g., M. R. C. McDowell and J. P. Coleman, Introduction to the Theory of Ion-Atom Collisions, North Holland, Amsterdam, 1970, pp. 178ff.
- ⁴²M. B. Faist and R. D. Levine, J. Chem. Phys. 64, 2953 (1976). See also M. B. Faist and R. B. Bernstein, J. Chem. Phys. 64, 2971 (1976).
- ⁴³B. Andresen, A. Kuppermann, and A. E. deVries, Z. Phys. A 289, 1 (1978); B. Andresen and A. Kuppermann, Z. Phys. A 289, 11 (1978).
- ⁴⁴W. H. Miller and T. F. George, J. Chem. Phys. 56, 5637 (1972). See also R. K. Preston, C. Sloane, and W. H. Miller, J. Chem. Phys. 60, 4961 (1974).
- ⁴⁵P. Habitz and C. Voltava, J. Chem. Phys. 72, 5532 (1980).
- ⁴⁶A. Russek, Phys. Rev. A 4, 1918 (1971).
- ⁴⁷E. B. Stechel, T. G. Schmalz, and J. C. Light, J. Chem. Phys. 70, 5640 (1979).
- ⁴⁸L. I. Ponomarev, S. I. Vinitzky, and F. R. Vukajlović, J. Phys. B 13, 847 (1980).

Figure Captions

Fig. 1. Adiabatic potential energy curves as a function of internuclear distance for the three lowest $1\Sigma^+$ states of KH. The curves are the results of the ab initio pseudopotential calculations as obtained by method 2I for the solid curve and method 2H for the dashed curve. The two asymptotic values for the C state differ because in fitting the 2I potential curve the experimental 5^2S excitation energy of 2.61 eV was used, whereas for the 2H potential curve the numerically computed value of 2.55 eV was used. This difference has a negligible effect on the scattering calculations. The potential curves for the B state both dissociate to the correct atomic 4^2P excitation energy of 1.61 eV. The points are the experimentally determined RKR values for the X and A potential curves (from references 7 and 10).

Fig. 2. First derivative coupling terms, as defined by equations (19) and (37), for the three lowest adiabatic $1\Sigma^+$ states of KH as functions of internuclear distance. States 1, 2, and 3 correspond to the X, A, and C states of figure 1. (Since the difference between methods 2I and 2H involves only the treatment of the core, the derivative couplings are the same for both methods.)

Fig. 3. The diagonal matrix elements $H_{kk}^d(R)$ for the $1\Sigma^+$ states of KH in the P-diabatic basis as functions of internuclear distance. The solid and dashed curves are the results of transforming the corresponding solid and dashed adiabatic curves shown in figure 1.

Fig. 4. Same as figure 3 except for the off-diagonal elements $H_{jk}^d(R)$.

Fig. 5. Transition probabilities $P_{jk}(E)$ as functions of the reciprocal of the total energy for $\epsilon = 0$. The zero of energy is the asymptote

of the X state. The top plot is for excitation of K from the 4^2S to the 4^2P state, the lower left plot is for excitation of K from the 4^2S to the 5^2S state, and the lower right part is for excitation of K from the 4^2P to the 5^2S state. In the top plot the left and right arrows along the abscissa indicate the energetic thresholds for excitation to the 5^2S and 4^2P state, respectively. The arrows in the lowest two plots are the threshold for the excitation to the 5^2S state. Note that the energy scale for the upper and lower left plots coincide and are aligned vertically with each other, whereas the energy scale for the lower right plot is expanded. In each plot the solid and dashed curves are the probabilities computed using the adiabatic potential curves and nonadiabatic couplings obtained by methods 2I and 2H, respectively.

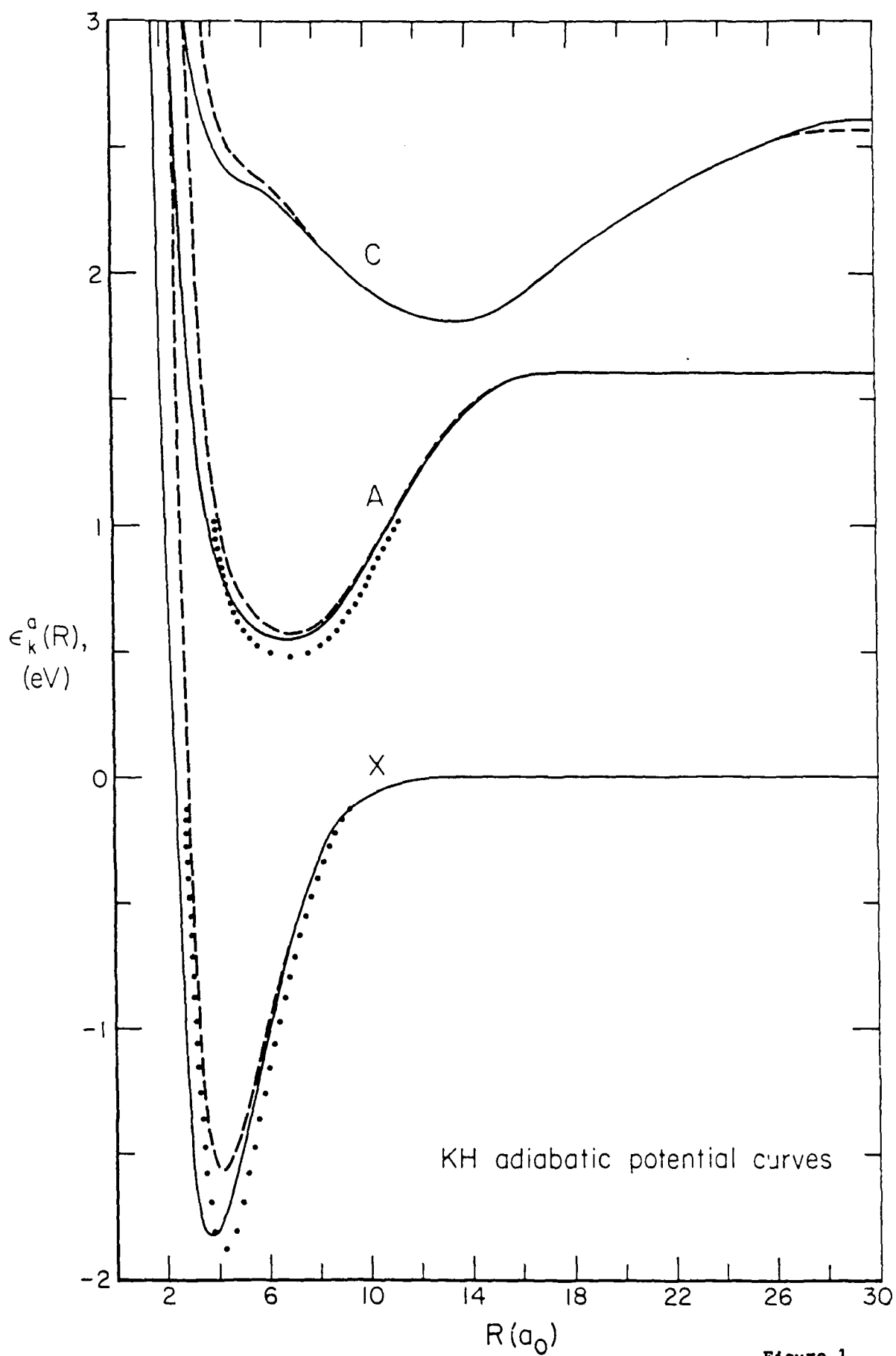


Figure 1

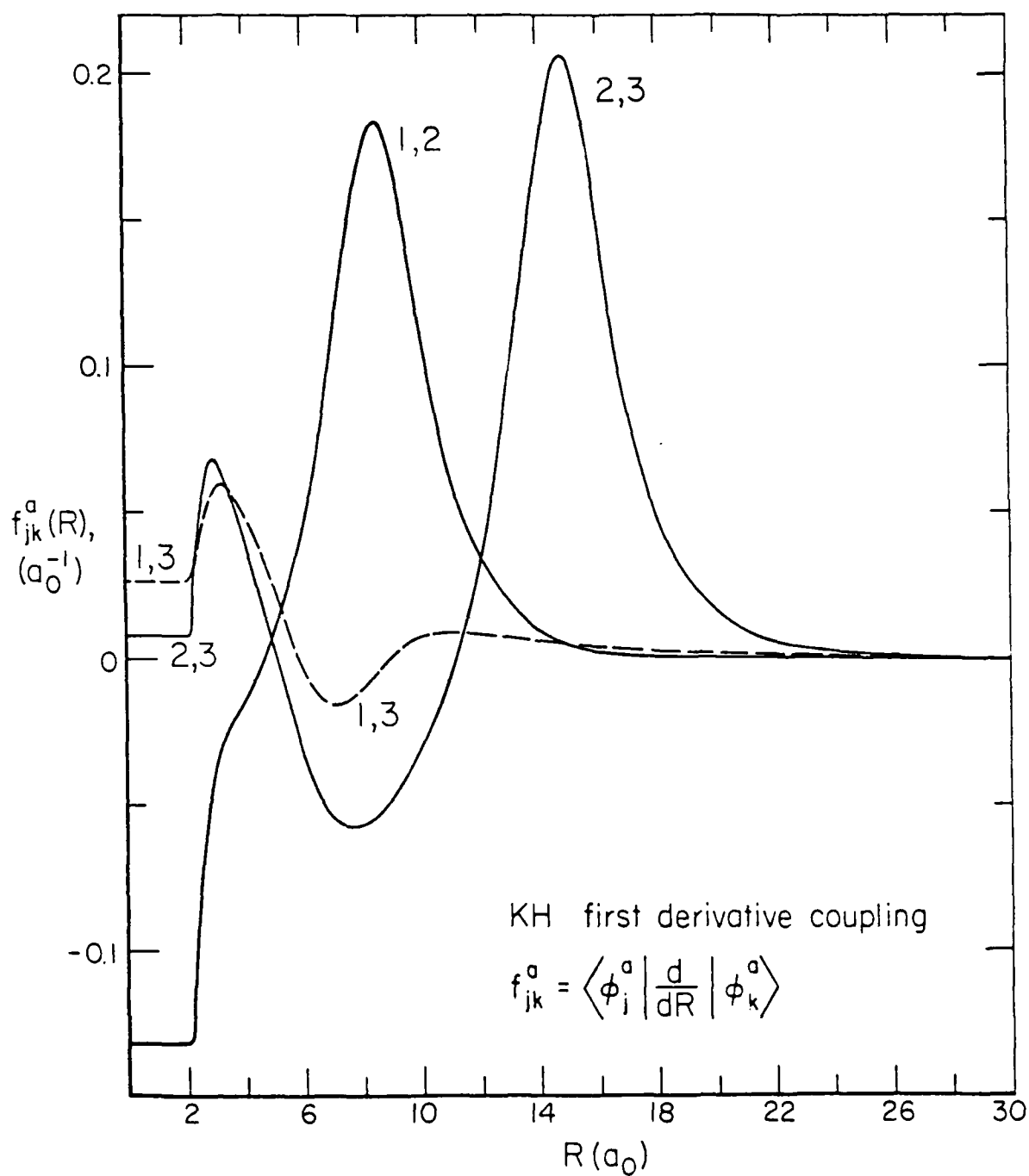


Figure 2

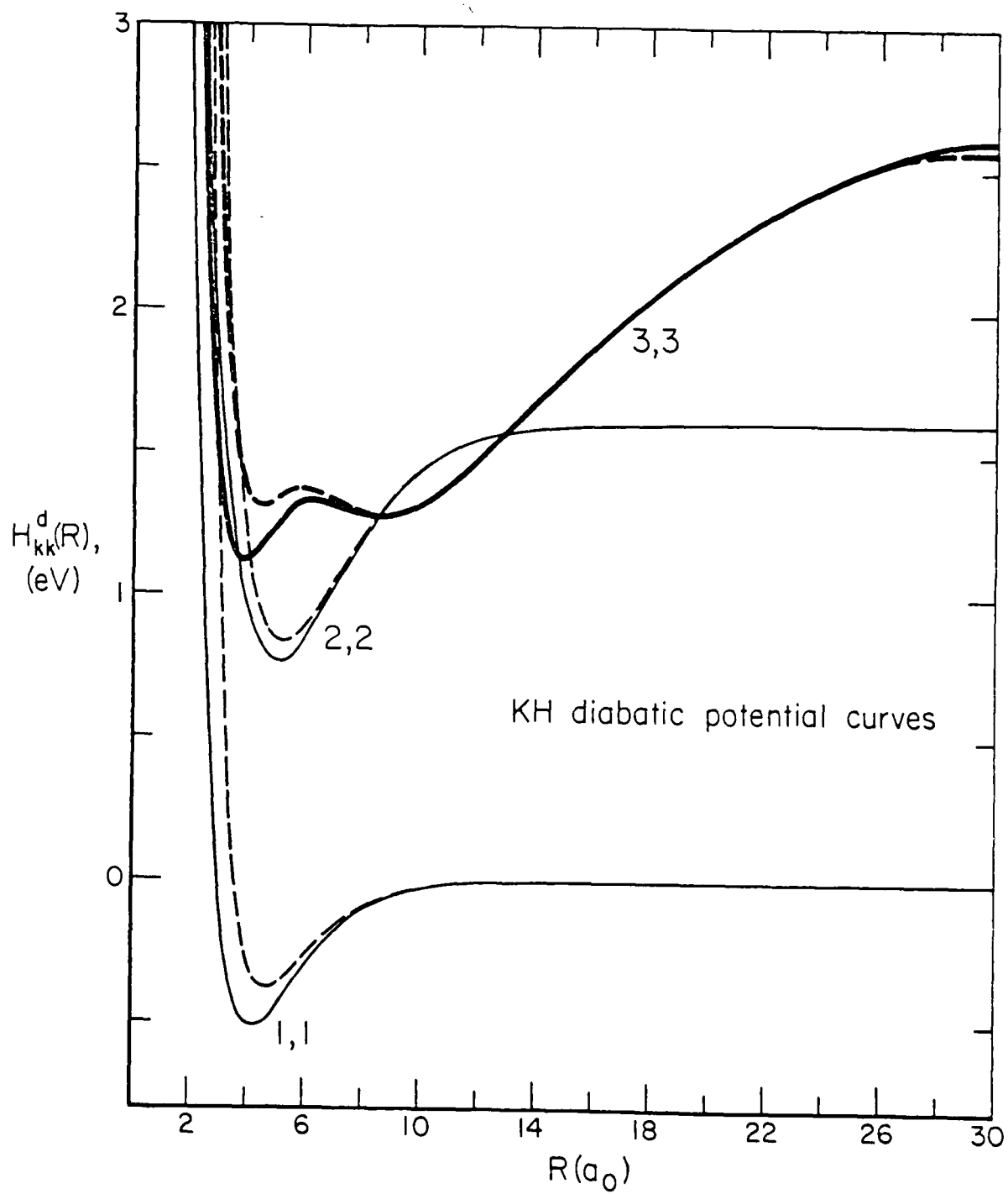


Figure 3

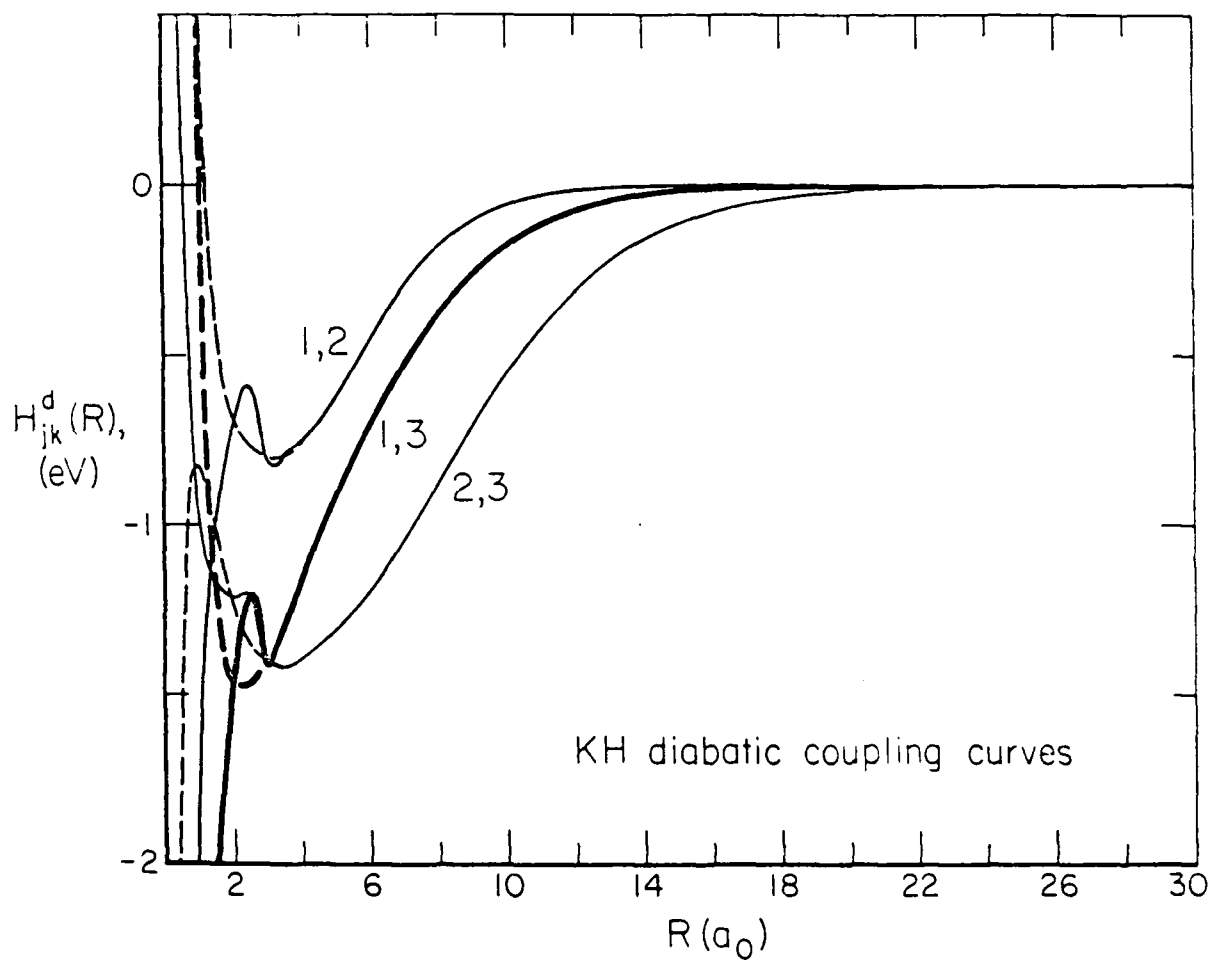


Figure 4

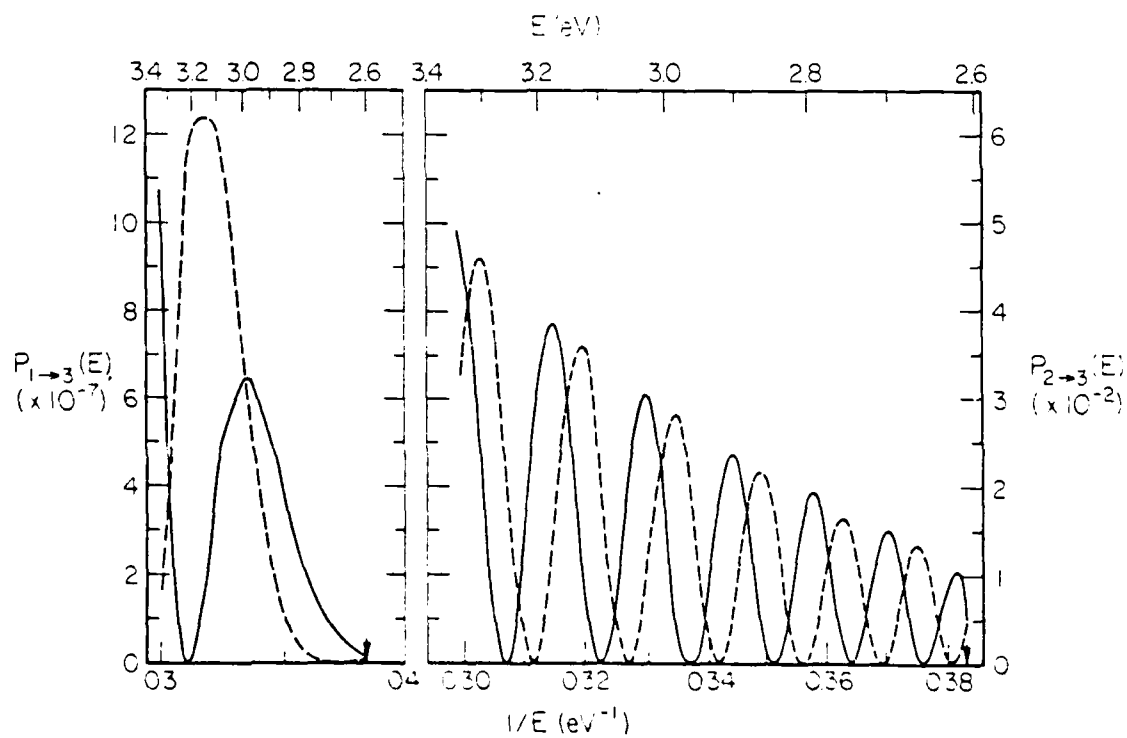
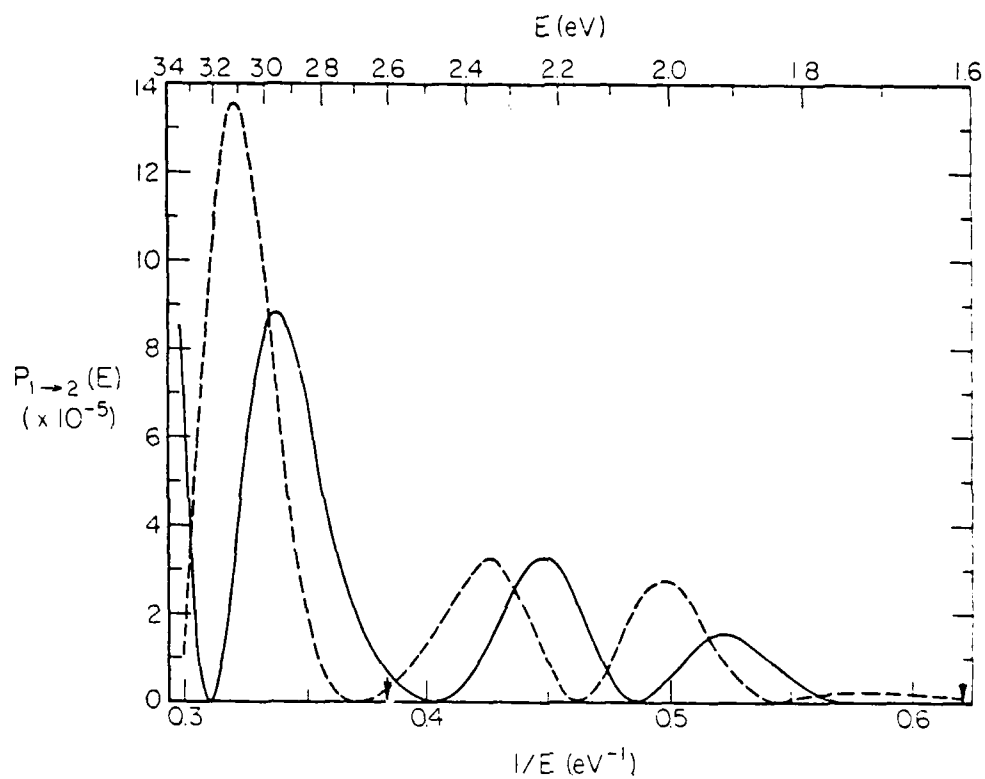


Figure 5

UNCLASSIFIED

SECURITY CLASSIFICATION OF THIS PAGE (When Data Entered)

REPORT DOCUMENTATION PAGE		READ INSTRUCTIONS BEFORE COMPLETING FORM
1. REPORT NUMBER AFOSR-TR-81-0007	2. GOVT ACCESSION NO. AD-A094511	3. RECIPIENT'S CATALOG NUMBER
4. TITLE (and Subtitle) COMPUTATIONAL STUDY OF NONADIABATIC EFFECTS IN ATOM-MOLECULE REACTIVE SCATTERING		5. TYPE OF REPORT & PERIOD COVERED Final 15 March 79-1 October 80
7. AUTHOR Dr. Michael J. Redmon		8. CONTRACT OR GRANT NUMBER(s) F49620-79-C-0050
9. PERFORMING ORGANIZATION NAME AND ADDRESS Battelle's Columbus Laboratories 505 King Avenue Columbus, OH 43201		10. PROGRAM ELEMENT, PROJECT, TASK AREA & WORK UNIT NUMBERS 61102F 2303/B1
11. CONTROLLING OFFICE NAME AND ADDRESS Air Force Office of Scientific Research (AFSC) Directorate of Chemical & Atmospheric Sciences (NC) Bolling AFB, D.C. 20332		12. REPORT DATE 10 December 1980
14. MONITORING AGENCY NAME & ADDRESS (if different from Controlling Office) 1114		13. NUMBER OF PAGES 115
		15. SECURITY CLASS. (of this report) UNCLASSIFIED
16. DISTRIBUTION STATEMENT (of this Report) Approved for public release, distribution unlimited		15a. DECLASSIFICATION/DOWNGRADING SCHEDULE
17. DISTRIBUTION STATEMENT (of the abstract entered in Block 20, if different from Report)		

19. KEY WORDS (Continue on reverse side if necessary and identify by block number)

quantum mechanics
scattering theory
chemical dynamics
kinetics

chemical reactions
combustion
chemical lasers
gas dynamics
state-to-state chemistry

potential energy surfaces

20. ABSTRACT (Continue on reverse side if necessary and identify by block number)

A research program that attempts to bring together the computational tools necessary for studying nonadiabatic transitions in atom-diatomic molecule collisions is described. Recent results, including rate constants for state-to-state reactions involving $F+H_2(V=0)$ and $H+H_2(V=1)$, are presented. Systematic approaches to fitting potential energy surfaces obtained from *ab initio* quantum chemistry are investigated. A practical formalism for accurately treating non-adiabatic electronic couplings is developed, and tested in an application to electronic quenching in $K+H$ collisions. It is argued that these developments

DD FORM 1 JAN 73 1473

UNCLASSIFIED

SECURITY CLASSIFICATION OF THIS PAGE (When Data Entered)

UNCLASSIFIED

SECURITY CLASSIFICATION OF THIS PAGE(When Data Entered)

provide the theoretical tools necessary for a computational study of rotational, vibrational and electronic transitions in selected atom-diatomic molecule reactions.

UNCLASSIFIED

SECURITY CLASSIFICATION OF THIS PAGE(When Data Entered)

**DAT
FILM**